

Intermediate water masses, a major supplier of oxygen for the eastern tropical Pacific ocean” by Olaf Duteil et al.

A. Reply to Referee #1

Main Objective of this Study and General Comments

This study investigates the impact of intermediate water masses (IMW) and its pathway and supply along Equatorial Intermediate Current System (EISC) on dissolved oxygen content in the Pacific Oxygen Minimum Zone (OMZ) (in the eastern tropical Pacific ocean). The authors utilized a suite of simulations to address these questions. The manuscript consists of mean state diagnostics and evaluations from suite of models (NEMO (ocean stand-alone simulation), UVIC (coupled, energy moisture balance model, forced wind stress), GFDL (coupled) and ii) sensitivity simulations (or transient simulations over 60 years) (oxygen restoring, conservative tracer release, and Lagrangian tracking of tracers) elucidating the role of subtropical IMW on dissolved oxygen supply (through EICS) in eastern tropical Pacific ocean. Despite the limitations (or discrepancies) in simulating properties of IWM in the current climate models, the authors did a nice set of simulations tackling how bias in IMW and EICS could impact on dissolved oxygen (and possibly impact on projections of OMZs due to climate change). This could provide insights on improving ocean bio-geochemistry in ESMs and I think the work contains interesting and important results.

We thank the reviewer for her/his positive evaluation.

However, I have several comments and some sections and figure presentations should be revisited before publication. Therefore, I suggest a major revision. I state specific comments below and hope this helps to improve the manuscript.

Major Comments

[1] The heterogeneous subset of models (simulations) will be an advantage exploring model and resolution dependencies (as author stated in L116–118) on IMW characteristics and tracers (here dissolved oxygen) but also makes the results difficult to interpret to some extent. I still think the results will have impacts from not only the differences in model structures and resolutions, but also the forcing (forcing dataset, prescribed vs. coupled) and model integration time (spinup states) (some specific comment on forcing dataset is stated below). I would like to ask authors to discuss further on these points since for example, the wind and buoyancy forcing bias could be one of the reasons introducing errors in climate (and ocean) models as stated in the introduction.

We agree with the reviewer that extracting information from a heterogeneous subset of simulations is not straightforward and needs a specific conceptual reasoning, that we clarify in a first step. In a second step, we reply specifically to the comments of the reviewer.

1. Conceptual reasoning

We compare the oxygen levels in a set of models characterized by different resolutions, integration time scale, forcings, etc.. Despite all these differences, we found common behaviours (part 3.1): the properties of the intermediate waters are poorly represented in all simulations that we analyzed and we found a correlation between oxygen levels in intermediate waters and oxygen levels in tropical regions (part 3.1 of the ms).

It suggests that intermediate waters affect oxygen levels and OMZ volume in tropical regions. We test this hypothesis using a “what if ?” experiment : “If the oxygen levels are realistic south of 30°S and/or below 1500m does it have an impact on OMZs ?”. These sensitivity simulations are performed using a single model framework: same resolution, same forcings, same integration time. (part 3.2)

Another second hypothesis that we investigate is “do the intermediate circulation and associated jets play a large role in setting oxygen levels in the equator region ?”. To reply to this question, we performed a set of sensitivity simulations using again a single model framework: same integration time, same forcings, but different spatial resolution. (part 4.2).

In addition (part 4.3) we compare the oxygen levels in a climate model suite: similar model framework, same integration time, different ocean resolution.

In summary, we investigate the mechanisms impacting tropical oxygen levels at intermediate depths in a very heterogeneous set of models, by performing dedicated sensitivity simulations that are easy to interpret.

2. Reviewer comment on the heterogeneity of the models and model set-ups that makes it difficult to pinpoint causes for differences of the simulations.

- Atmospheric forcing

We agree that the atmospheric forcing data play a large role in setting ocean properties. Differences in wind stress between reanalyses data are of the order of 5-20 % (zonal mean wind stress), as shown by the figure below (Chauduri et al., 2013)

Chaudhuri, Ayan & Ponte, Rui & Forget, Gael & Heimbach, Patrick. (2013). A Comparison of Atmospheric Reanalysis Surface Products over the Ocean and Implications for Uncertainties in Air-Sea Boundary Forcing. *Journal of Climate*. 26. 153-170. 10.1175/JCLI-D-12-00090.1.

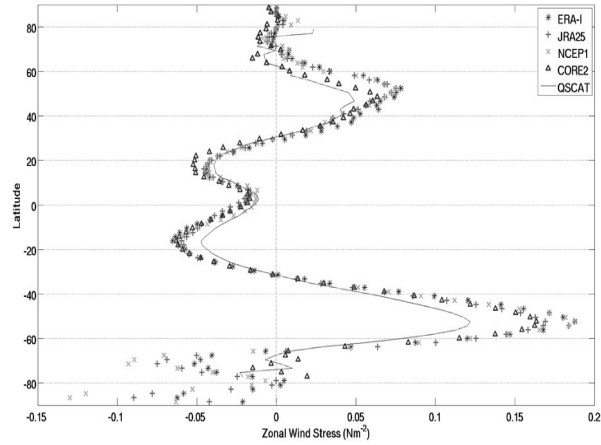


Figure 1: Zonally averaged profiles of zonal wind stress from 1999–2006 for ERA-Interim, JRA-25, NCEP1, CORE2, and QuikSCAT (Chauduri et al., 2013).

Large differences exist especially in the eastern tropical Pacific Ocean where the wind is weak. The Figure 2 below shows the relative difference in wind speed between NCEP and CORE (Large and Yeager, 2009), i.e., it shows that winds of the different products in the eastern tropical Pacific differ by up to 50%.

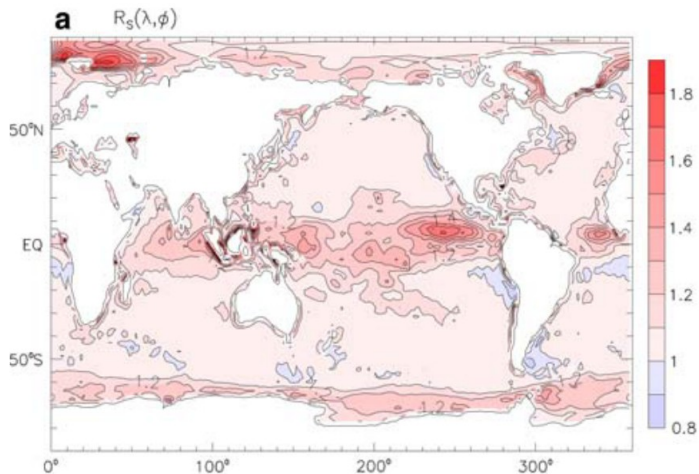


Figure 2: Global distributions of the multiplicative speed applied to NCEP wind vectors to obtain CORE wind vectors (Large and Yeager, 2009)

Large, W.G., Yeager, S.G. /2009). The global climatology of an interannually varying air-sea flux data set. *Clim Dyn* 33, 341–364. 10.1007/s00382-008-0441-3

To test this impact, we performed an experiment using the UVIC model using 2 different wind products (NCEP and COREv2 – Large and Yeager, 2009) (Figure A1). While the shape of the OMZ shows slight differences, the volume of the OMZ and the mean oxygen levels in the tropical

regions and in the mid latitudes are similar. Consistent with the Figure 2, higher oxygen levels at 30°S lead to higher oxygen levels in the tropical ocean and to a smaller OMZ volume (Figure 3)

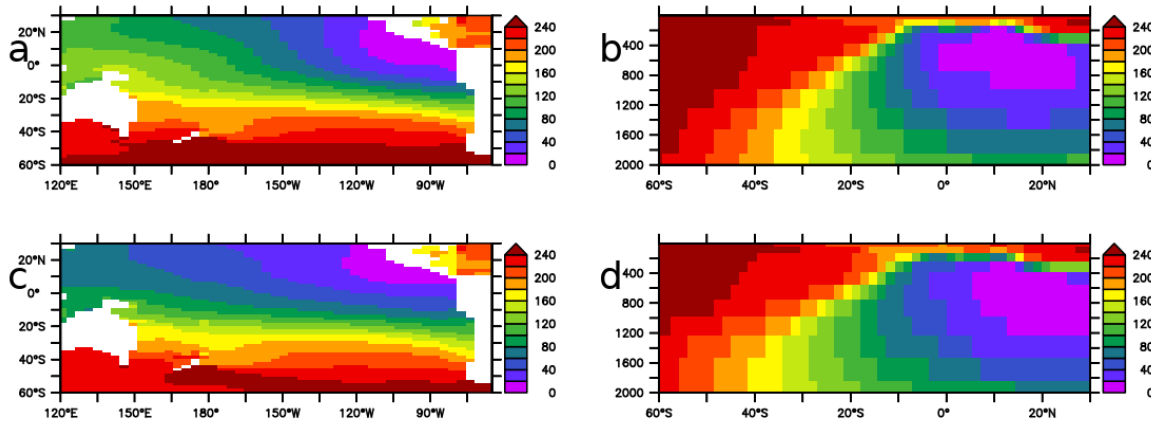


Figure 3 : Oxygen levels in UVIC (10000 years integration) a- mean 500-1500 m forcing NCEP. b- section 120°W forcing NCEP. c- mean 500-1500 m forcing COREv2, d- section 120°W forcing COREv2.

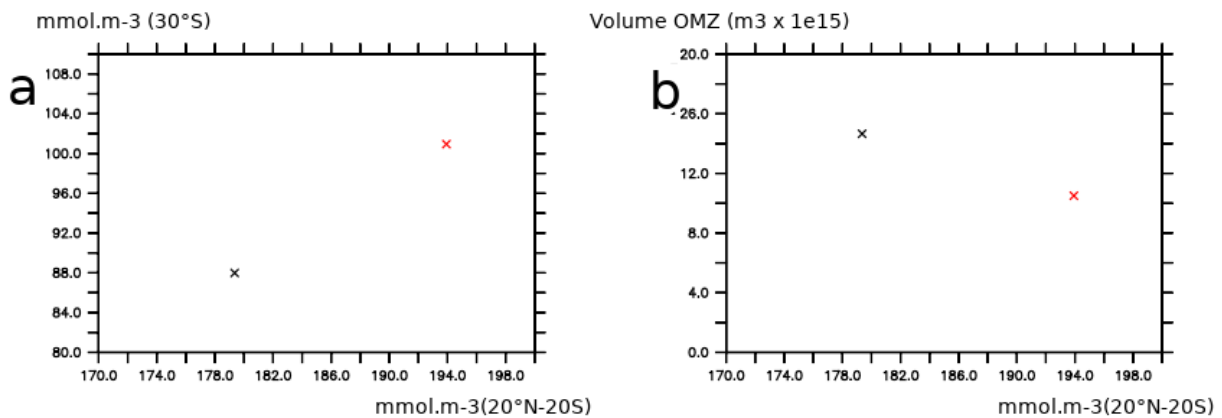


Figure 4 : a - Oxygen levels in UVIC (10000 years integration) at 30°S (zonal mean in the Pacific Ocean from surface to 2000 m depth) and in the tropical regions (20°S-20°N, averaged over the whole Pacific Ocean). b - Oxygen levels in UVIC (10000 years integration) at 30°S (zonal mean in the Pacific Ocean, from surface to 2000 m depth) and volume of the OMZ in the Pacific Ocean. The configuration forced by COREv2 is shown in black, the configuration forced by NCEP is shown in red.

Coupled ocean atmosphere experiments

Coupled ocean-atmosphere experiments introduce further discrepancies compared to the use of realistic atmospheric forcings. However, the mean surface velocity is similar in the suite of GFDL models (especially GFDL01 and GFDL025) that we analyzed, suggesting that the effect of atmospheric forcing is likely not dominant when comparing this subset of models (part 4.3).

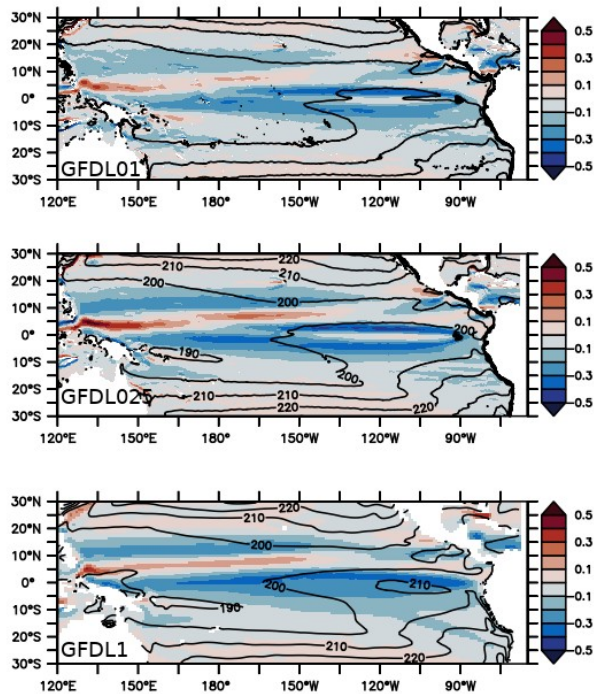


Figure 5: ocean zonal surface velocity (ms-1) in GFDL01, GFDL025 and GFDL1

Model integration time

In complement, the spinup state of the model also impacts the oxygen levels as the deep ocean needs thousands of years to be in equilibrium. It may explain why UVIC (integrated for 10000 years) is characterized by much larger oxygen levels than the GFDL model suite (integrated for 190 years). As an example, the Figure 6 shows the evolution of oxygen levels during spinup in NEMO2. Larger oxygen levels at 30°S (e.g after 1000 years of integration) are characterized by a smaller OMZ volume (which is consistent with Fig 2) (Figure 7)

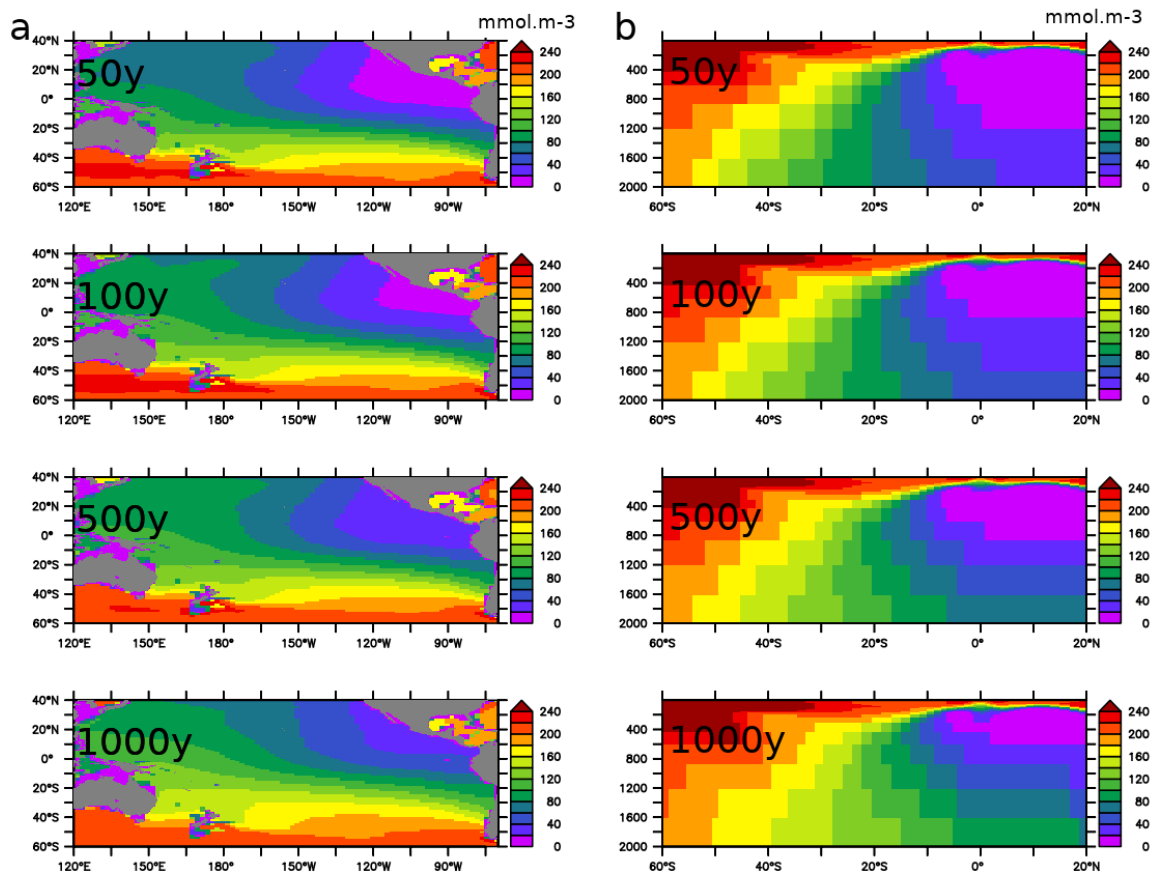


Figure 6 : oxygen levels at a - intermediate depth (average 500 – 2000 m) and b - 120°W in NEMO2 after 50, 100,500 and 1000 years integration

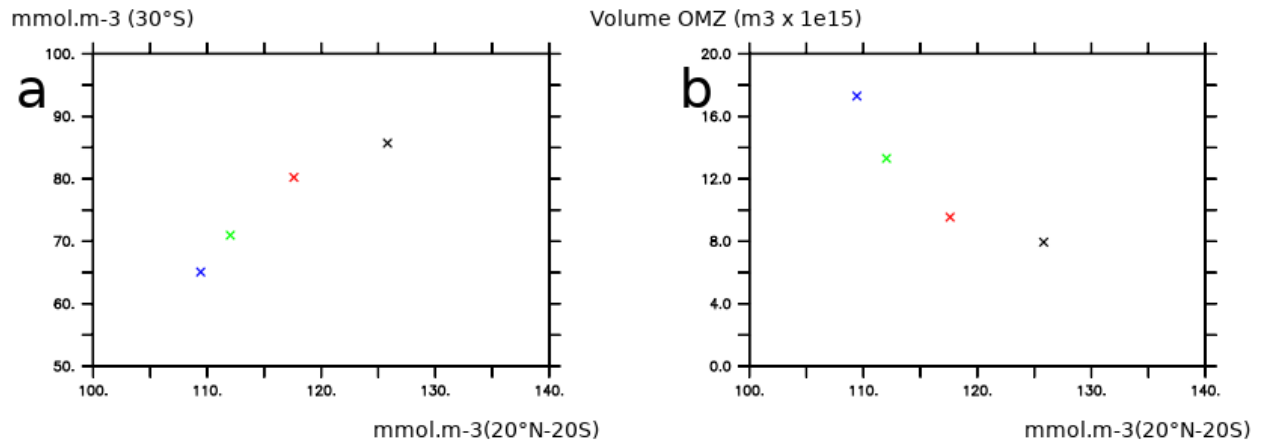


Figure 7 : a - Oxygen levels in NEMO2 at 30°S (zonal mean in the Pacific Ocean from surface to 2000 m depth) and in the tropical regions (20°S-20°N, averaged over the whole Pacific Ocean from surface to 2000 m depth). b - Oxygen levels in NEMO2 at 30°S (zonal mean in the Pacific Ocean from surface to 2000 m depth) and volume of the OMZ in the Pacific Ocean. The color of the cross depends of the integration duration (black : 50 years, red : 100 years, green : 500 years, blue 1000 years).

3. Conclusion

The differences induced by the different forcings and integration time have (not surprisingly) an impact on water masses and oxygen levels. Despite the heterogeneity of our simulations, our results nevertheless suggest a strong coupling between subtropical and tropical oxygen content and justify our questioning and the experiments performed in the part 3 and 4 of this study (see 1. Conceptual reasoning)

[2] Regarding to sensitivity of tropical IWM oxygen to subtropical and deep dissolved oxygen levels, the authors refer AAIW, NPIW (and the upper part of the PDW) as IWM in this study. I was wondering what will be the relative contributions of each water masses to dissolved oxygen supply, ventilation in the eastern tropical Pacific ocean (particularly North (NPIW) vs South (AAIW)). My impression is that AAIW could be more dominant (e.g. Talley, 2013) but I would like to know what sensitivity simulations indicates. At least, I think it is possible to obtain insights from the Lagrangian tracking diagnostics (or if possible, conducting additional restoring simulations with 30°S boundary only for example).[Reference] Talley, Lynne D., (2011), Descriptive Physical Oceanography: An Introduction, Academic Press.

We perform a complementary experiment using NEMO2 where the oxygen levels are forced (see Minor Comment 4) to WOA solely south of 30°S (experiment NEMO2_30S). The experiment where oxygen is restored both to the south and to the north. NEMO2_DEG30 has been renamed NEMO2_30S30N. It shows clearly that AAIW has a dominant impact in setting tropical Pacific Ocean intermediate oxygen levels and the OMZs volume. This is not surprising as AAIW recirculates till about 20°N and NPIW has a much smaller, regional extension (Talley, 2011)

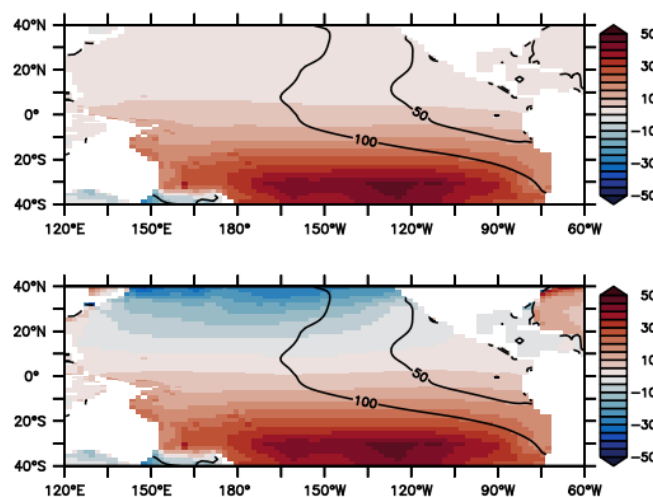


Figure 8: NEMO2-30S minus NEMO2-REF and NEMO2_30S30N minus NEMO2_REF (average 500-2000 m).

[3] The core of the study is based on a suite of sensitivity simulations from NEMO(NEMO2). In the first reading, I struggled a bit on connecting aim and each sensitivity experiments. The dissolved oxygen restoring simulations aim on investigating sensitivity of tropical IWM oxygen to subtropical and deep dissolved oxygen levels (as stated in section 3.2) and the conservative tracer release simulations are more dedicated to investigate spreading of tracers towards the eastern tropical Pacific (transport by the EICS, as stated in section 4.1). While the standard structure of the manuscript is to introduce overall data and methods in the beginning, (section 2), I suggest to move some of the objective and details of sensitivity experiments to each corresponding sections (referring to sections 3.2 and 4.1) so it is much easier to follow the aim bridging to sensitivity experiments (I think it is still fine to keep brief general descriptions in section 2 including Table 1). Alternatively, the methods section could be revised to include additional descriptions connecting to corresponding result sections. I will leave this decision to the authors regarding to the structure of the paper but I think the flow could be improved.

We decided to keep the original, classical, structure but agree that the methodology section need to be better connected with the results / discussions. We therefore added the following lines :

“L126: The mean state of the oxygen distributions is discussed below in section 3.1 “IWM Oxygen levels in models”

“L159 : The sensitivity of tropical IWM oxygen to subtropical and deep oxygen levels is discussed in section 3.2”

“L187 : The transport by the EICS is discussed in section 4.2 (tracers levels and Lagrangian pathways).”

[4] Another major issue is the figures. Figure labels and captions are not easy to interpret (and in some part, the authors are referring to figure does not appear,e.g.L267, Fig.4i). Therefore, I suggest the authors to carefully revisit all the figures and add necessary caption, labels for better presentation. For example, for time series plots (e.g.Fig. 2,3g–i,8), the difference in color (models, configurations etc.) should also be informed in the label (not just in figure captions) because it is not easy to follow.

The figures/labels/captions are revised in the final version of the ms. See the new set of figures at the end of the reply. When necessary, the figure / subpanel number has been modified in the text to match the new set of figures.

Similar issues for multiple maps (such as Fig.5), it will be reader friendly to label maps with "zonal advection", "meridional advection" etc.

The transport terms (Fig 4) are labeled in the final version of the ms. See the new set of figures at the end of the reply.

Also, some of the model names(labels) are not obvious because those are overlaid on color shading (e.g. Fig.9).

The names are labeled in a more obvious way in the final version of the ms. See the new set of figures at the end of the reply.

I put few more specific suggestions below and hope this helps to point out the difficulties I am referring to.

Thanks to the reviewer for these suggestions. We have rechecked all captions to make sure that they are correctly describing the panels.

[4.1] Fig.1caption, (L762–763) oxygen levels (mean 500 - 1500m) at 160W, I think color shading in b) is not vertical mean (because it is depth-latitude section). Also, is dissolved oxygen in Fig.1from observations such as World Ocean Atlas?

A new caption has been written.

[4.2] Regarding to Fig.4, I have several suggestions to improve figure presentation. I am still a bit confused what is in color shading and contours. For example, in L789,it states the vertical current as contour in c) but the contours do not look like vertical current values. Also the continent shading (ing) is missing (no gray shaded). Similar confusion occurred to me in other panels and I suggest to revisit and clearly state what is presented in color shading and contours for each panels with units.

The Figure 4 has been revisited (missing shading of the continent, captions, legend). See the new set of figures at the end of the reply.

Also, why did you only present the results from NEMO2-30DEG (not including NEMO2-30DEG1500M or NEMO2-30DEG1500M minus NEMO2-30DEG)?

The experiment NEMO2-30DEG has been renamed NEMO2_30S30N for clarity reasons (see above comment). We show in Fig 4 both the transport terms of NEMO2_30S30N and of NEMO2_30S30N minus NEMO2_REF. We do not show NEMO2_30S30N1500M as from Figure 3i it becomes clear that the processes transferring oxygen from the deeper layer toward the intermediate ocean are vertical advective processes. This is now stated explicitly in the new version of the ms.

[4.3] Add information labels for Fig.7a)–c)the first release, and d)–e)the second release, respectively.

Information labels have been added and the figure revisited. See the new set of figures at the end of the reply.

[4.4]Add information labels (like figure title) for Fig.9, zonal sections and meridional sections,

respectively.

Information labels have been added and the figure revisited. See the new set of figures at the end of the reply.

3 Minor Comments

[1] I am curious whether CORE v2 climatological forcing (used for NEMO) and NCEP/NCAR climatological forcing (wind stress, used for UVIC) makes a difference in paper spinup states. As far as I know, CORE v2 forcing is based on NCEP/NCAR reanalysis but it has several corrections and adjustments in the forcing and difference between the two could lead to different results, particularly after long-term spinup. Do authors think this is a minor thing ?

The different climatological forcings have indeed a significant impact (see Figure 3 of our response). However we think that differences in resolution play a larger role by resolving additional processes (in particular deep equatorial jets)

[2] Are all the GFDL model simulations integrated for the same period following high-resolution (GFDL01) for comparison (I assumed 200 years from Busecke et. al.,2018) or the low-resolution configurations are integrated for longer durations ?

All configurations have been integrated for 190 years (more precisely 48 years physics only + 142 years biogeochemical cycles), including the lower resolution version. This is now clearly stated in the new Table 1.

[3] Because of the high resolutions configurations for GFDL01, the integration time is limited but does this impact on IWM (and upper part of PDW) characteristics and tracers (i.e. insufficient spinup, drift in certain properties etc.)? Upper ocean could be quasi-equilibrated (say few hundred meters) but I am wondering about mid~deep ocean you are more focusing on in this study.

We agree with the reviewer, the model spin-up has a large impact on ocean properties. The mid-depth (500 – 1500 m) ocean is not fully equilibrated after 100/200 years. However, the experiments part 3.2 : “If the oxygen levels are realistic south of 30°S and/or below 1500m does it have an impact on OMZs ?” and 4.2/4.3 “do the intermediate circulation and associated jets play a large role in setting oxygen levels in the equator region ?” (see 1 - Conceptual reasoning) clearly show that a timescale of 100 - 200 years is sufficient to investigate the connectivity between mid-latitude / tropical regions, as well as the role of the intermediate current system in controlling oxygen (and more generally tracers) concentration. Even if a short integration timescale does not allow to characterize the steady state and the relative importance of all the processes at play, it permits nevertheless to assess the importance of specific processes (especially that the experiments, e.g the GFDL suite of models, have been integrated for the same duration (190 years).

[4] Regarding to dissolved oxygen restoring, are the boundaries (and depth inter-face at 1500m) all in the Pacific ocean only (e.g. thinking of for example, 30°N and 30°S zonal walls and 1500m layer in the entire Pacific ocean) or globally ? Also, how strong (i.e. timescale) is the restoring in these simulations ?

The term “restoring” is maybe inadequate and has been replaced by “forcing” L132, 139 and 142. of the manuscript including corrections as the oxygen levels are forced to the WOA monthly climatology. The latitude where the forcing is applied has been set globally (however as it is a “forcing”, it does not make any difference if it were applied solely in the Pacific Ocean).

[5] Regarding to the respiration rate (in L144), did you set all the simulations respiration rate (similar to fixing oxygen utilization rate I would assume) to NEMO2-REF?

Respiration rates (as all other biogeochemical fluxes) are the same in all the experiments, as stated L147 : “ The respiration rate (oxygen consumption) is identical in NEMO2-REF, NEMO2-30S30N and NEMO2-30S30N1500M”. Solely the oxygen concentrations are forced by WOA values at 30N/30S/1500m depth. Forcing phosphate levels would complicate the picture (as stated L150-151), as the resulting differences of productivity and respiration would counteract the difference of advection of modified oxygen concentrations. Quantifying the sensitivity of respiration to a change in nutrients is an important aspect, but is outside the scope of this study which focuses on the transport of oxygen by intermediate water masses. Furthermore our Figure 2 (correlation oxygen content at 30°S and in tropical regions) suggests that differences in ocean circulation are dominant compared to differences in biology in the simulations that we consider.

[6] I am a bit confused by the locations of particle release and IETP/IWTP regions you were referring to (L363–383, Fig.7 and 8). While the the locations of particle release is in sections (shown as black bold lines (or dot) in Fig.7), I thought the IETP/IWTP are basins in specific rectangles and this is different from the locations of particle release (it contains of course) if I understand correctly. If that is the case, I suggest to revise the main text and Figure to include these information more explicitly (I think adding boxes in Fig.7 could help and you can refer to that interpreting Fig.8).

A new Figure 8a has been added, which shows the IETP/IWTP regions and the release locations R1 and R2. We state more explicitly in the text:

L389 : “The release location R1 is the eastern tropical Pacific (100°W, 5°N-5°S, 1000 m depth) . R1 is included in the larger Intermediate Eastern Tropical Pacific (IETP) ocean region (160°W – coast / 10°N-10°S / 200 – 2000 m)”

L405 : “The location of the second release R2 (160°E, 5°N-5°S, 1000 m depth) is included in the Intermediate Western Tropical Pacific (IWTP) ocean region (160°W – coast / 10°N-10°S / 200 – 2000 m) (Fig 7b)”

[7] Just for clarification: do ocean stand-alone simulations (i.e. NEMO and UVIC) paper also use preindustrial pCO₂ for spinup (related to mean state diagnostics)?

Preindustrial pCO₂ is used. This is now stated in the text L117.

[8] In section 2.1, Table 1, and part of the main text: The author mix use the NEMO and NEMO2 through the manuscript and I have got a bit confused. Since all the simulations use NEMO2, you should make the terminology consistent through the text after introducing (or just NEMO, I will leave this to the authors).

Three versions at 2°, 0.5° and 0.1° horizontal resolution of the general NEMO model engine (Madec et al., 2017) are used : NEMO2 (with biogeochemical cycles), NEMO05, NEMO01 (physics only). We refer specifically to these versions in the text.

L132 : we refer to generally to the NEMO model engine and state that explicitly to avoid confusion : "we perform two different sets of sensitivity simulations using the general NEMO model engine"

[9] For Table 1, I would suggest to include model integration time information.

The model integration time has been added in the Table 1 (see last section of this document)

3.1 Line Specific Comments

[L70] Cabre et I., : should be Cabre "et al."

This is corrected in the final version of the ms

[L85] eastern tropical (20°S-20°N): I think you should add longitude information since you mentioned "eastern" tropical Pacific.

We added "east of 160°W" in the final version of the ms

[L104](see Keller 2012 for ... : delete "Keller" (duplicates).

This is corrected in the final version of the ms

[L124] more than 50 years: suggest to change to "60 years" (the same as the statement in latter section, L160).

This is corrected in the final version of the ms

[L167] 5 daily means: I think "5-day mean" is more common.

This is corrected in the final version of the ms

[L262–263] Where is the information (figure) of total advective term? Fig. 4g is the vertical advection term difference and I could not find specific information on total term in the figure (although it is possible to infer from all the terms).

The objective of the Figure 4 is to better explain the differences between the model experiments (Fig 3g). As the patterns are mostly zonal, we did not show in Fig 4 the total term (the zonal mean of the total term is already displayed in Fig. 3g).

[L301]Tsuchuya jets: should be "Tsuchiya jets".

This is corrected in the final version of the ms

B. Reply to Referee #2

This paper highlights the role of intermediate waters as the O₂ supply pathway for the waters of oxygen minimum zones primarily focusing on the Pacific basin. This study consists of three model simulation with different source code, resolution and biogeochemical parameterizations. In general current generation of earth system models tend to have difficulties representing this mode of oxygen supply, thus overestimating the size of low-oxygen waters.

Here are main conclusions;

- (1) the O₂ concentration of these water masses in the subtropics is biased in models. If restoring is used to correct the model bias in O₂ entering into the subtropics, the tropical O₂ representation improves significantly.
- (2) the ocean jets and eddies play major role for the O₂ transport of intermediate water, as supported by the runs with different model resolutions. Coarse resolution models must rely on parameterization for this process.
- (3) Due to tropical upwelling, the biases in the deep and intermediate water can impact on the entire upper ocean water column.

I think these points are not really surprising, but the authors have done a detailed, systematic analysis of oxygen responses to model resolution and source water properties to support these conclusions. In my view, this paper is publishable perhaps with a few minor revisions.

We thank the author for her/his positive feedback.

Below are my technical comments. Main text has several typos. It will benefit from a careful proofreading.

The final version of the ms has been carefully proofread.

Fig 2b. If I'm reading this figure correctly, it is remarkable that not a single model can capture the peak of O₂ at about 800m. I think this feature should be pointed out more clearly in the main text at about page 6. The caption does not indicate which line is WOA. I think it is obvious that the observation is the thick black line, but it needs to be spelled out in the caption.

The "missing" O₂ peak is indeed a remarkable feature in the models. We point that out more clearly in the new version of the ms.

We added to the paragraph L209-213 : "The IWM oxygen maximum is apparent at 30°S throughout the lower thermocline (600 – 1000 m) in observations (Fig 2b), consistent with the circulation of IWM with the gyre from the mid/high latitude formation regions towards the northwest in subtropical latitudes, and followed by a deflection of the waters in the tropics towards the eastern basin", the sentence L213 : " This oxygen peak is missing in all the models analyzed here".

The figure 2 has been updated and is reproduced at the end of the reply.

Fig 3 and main text in page 7. I really like this figure and the discussion in the main text, up to panel f. Then I'm confused. The figure caption says the panels g, h, i are zonal mean tendencies of O₂. The main text talks about something different about deep O₂. It doesn't even mention how these tendencies are calculated. This probably means there is some version inconsistency between Figure 3 and the main text. This obviously needs a revision.

The text L229 (page 7) to which the reviewer refers reads : "The difference NEMO2-30DEG1500M – NEMO2-30DEG (Fig 3f-h) shows a deep positive anomaly in oxygen, as oxygen levels are lower than in observations by 30-40 mmol.m⁻³ in the eastern tropical regions". The reference to Fig 3 f-h is wrong. It has been corrected in the new version of the ms.

We added a brief description of the budget terms L265 :

"The oxygen budget is :

$$\frac{dO_2}{dt} = Adv_x + Adv_y + Adv_z + Diff_{Dia} + Diff_{Iso} + SMS$$

where Adv_x, Adv_y, Adv_z , are respectively the zonal, meridional and vertical advection terms, $Diff_{dia}$ and $Diff_{iso}$ are the diapycnal and isopycnal diffusion. SMS (Source Minus Sink) is the biogeochemical component (respiration at depth, below the euphotic zone)

L284 and in some other places; What is meant by the "upper layer"? I interpreted as the surface, but please be more specific (such as the surface or sigma-theta level or z-level).

The upper layer corresponds to the mixed layer. This is clearly specified in the new version of the ms.

The text related to Fig 4 is confusing, if I read it correctly, the net advective transport divergence is not affected but is not shown (L262-263). Is the change in O₂ concentration entirely caused by the eddy parameterization part of the transport? In my opinion this type of budget analysis may be more interesting if it is applied to contrast the low-and high-resolution runs and separate the mean flow and (resolved or parameterized) eddy contribution.

We show below the total advective transport in NEMO2_REF and its anomaly (NEMO2_30S30N minus NEMO2_REF) (Figure 7)

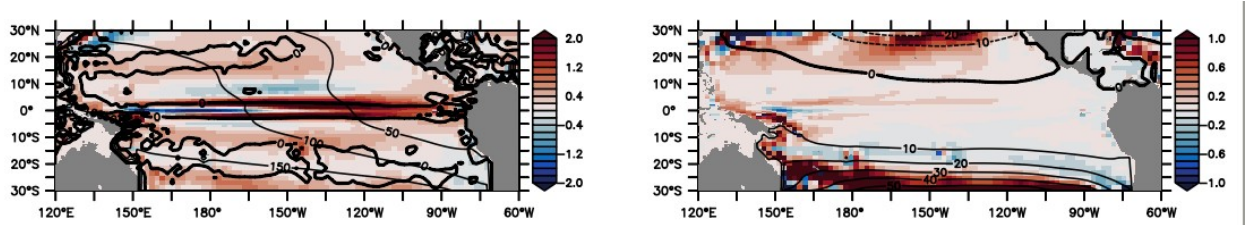


Figure 7: left : total advection term in NEMO2_REF. Right : difference in the total advection term between NEMO2_30S30N – NEMO2_REF

The Fig 7 right panel in our response letter shows clearly that the total advection terms are similar in NEMO2_30S30N and NEMO2_REF at the equator. In contrast, the differences are large in the gyres as the anomaly is advected by the strong westward currents. In the tropics, most of the anomaly is due to isopycnal mixing (or “eddy parameterization” transport as stated by the reviewer), see Fig 4b in the new version of the ms. This is maybe not surprising as the intermediate currents are weak in NEMO2 (coarse resolution). Higher resolutions models will likely be characterized by the imprint the of zonal jets. We agree with the reviewer, a similar experiment but performed at high resolution would be very useful to quantify precisely the impact of these jets. Unfortunately a high resolution eddy resolving simulation coupled with biogeochemical cycle was not available due to computational expenses (which is the reason why we compare coarse and high resolution simulations coupled to a single passive tracer in part 4 of this ms).

C. Updated Figures and Table

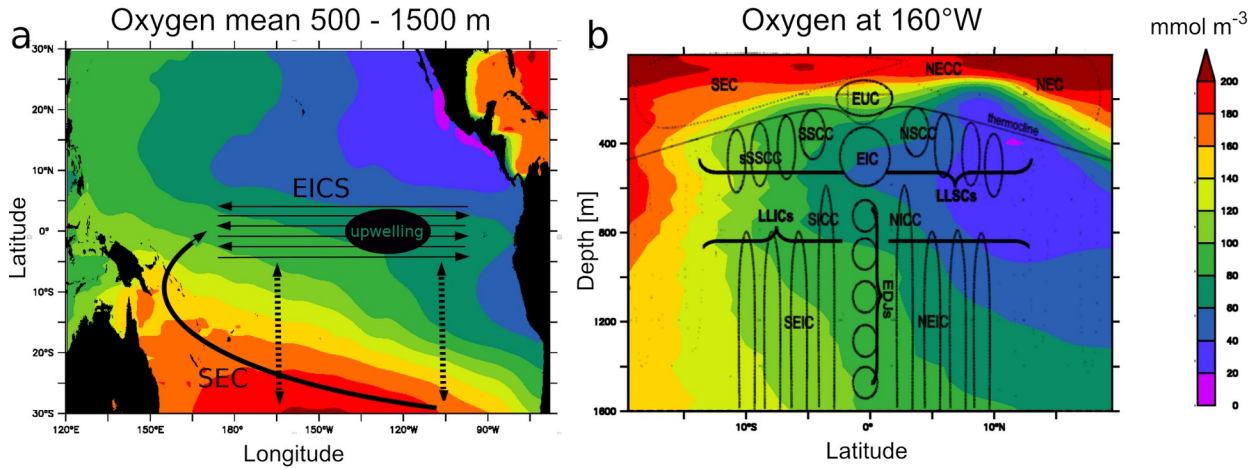


Figure 1 : a- schema summarizing the intermediate water masses (IWM) pathway from the subtropics into the equatorial regions. EICS : Equatorial Intermediate Current System. SEC : South Equatorial Current. Dashed line : isopycnal diffusive processes. Observed (World Ocean Atlas) oxygen levels (mmol.m⁻³) in the lower thermocline (mean 500-1500m) are represented in color. b - schema (adapted from Menesguen et al., 2019) illustrating the complexity of the EICS, extending below the thermocline till more than 2000 m depth (see section 4.1 for a detailed description). Observed (World Ocean Atlas) oxygen levels at 160°W are represented in color.

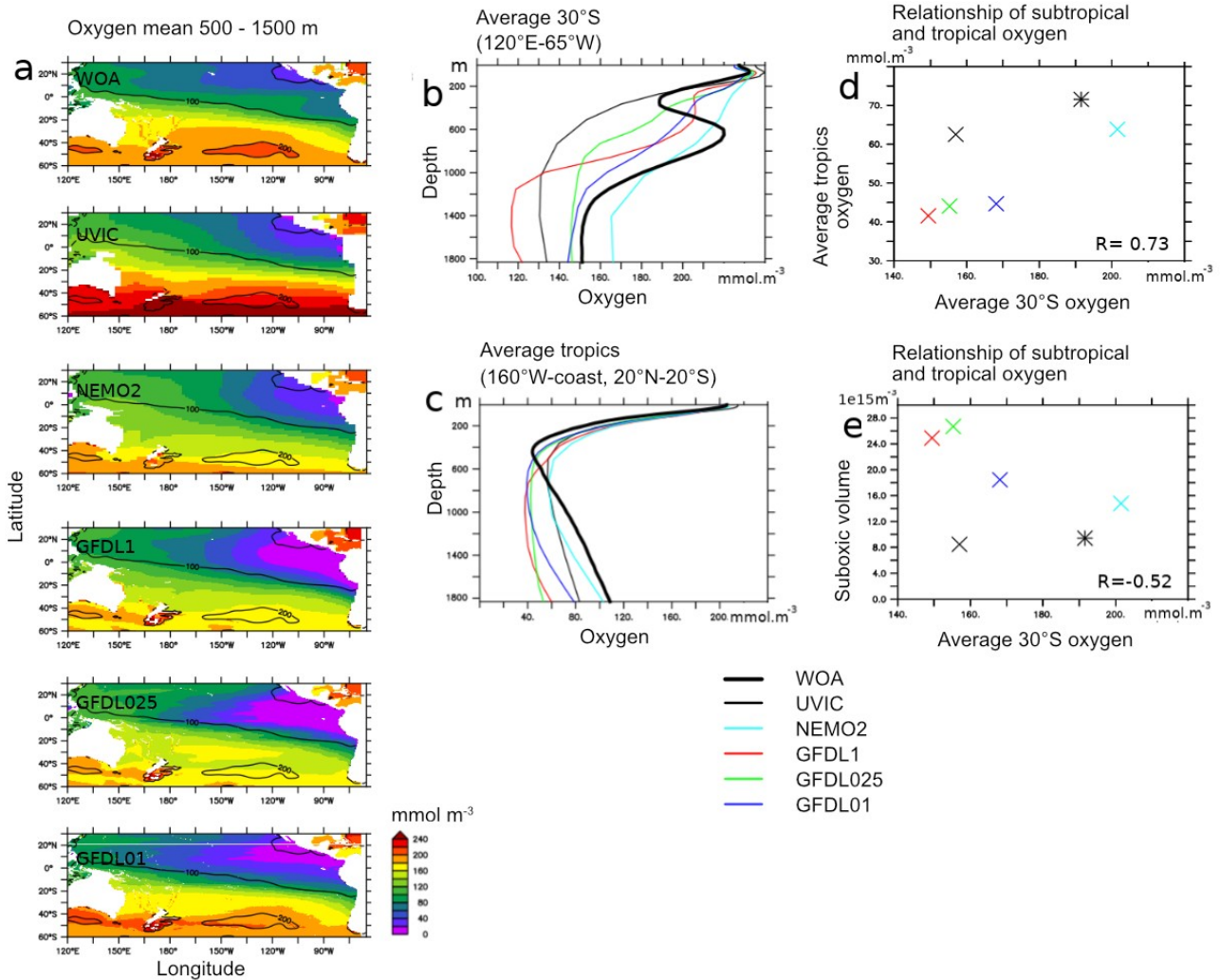


Figure 2 : a- oxygen levels (mmol.m^{-3}) in observations (World Ocean Atlas - WOA) (mean 500 – 1500 m) and models (UVIC, NEMO2, GFDL1, GFDL025, GFDL01). Contours correspond to WOA values. b: average “30°S” (120°E-65°W, 30°S) c : average “tropics” (160°W-coast, 20°N-20°S). d: average “30°S” vs “tropics”. e: average “30°S” vs volume of tropical suboxic ocean (oxygen lower than 20 mmol.m^{-3}) regions ($1\text{e}15\text{m}^3$). b-e : UVIC : black, NEMO2 : cyan, GFDL1 : red, GFDL025, green; GFDL01 : blue, WOA: bold line (b,c) and star (d,e).

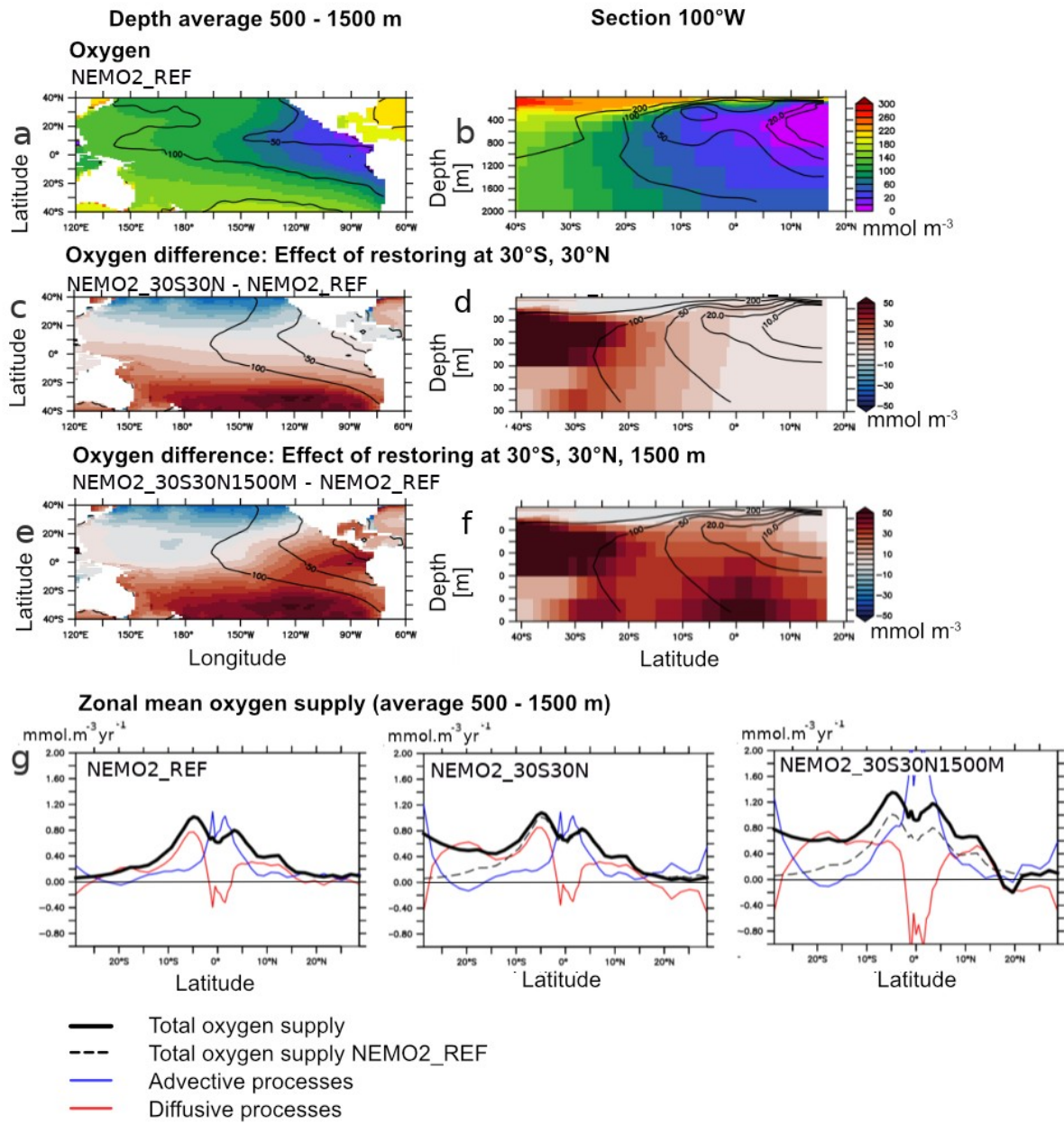


Figure 3 : a,b: Oxygen (mmol.m⁻³) in the experiments NEMO2_REF (color) and World Ocean Atlas (contour) (a- average 500-1500 m, b- 100°W). c,d: Oxygen (mmol.m⁻³) difference (c- average 500 – 1500m, d- 100°W) between the experiments NEMO2_30S30N minus NEMO2_REF. e,f : Oxygen (mmol.m⁻³) difference (e- average 500-1500m, f- 100°W) between the experiments NEMO2_30S30N1500M minus NEMO2_REF. g- basin zonal average (average 500 - 1500 m) of the oxygen total supply (bold) (mmol.m⁻³.year⁻¹), advective processes (blue) and isopycnal diffusion (red) in NEMO2_REF, NEMO2_30S30N, NEMO2_30S30N1500M. The dashed line is the oxygen total supply in NEMO2_REF.

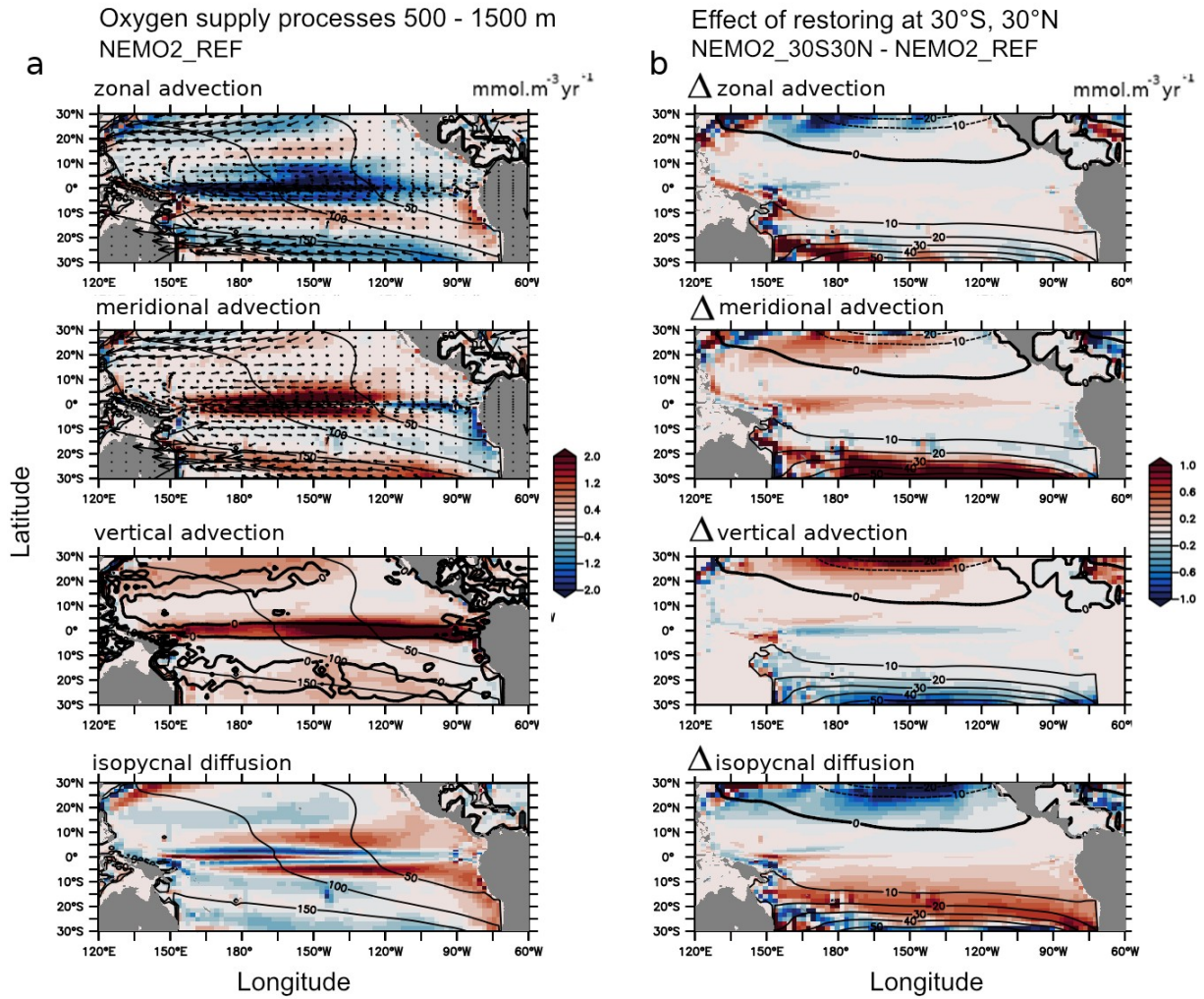
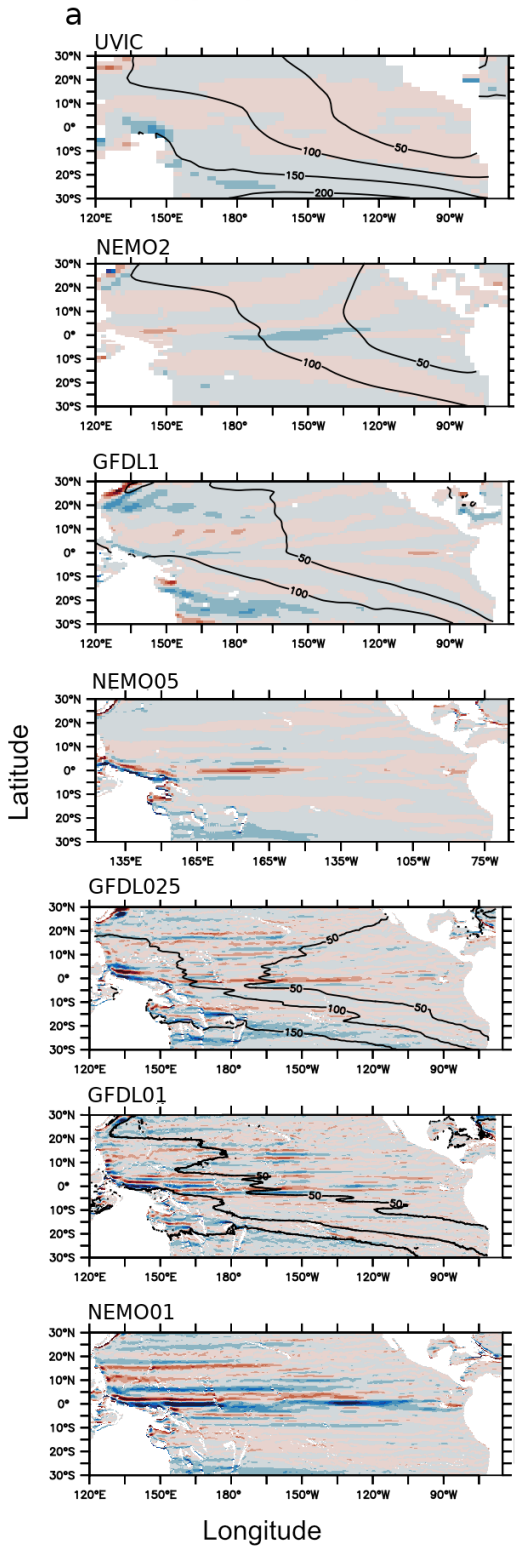


Figure 4 : a- Oxygen supply processes ($\text{mmol.m}^{-3}.\text{year}^{-1}$ – average 500 - 1500m) in NEMO2_REF : zonal advection, meridional advection, vertical advection, isopycnal diffusion. The mean meridional and zonal currents are displayed as vectors (meridional, zonal advection). The mean vertical current (0 isoline) is represented as bold contour (vertical advection). Oxygen levels (mmol.m^{-3}) are displayed in black contour. b- Difference in oxygen supply processes ($\text{mmol.m}^{-3}.\text{year}^{-1}$ – average 500-1500m) between NEMO2_30S30N and NEMO2_REF : zonal advection, meridional advection, vertical advection, isopycnal diffusion. The NEMO2_30S30N – NEMO2_REF oxygen anomaly (mmol.m^{-3}) is displayed in contour.

Zonal velocity component at 1000 m (colors) and oxygen (contours)



Zonal velocity component at 100°W (colors) and oxygen (contours)

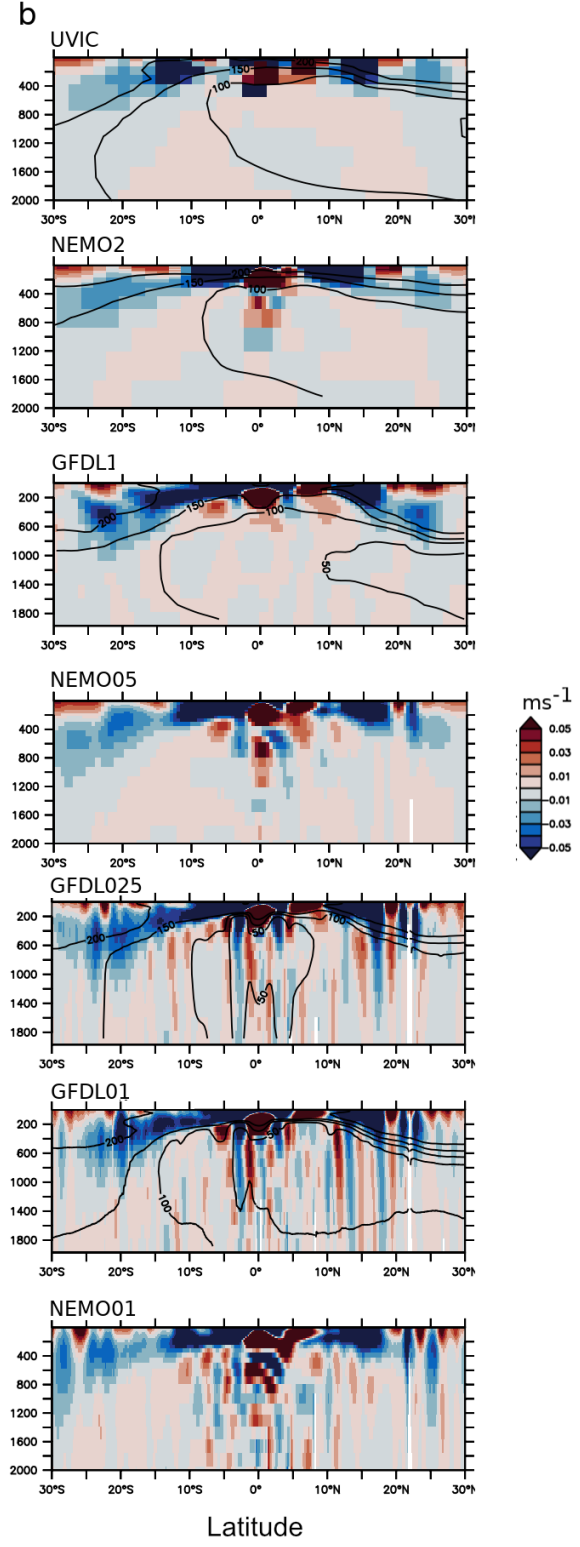
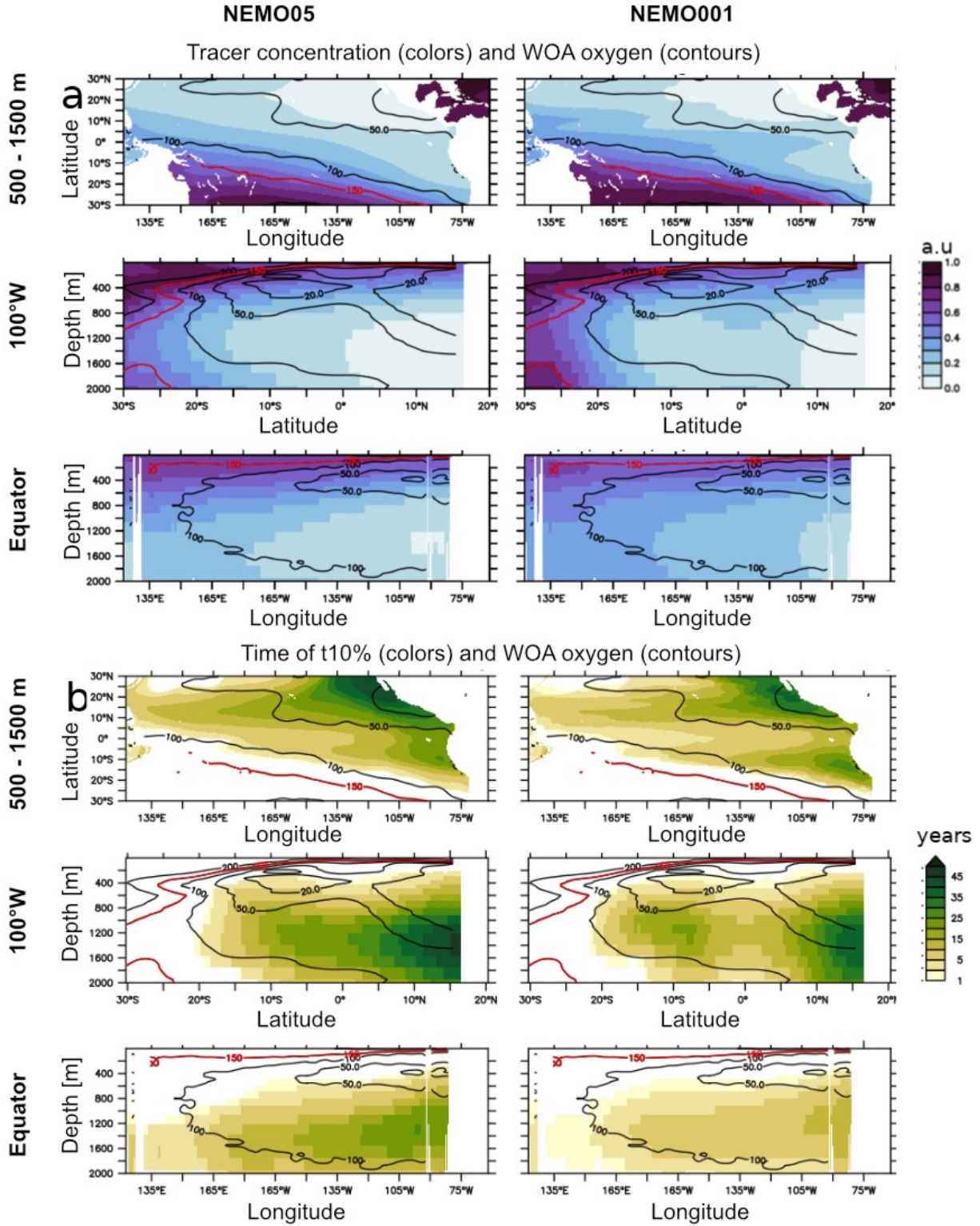


Figure 5 : mean currents velocity (ms^{-1}) at a- 1000 m depth b- 100°W in UVIC, NEMO2, NEMO05, GFDL025, GFDL01, NEMO01. The mean oxygen levels (mmol.m^{-3}) (when coupled circulation-biogeochemical experiments have been performed – see Table 1) are displayed in contour



Fig

Figure 6: a : tracer concentration (arbitrary unit) after 60 years integration in NEMO05 and NEMO01: average 500-1500m, section 100°W, equatorial section. b: Time (years) at which the released tracer reaches the concentration 0.1 ($t_{10\%}$) in NEMO05 and NEMO01: average 500-1500m, section 100°W, equatorial section. In all the subpanels, the WOA oxygen levels are displayed in contour. The red contour is the WOA 150 mmol.m^{-3} oxygen isoline, used to initialize the tracer level.

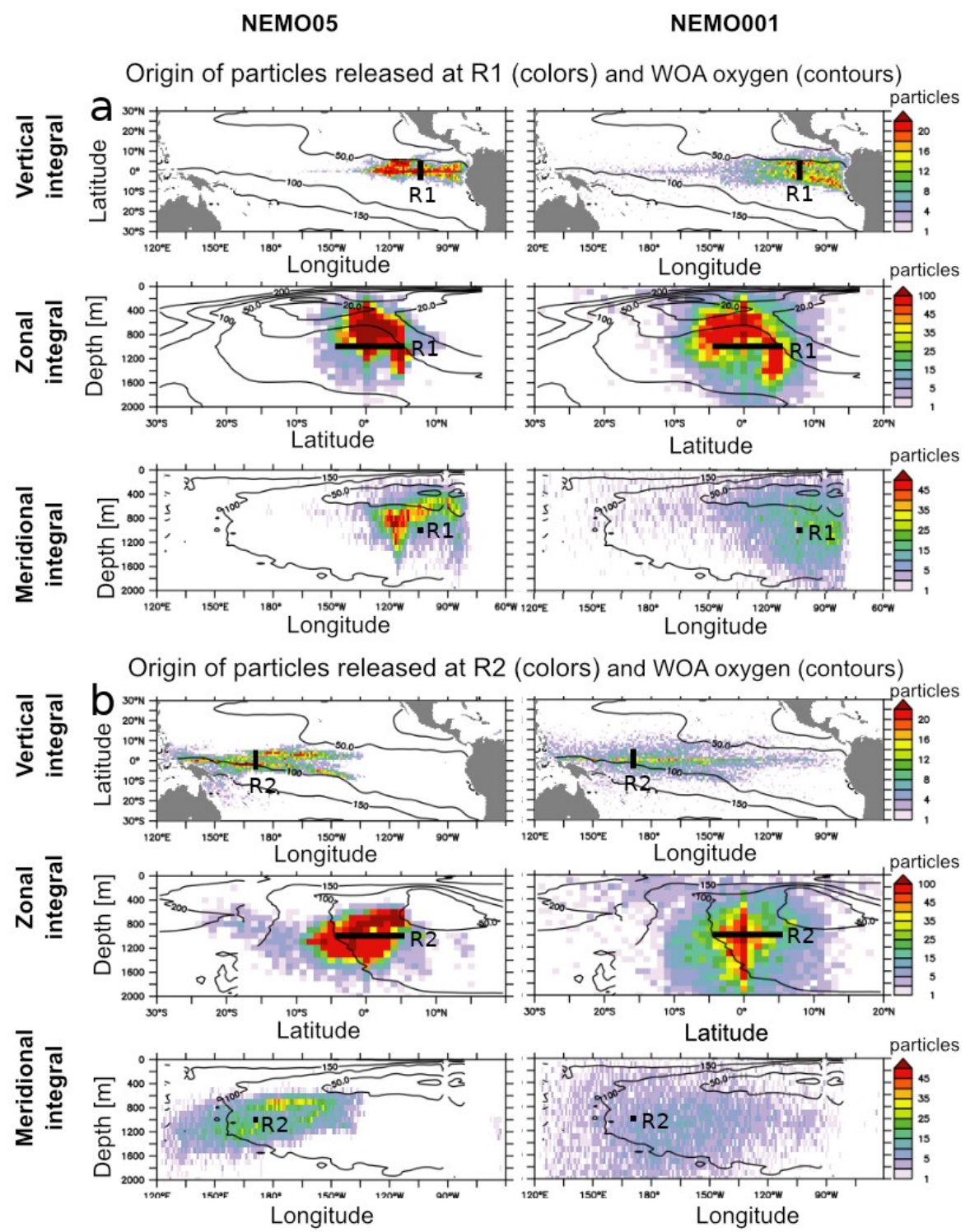


Figure 7 : Density (number of particles in a $1^\circ \times 1^\circ \times 100\text{m}$ depth box) distribution of the location of released Lagrangian particles (15 years backward integration starting from the final experiment state) in NEMO05 and NEMO01. The release location is identified in bold and is located a- at $100^\circ\text{W}/5^\circ\text{N}-5^\circ\text{S}/1000\text{ m}$ depth (R1). b- at $160^\circ\text{E}/5^\circ\text{N}-5^\circ\text{S}/1000\text{ m}$ depth (R2). The particles have been integrated vertically, zonally and meridionally. The observed mean oxygen levels (WOA) are displayed in contour.

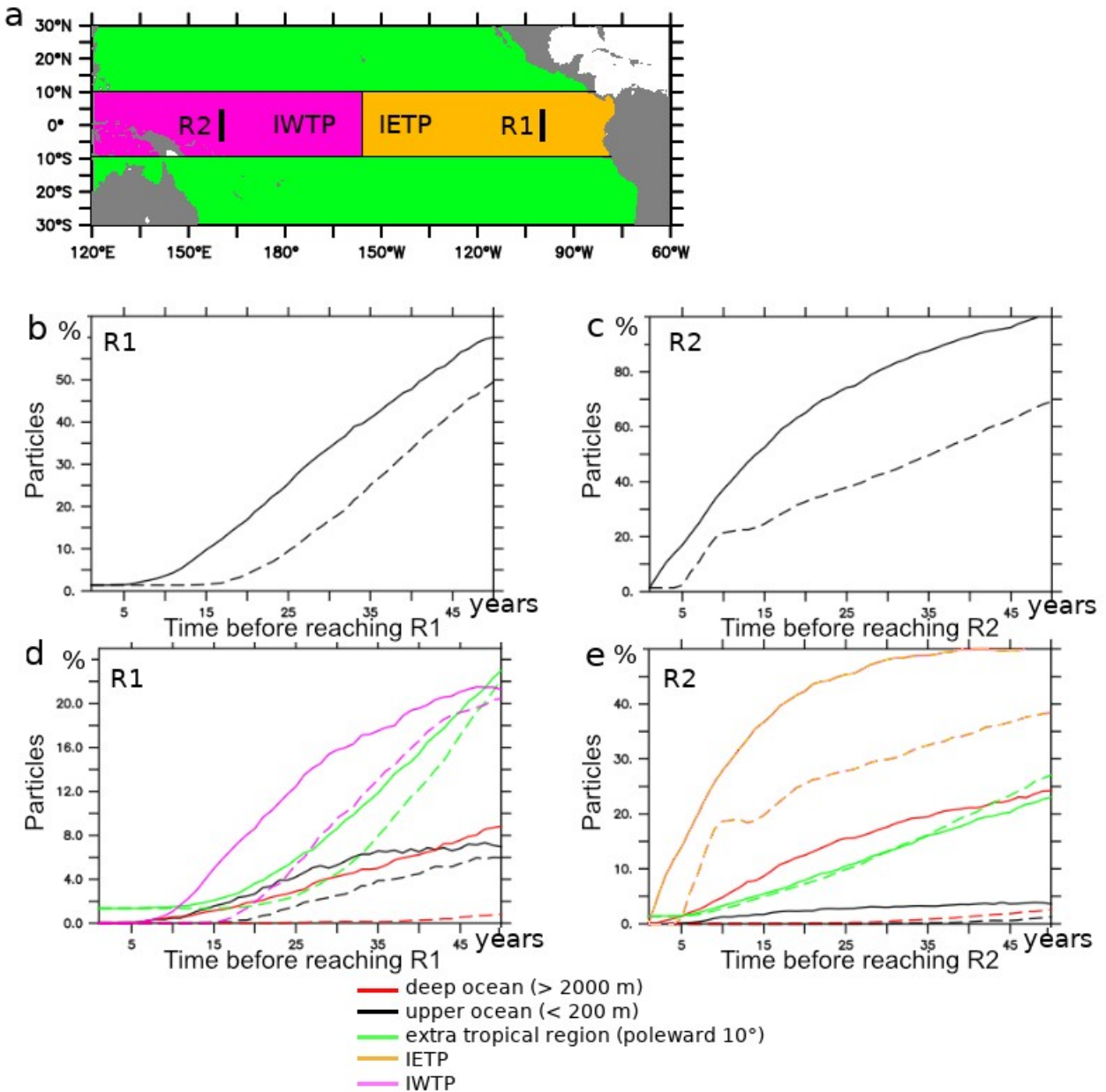


Figure 8 : a- schema summarizing the releases (R1: 100°W / 5°N-5°S / 1000 m , R2: 160°E / 5N°5S / 1000 m) location, the IETP (Intermediate Eastern Tropical Pacific), IWTP (Intermediate Western Tropical Pacific) regional extension. b- percentage of particles (release R1) originating from outside the IETP ocean region. b- percentage of particles (release R2) originating from outside the IWTP ocean region. d- percentage of particles (release R1) originating from the upper ocean (shallow than 200 m), the deeper ocean (deeper than 2000 m), subtropical regions (poleward 10°), the IWTP. e- percentage of particles (release R2) originating from the upper ocean (shallow than 200 m), the deeper ocean (deeper than 2000 m), subtropical regions (poleward 10°), the IETP.

Mean kinetic energy

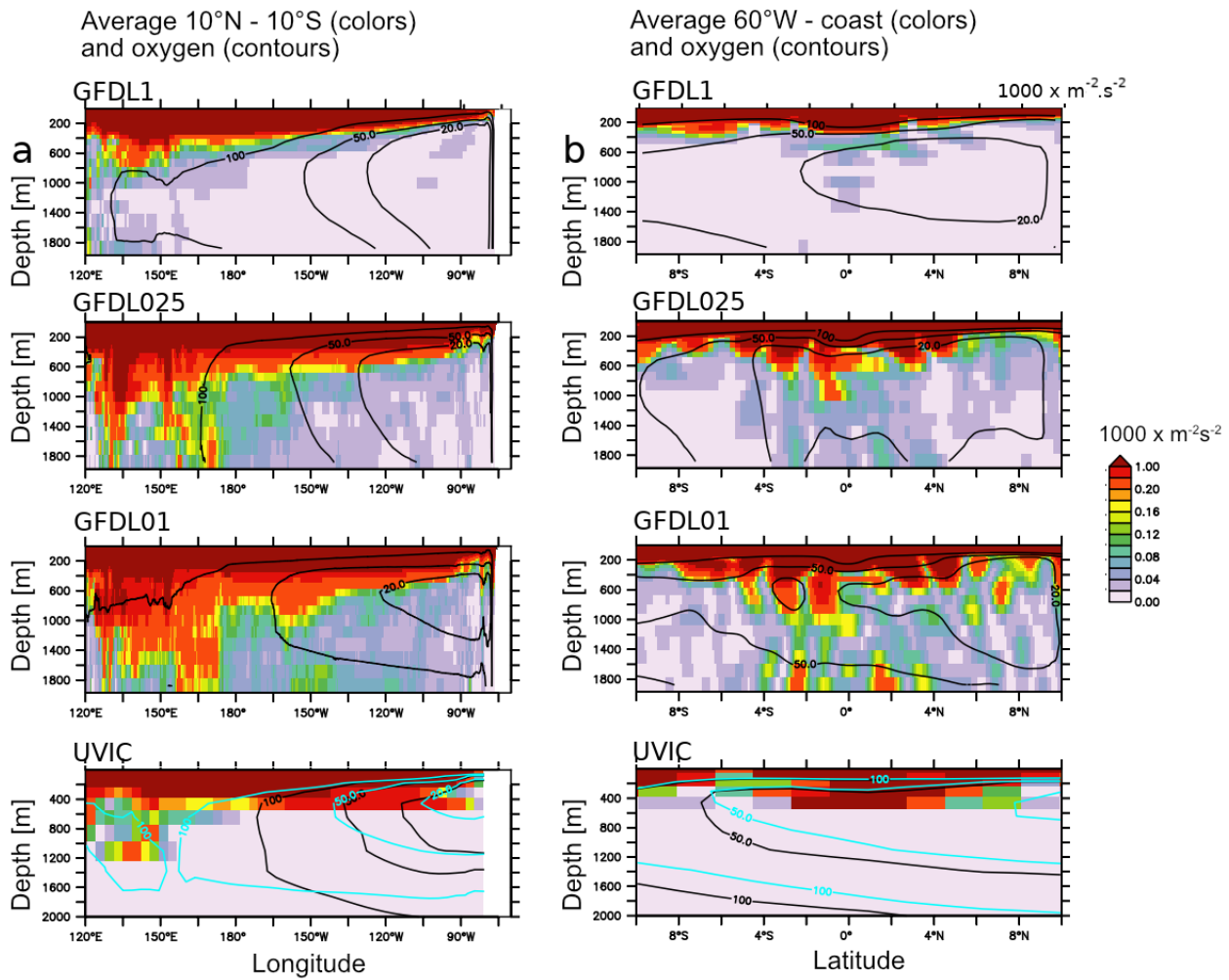


Figure 9 : a - Mean Kinetic Energy ($\text{m}^2\text{s}^{-2} \times 1000$) (average 10°N - 10°S) in GFDL01, GFDL025, GFDL01, UVIC, b - similar to a. but average 160°W - coast. Oxygen levels (mmol.m^{-3}) are displayed in black contour. The blue contour corresponds to UVIC GD13 (Getzlaff and Dietze, 2013, including an anisotropical increase of lateral diffusion at the equator)

Table 1 :

Model	Resolution	Atmosphere	Integration (years)	BGC	Model Reference (circulation)	Model Reference (BGC)	
Mean state comparison							
UVIC	2.8°	Coupled (temperature, humidity) Forced (NCEP/NCAR wind stress)	10000	UVIC-BGC	Weaver et al., 2001	Keller et al., 2012	
NEMO2	2° (0.5 eq)	Forced COREv2 “normal year”	1000	NPZD-O2	Madec et al., 2015	Kriest et al, 2010 Duteil et al., 2014	
GFDL1	1°	Coupled	190	BLING	Delworth et al, 2012, Griffies et al, 2015	Galbraith et al., 2015	
GFDL025	0.25 °	Coupled	190	BLING			
GFDL01	0.1°	Coupled	190	BLING			
Process oriented experiments							
Model	Resolution	Atmosphere	Integration (years)	BGC	Characteristics		
NEMO2 -REF -30N30S -30N30S1500M (section 2.2.1)	2° (0.5 eq)	Forced COREv2 1948-2007	60	NPZD-O2	<ul style="list-style-type: none"> - control experiment - O2 restoring to WOA at 30°N/30°S - O2 restoring to WOA at 30°N/30°S/1500m 		
NEMO05 (section 2.2.2)	0.5°	Forced COREv2 1948 - 2007	60	Tracer release	<ul style="list-style-type: none"> - Tracer initialized to 1 (O2 WOA > 150 mmol.m-3) or 0 (O2 WOA < 150 mmol.m-3) 		
NEMO01 (section 2.2.2)	0.1°	Forced COREv2 1948 – 2007	60	Tracer release			

1 **Intermediate water masses, a major supplier of oxygen for the eastern tropical Pacific ocean**

2 Olaf Duteil (oduteil@geomar.de)(1), Ivy Frenger(1), Julia Getzlaff(1)

3 (1) GEOMAR, Kiel, Germany

4

5 **Abstract**

6 It is well known that Intermediate Water Masses (IWM) are sinking in high latitudes and ventilate
7 the lower thermocline (500 – 1500 m depth). We here highlight how the IWM oxygen content and
8 the IWM pathway along the Equatorial Intermediate Current System (EICS) towards the eastern
9 tropical Pacific ocean are essential for the supply of oxygen to the lower thermocline and the
10 Oxygen Minimum Zones (OMZs). To this end, we assess here a heterogeneous subset of ocean
11 models characterized by a horizontal resolution ranging from 0.1° to 2.8°. Subtropical oxygen
12 levels in the lower thermocline, i.e., IWM are statistically correlated with tropical oxygen levels and
13 OMZs. Sensitivity simulations suggest that the oxygen biases of the subtropical IWM oxygen levels
14 contribute to oxygen biases of the tropical thermocline : an increase of the IWM oxygen by 60
15 mmol.m⁻³ results in a 10 mmol.m⁻³ increase in the tropical ocean in a timescale of 50 years. In the
16 equatorial regions, the IWM recirculates into the Equatorial Intermediate Current System (EICS).
17 By comparing tracer and particle release simulations, we show that a developed EICS increases
18 eastern tropical ventilation by 30 %. Typical climate models lack in representing crucial aspects of
19 this supply: biases in IWM properties are prominent across climate models and the EICS is
20 basically absent in models with typical resolutions of ~1°. We emphasize that these biases need to
21 be reduced in global climate models to allow reliable projections of OMZs in a changing climate.

22

23 **1. Introduction**

24 Oxygen levels in the ocean are characterized by high values in the high latitudes and the subtropical
25 gyres, while concentrations decrease to close to zero in the tropical oceans in the Oxygen Minimum
26 Zones (OMZs). While OMZs are natural features, climate change is potentially responsible for their
27 expansion (Breitburg et al., 2018), leading to a reshaping of the ecosystems and a potential loss of
28 biodiversity. In order to perform robust projections there is a need to better understand the processes
29 at play that are responsible for the supply of oxygen to the OMZ. We focus here on the Pacific
30 ocean, where the largest OMZs are located (Karstensen et al., 2008; Paulmier and Ruiz-Pino. 2009)

31

32 Oxygen rich waters are supplied into the ocean by subduction processes (Karstensen et al., 2008).

33 Oxygen solubility increases with lower temperatures, thus waters formed in the Southern Ocean
34 and in the North Pacific are characterized by particularly high oxygen values. In particular, the

35 Antarctic Intermediate Water (AAIW) (Molinelli, 1981) ventilates large areas of the lower
36 thermocline of the Pacific Ocean (Sloyan and Rintoul., 2001) and is characterized by oxygen values
37 larger than 300 mmol.m^{-3} at subduction time (Russel and Dickson, 2003). The oxygenated core of
38 the AAIW in the tropical Pacific is located at about 500-1200 m depth at 40°S (Russell and
39 Dickson, 2003) and with this at a depth directly below the depth of the OMZs in the eastern Pacific;
40 the Pacific AAIW mixes down to 2000 m depth with the Pacific Deep Water (PDW) as determined
41 by the OMP (Optimum Multiparameter) analysis (Pardo et al., 2012; Carrasco et al., 2017). The
42 oxygen rich ($> 200 \text{ mmol.m}^{-3}$ at 40°S) AAIW spreads from its formation side in the Southern Ocean
43 to the subtropical regions ; conversely the oxygen poor PDW (below 150 mmol.m^{-3}), extends till
44 3000m depth and recirculates poleward (Koshlyakov and Tarakanov, 2003). The northern part of
45 the Pacific basin is characterized by the North Pacific Intermediate Water (NPIW) (Talley, 1993)
46 confined to the northern Pacific conversely to the AAIW, which spreads far northward as its
47 signature reaches 15°N (Qu and Lindstrom., 2004). AAIW, NPIW and the upper part of the PDW
48 are oxygenated water masses occupying the lower thermocline between 500 and 1500 m depth. We
49 will refer to these waters as Intermediate Water Masses (IWM) in the following.

50

51 In the subtropics, the IWM (more particularly the AAIW) circulates into the intermediate flow of
52 the South Equatorial Current and the New Guinea Coastal Undercurrent (Qu and Lindstrom, 2004)
53 where it retroflects in the zonal equatorial flows of the Southern Intermediate Countercurrent
54 (SICC) and Northern Equatorial Intermediate Current (NEIC) within about $\pm 2^\circ$ off the equator
55 (Zenk et al., 2005; Kawabe et al., 2010) (Fig 1). These currents are part of the Equatorial
56 Intermediate Current System (EICS) constituted by a complex system of narrow jets extending
57 below 500 m in the lower thermocline (Firing, 1987; Ascani et al., 2010; Marin et al. 2010; Cravatte
58 et al., 2012, 2017; Menesguen et al., 2019). While the existence of this complex jet system has been
59 shown to exist in particular using argo floats displacements (Cravatte et al., 2017) the spatial
60 structure and variability of the jets are still largely unknown. In addition, there is little knowledge
61 about their role in transporting properties such as oxygen.

62

63 The simulation of the supply of oxygen to the eastern tropical Pacific is a difficult task as it depends
64 on the realistic simulation of the IWM properties (in particular the oxygen content) and the IWM
65 pathway (through the EICS). —It is known that current climate models, in particular CMIP5
66 (Coupled Model Intercomparison Project phase 5) models, have deficiencies in correctly
67 representing the IWM, and in particular the AAIW. They generally display too shallow and thin
68 IWM, with a limited equatorward extension compared to observations (Sloyan and Kamenkovich,

69 | 2007; Sallee et al., 2013; Meijers, 2014; Cabre et al., 2015; Zhu et al., 2018 for the south Atlantic
70 | ocean). Discrepancies in the simulated properties of IWM compared to observations are due to a
71 | combination of many errors in the climate models, including simulation of wind and buoyancy
72 | forcing, inadequate representation of subgrid-scale mixing processes in the Southern Ocean, and
73 | midlatitude diapycnal mixing parameterizations (Sloyan and Kamakovich, 2007; Zhu et al., 2018).
74 | In addition, the representation of the EICS is lacking in coarse resolution models (Dietze and
75 | Loepfien, 2013; Getzlaff and Dietze, 2013). Higher resolution (0.25° , $1/12^\circ$) configurations partly
76 | resolve the EICS but with a smaller amplitude than observed (Eden and Dengler, 2008; Ascari et
77 | al., 2015). The mechanisms forcing the EICS are complex and still under debate (see the review by
78 | Menesguen et al., 2019).

79 | -

80 | In this study we focus on the impact of IWM (and of the deficiencies in the representation of their
81 | properties and transport) on the oxygen content in the eastern tropical Pacific in a set of model
82 | simulations. Section 2 gives an overview of all models that we used as well as of the sensitivity
83 | simulations. Next, we assess to which extent the IWM modulate (or drive) the oxygen levels in the
84 | eastern tropical (20°S – 20°N ; [160°W-coast](#)) Pacific ocean in this set of models. The role of the
85 | IWM depends i) on the oxygen content of the IWM in the lower thermocline of the subtropical
86 | regions (section 3) and ii) on the zonal recirculation of the oxygen by the EICS toward the [eastern](#)
87 | part of the basin (section 4). We conclude in section 5.

88

89 | **2. Analyzed models and experiments**

90 | **2.1 Mean state**

91 | We analyze the mean state of the oxygen fields, OMZ, EICS of the following model experiments
92 | (see Table 1), which previously have been used in recent studies focusing on the understanding of
93 | the tropical oxygen levels mean state or variability:

94 | - [thea](#) NEMO (Nucleus for European Modelling of the Ocean) [model configuration \(Madec et al.,](#)
95 | [2017\)](#) with a resolution of 2° , refined meridionally to 0.5° in the equatorial region [\(NEMO2\)](#)
96 | [\(NEMO2 configuration\)](#). The circulation model is coupled to a simple NPZD (Nutrient
97 | Phytoplankton Zooplankton Detritus) biogeochemical model that comprises 6 compartments (e.g
98 | used in Duteil et al., 2018; Duteil, 2019). The simulation has been forced by climatological forcings
99 | based on the Coordinated Reference Experiments (CORE) v2 reanalysis (1948-2007) (Large and
100 | Yeager, 2009) and integrated for 1000 years.

101 | - the UVIC (University of Victoria) model (e.g used in Getzlaff et al., 2016; Oschlies et al., 2017),
102 | an earth System Model (ESM) that has a horizontal resolution of 1.8° latitude x 3.6° longitude. The

103 experiment has been integrated for 10000 years. The biogeochemical model is a NPZD-type model
104 of intermediate complexity that describes the full carbon cycle (see Keller [et al.](#), [Keller](#) 2012 for a
105 detailed description). This model is forced by monthly climatological NCAR/NCEP wind stress
106 fields.

107 - the GFDL (Geophysical Fluid Dynamics Laboratory) CM2-0 suite (Delworth [et al.](#), 2012; Griffies
108 [et al.](#), 2015, Dufour [et al.](#), 2015): the suite is based on the GFDL global climate model and includes
109 a fully coupled atmosphere with a resolution of approximately 50 km. It consists of three
110 configurations that differ in their ocean horizontal resolutions: GFDL1 with a nominal 1°
111 resolution, GFDL025 with a nominal 0.25° and GFDL01 with a nominal 0.1° resolution (e.g used in
112 Frenger [et al.](#), 2018 and Busecke [et al.](#), 2019 for studies on ocean oxygen). [The climate models are](#)
113 [forced with preindustrial atmospheric pCO2 concentrations](#). At simulation year 48, the simplified
114 ocean biogeochemistry model miniBLING is coupled to the models, with three prognostic tracers,
115 phosphate, dissolved inorganic carbon and oxygen (Galbraith [et al.](#), 2015). Due to the high
116 resolution of GFDL01, the integration time is limited. We here analyze simulation years 186 to 190.
117 [All the models \(NEMO2, UVIC, GFDL suite\) are forced using preindustrial atmospheric pCO2](#)
118 [concentrations](#).

119 [The heterogeneity of the configurations that we analyze permits to determine whether the simulated](#)
120 [oxygen distributions of the models display systematic biases or are strongly configuration](#)
121 [dependent \(e.g dependent on resolution\). Differences in model resolution but also in atmosphere](#)
122 [forcings or spinup duration strongly impact oxygen distribution \(see Annex A\). However, the](#)
123 [heterogeneity of the configurations that we analyze permits to determine whether the simulated](#)
124 [oxygen distributions display systematic biases / similar patterns.](#)

125
126 [The mean states of the oxygen distributions are discussed below in section 3.1 “IWM Oxygen levels](#)
127 [in models”.](#)

128 -

129
130 2.2 Sensitivity simulations

131 In order to disentangle the different processes at play we perform two different sets of sensitivity
132 simulations [using the ewith one of the models](#), [NEMO model engine](#). NEMO allows to test effects
133 of increasing the ocean resolution and to integrate the model over a relatively long time span. All
134 sensitivity experiments are integrated for [60 more than 50](#) years (1948 to 2007) using the CORE

135 (Coordinated Ocean-Ice Reference Experiments) v2 interannual (Large and Yeager, 2009) forcings.
136 This time scale permits the recirculation from the interior subtropical regions to the tropical area (as
137 suggested in the model study by SenGupta and England, 2007).

138

139 | 2.2.1 Oxygen forcing restoring to observations in the subtropical regions

140 In the first set of experiments the focus is on the role of the lower thermocline oxygen content for
141 the ventilation of the eastern equatorial Pacific. We use NEMO2, the oceanic component of the
142 IPSL-CM5A (Mignot et al., 2013), that is part of CMIP5. NEMO2 shows mid-latitudes oxygen
143 biases consistent with CMIP5 models. We compare three experiments :

144 - NEMO2-REF: the experiment is integrated from 1948 to 2007 starting from the spinup state
145 described in 2.1.

146 | - NEMO2-30S30NDEG: the oxygen boundaries are forced restored to observed oxygen
147 concentrations (WOA) at the boundaries 30°N and 30°S : the mid-latitude supply of oxygen by the
148 IWM is therefore correctly represented.

149 | - NEMO2-30S30NDEG1500M: same as NEMO2-30S30NDEG ; in addition oxygen is also forced
150 restored at the depth interface of 1500m, mimicking a correct oxygen state of the deeper water
151 masses (lower part of the AAIW, upper part of the PDW)

152

153 We focus with the above three experiments on the transport of IWM oxygen levels to the tropical
154 ocean and the OMZs. The respiration rate (oxygen consumption) is identical in NEMO2-REF,
155 NEMO2-30S30NDEG and NEMO2-30S30NDEG1500M in order to avoid compensating effects
156 between supply and respiration that depends on biogeochemical parameterizations (e.g Duteil et al.,
157 2012). We aim to avoid such compensating effects to ease interpretation and be able to focus on the
158 role of physical transport. The sensitivity of tropical IWM oxygen to subtropical and deep oxygen
159 levels is discussed in section 3.2

160

161 | 2.2.2 Conservative Tracer Release in oxygenated waters

162 In a second set of experiments, we performed tracer release experiments in a coarse 0.5°
163 (NEMO05) and high resolution 0.1° (NEMO01) configurations of the NEMO model engine (Table
164 1) to examine the transport of oxygenated IWM from the subtropical regions into the oxygen
165 deficient tropics. NEMO01 is a configuration based on NEMO05 and where a 0.1° two-ways nest
166 has been embedded in the whole Pacific Ocean, from 49°S to 31°N (Czeschel et al, 2011). In these
167 experiments, we initialized the regions with climatological (WOA) oxygen levels greater than 150
168 mmol.m⁻³ with a value of 1 (and 0 when oxygen is lower than 150 mmol.m⁻³). In the model

169 simulations, the tracer is subject to the same physical processes as other physical and
170 biogeochemical tracers, i.e. advection and diffusion but it does not have any sources and sinks. The
171 experiments have been integrated for 60 years (1948 – 2007) using realistic atmosphere forcing
172 (COREv2). NEMO05 and NEMO01 display a similar upper ocean circulation (Fig 5) but NEMO05
173 does not simulate a developed EICS contrary to NEMO01.

174

175 In order to complement the tracer experiment we performed Lagrangian particle releases.
176 Lagrangian particles allow to trace the pathways of water parcels due to the resolved currents, and
177 to track the origin and fate of water parcels. They are not affected by subgrid scale mixing
178 processes. The particles are advected offline with 5-days daily means of the NEMO05 and
179 NEMO01 currents. The NEMO01 circulation fields have been interpolated on the NEMO05 grid in
180 order to allow a comparison of the large scale advective patterns between NEMO01 and NEMO05.
181 We used the ARIANE tool (Blanke and Raynaud, 1997). A first particle release has been performed
182 in the eastern tropical OMZ at 100°W in the tropical region between 5°S - 5°N, a second release has
183 been performed in the western part of the basin at 160°E. The particles have been released in the
184 lower thermocline at 1000 m and integrated backward in time from 2007 to 1948 in order to
185 determine their pathways and their location of origin. We released 120 particles every 5 days during
186 the last year of the experiment, for a total of 8760 particles. [The transport by the EICS is discussed](#)
187 [in section 4.2 \(tracers levels and Lagrangian pathways\).](#)

188

189 **3. Intermediate water properties and oxygen content**

190 **3.1. IWM Oxygen levels in models**

191

192 The IWM subducted in mid/high latitudes are highly oxygenated waters. As part of the deficient
193 representation of IWM, the subducted “oxygen tongue” (oxygen values up to 240 mmol.m⁻³) is not
194 reproduced in most of the models part of CMIP5 (Fig 8 from Cabre et al., 2015, Fig 4 from Takano
195 et al., 2018) and in the models analyzed here (Fig 2a), with biases of about 20-60 mmol.m⁻³
196 (NEMO2, GFDL1, GFDL025, GFDL01). UVIC, a coarse resolution model, shows oxygenated
197 waters in the lower thermocline at mid latitudes (30°S-50°S); the oxygenation however arises due
198 to a too large vertical diffusion from the mixed layer rather than by an accurate representation of the
199 water masses.

200

201 GFDL01, even though still biased low, presents larger oxygen values than the coarser resolution
202 models GFDL1, GFDL025 and NEMO2. A possible explanation is a better representation of the
203 water masses and in particular the AAIW in eddy-resolving models (Lackhar et al., 2009).

204

205 ~~-~~The IWM oxygen maximum is apparent at 30°S throughout the lower thermocline (600 – 1000 m)
206 in observations (Fig 2b), consistent with the circulation of IWM with the gyre from the mid/high
207 latitude formation regions towards the northwest in subtropical latitudes, and followed by a
208 deflection of the waters in the tropics towards the eastern basin. This oxygen peak is missing in all
209 the models analyzed here.

210

211 Consistent with the low oxygen bias of models at subtropical latitudes (Fig 2b), models also feature
212 a bias in the tropical ocean (20°S-20°N) by 20 – 50 mmol.m⁻³ (Fig 2a, Fig 2c) at intermediate depths
213 in the eastern part of the basin (similarly to CMIP5 models, as shown by Cabre et al., 2015). The
214 basin zonal average of the mean oxygen level in the lower thermocline (layer 500 - 1500) m at 30°S
215 and in the eastern part of the basin (average 20°S – 20°N, 160°W-coast; 500-1500 m) are positively
216 correlated (Pearson correlation coefficient R=0.73) (Fig 2d, Annex A), suggesting a large role of the
217 IWM in controlling the oxygen levels in the tropical oceans.

218

219 The models presenting the poorest oxygenated water at 30°S display the largest volume of OMZs
220 (GFDL025 and GFDL1), though the negative correlation (Pearson correlation coefficient R=-0.52)
221 is less pronounced between the volume of the OMZs and the mean oxygen levels in the layer 500 -
222 1500 m at 30°S (Fig 2e). Reasons of this weaker correlation are due to the OMZs being a result of
223 several processes next to oxygen supply by IWM, e.g, vertical mixing with other water masses
224 (Duteil et al., 2011), isopycnal mixing in the upper thermocline (Gnanadesikan et al., 2013; Bahl et
225 al., 2019), supply by the upper thermocline circulation (Shigemitsu et al., 2017; Busecke et al.,
226 2019). A correlation, even weak, suggests a major role of the IWM in regulating the OMZ volume.

227

228 In order to better understand the role of IWM entering the subtropical domain from higher latitudes
229 for the oxygen levels in the eastern tropical Pacific Ocean, we perform sensitivity experiments (see
230 2.2.1) in the following.

231

232 3.2 Sensitivity of tropical IWM oxygen to subtropical and deep oxygen levels

233 3.2.1 Oxygen levels in the lower thermocline

234 The difference of the experiments NEMO2-30S30NDEG – NEMO2-REF (average 1997-2007) (Fig
235 3c,d) allows to quantify the effect of model biases of IWM at mid latitudes (30°N/30°S). As we
236 restore oxygen to observed levels at 30°S/°N (see 2.2.1), the difference shows a large anomaly in
237 oxygen levels at 30°S (more than 50 mmol.m⁻³) at lower thermocline level (500 – 1500 m)
238 corresponding to the missing deep oxygen maximum (Fig 3). The northern negative anomaly results
239 from a deficient representation of the north Pacific OMZ, i.e., modeled oxygen is too high for
240 NPIW. The northern low and southern high anomalies spread towards the tropics at intermediate
241 depth. A fraction -of the positive oxygen anomaly recirculates at upper thermocline level due to a
242 combination of upwelling and zonal advection by the tropical current system (for instance the EUC
243 at thermocline level is a major supplier of oxygen as shown in observations by Stramma et al., 2010
244 and in ocean models by Duteil et al., 2014, Busecke et al., 2019).

245

246 The difference NEMO2-30S30NDEG1500M – NEMO2-30S30NDEG (Fig 3e,f-hf) shows a deep
247 positive anomaly in oxygen, as oxygen levels are lower than in observations by 30-40 mmol.m⁻³ in
248 the eastern tropical regions. This anomaly is partially transported into the lower thermocline (500 -
249 1500 m). It shows that a proper representation of the deep oxygen level (> 1500 m) is important for
250 a realistic representation of the lower thermocline and OMZs. Causes of the oxygen bias of the
251 deeper water masses are beyond the scope of this study but may be associated with regional
252 (tropical) issues, such as an improper parameterization of respiration (e.g a too deep
253 remineralisation) (Kriest et al., 2010), or a misrepresentation of deeper water masses.

254

255 3.2.2 Oxygen budget and processes-

256 To assess the processes that drive the oxygen content of the (sub)tropical lower thermocline, we
257 analyzed the oxygen budget in NEMO2-REF and NEMO2-30S30NDEG. The budget is computed
258 calculated as an average between 500 and 1500m and shown in Fig 3g and Fig.4.

259

260 The oxygen budget is :

$$\frac{\delta O_2}{\delta t} = Adv_x + Adv_y + Adv_z + Diff_{Dia} + Diff_{Iso} + SMS$$

262 where Adv_x, Adv_y, Adv_z , are respectively the zonal, meridional and vertical advection terms, $Diff_{dia}$
263 and $Diff_{iso}$ are the diapycnal and isopycnal diffusion terms. SMS (Source Minus Sink) is the
264 biogeochemical component (i.e respiration below the euphotic zone)

265

266 In NEMO2-REF, the physical oxygen supply is balanced by the respiration. The oxygen supply in
267 the model is divided into advection, i.e., oxygen transport associated with volume transport, and
268 isopycnal diffusion, i.e., subgrid scale mixing processes that homogenize oxygen gradients (Fig 4a).
269 Diapycnal diffusion is comparatively small and can be neglected. The lower branches of the
270 subtropical gyres transport the oxygen from the eastern to the western part of the basin (Fig 4a,b).
271 Downwellings from the oxygen-rich mixed upper layer supply the interior of the subtropical gyres
272 (Fig 4e). At the equator, the EICS transport westward oxygen-poor water originating in the eastern
273 side of the basin (Fig 4a). Concomitantly, the meridional advection term transports oxygen
274 originating from the subtropics in the tropical regions (Fig 4b), which is upwelled (Fig 4e).
275 Isopycnal diffusion transfers oxygen from the oxygen-rich gyres to the poor oxygenated regions
276 (Fig 4d).

277

278 The anomalies generated at 30°S and 30°N by the restoring experiment generate a disbalance
279 between respiration (which remains identical in NEMO2-REF and NEMO2-30S30NDEG) and
280 supply. This disbalance is most apparent in the tropics by an increase (south) or decrease (north) of
281 isopycnal diffusion (Fig 4g, Fig 3gh, Fig 4b). Changes in the advective terms can be found along
282 the equator: as the vertical gradient of oxygen decrease (the intermediate ocean being more
283 oxygenated), the vertical supply from the upper ocean decreases in the south (increases in the north)
284 subtropical gyre and decreases at the equator (Fig 4bg). The meridional oxygen gradient between
285 the southern subtropical gyre and the equator strengthens, and so the meridional transport from the
286 subtropics to the equator, partly by the western boundary currents (Fig 4f). The changes in zonal
287 transport are comparatively small (Fig 4e). The total advective term does not present show
288 significant change however (Fig 4g).

289

290 In the experiment NEMO2-30S30NDEG1500, in complement to the isopycnal propagation of the
291 subtropical anomaly, the deep (> 1500 m) oxygen anomaly is upwelled in the eastern equatorial
292 (500 – 1500 m) part of the basin (see Fig 3g4i) showing a large increase in advective terms, mostly
293 due to an increase in vertical advection, consistent with the analysis by Duteil (2019) who showed
294 that vertical advection is the dominant process to supply oxygen from the lower to the upper
295 thermocline in the equatorial eastern Pacific Ocean in a similar NEMO2 configuration.

296

297 This simple set of experiment shows that in climate models oxygen in the lower thermocline (500 –
298 1500 m) ocean are partially controlled by properties of IWM that enter the tropics from higher
299 latitudes. This presumably applies to other (biogeochemical) tracers. IWM oxygen propagates

300 equatorward mostly by small scale isopycnal processes and the western boundary currents. Further,
301 upwelling in the tropics from deeper ocean layers (Pacific Deep Water, partially mixed with the
302 lower IWM) play an important role. Our budget analysis highlighted the importance of advective
303 processes in the equatorial region in the lower thermocline which we will examine more closely in
304 the following.

305

306 **4. Equatorial intermediate current system and oxygen transport**

307 4.1 Structure of the currents in the upper 2000 m in observations and models

308 The current structure of the models analyzed in this study (see section 2.1, Table 1) is shown in Fig.
309 5. In the upper mixed layer, the broad westward drifting South and North Equatorial Currents (SEC,
310 NEC) characterize the equatorial side of subtropical gyres. In the thermocline, the eastward flowing
311 equatorial undercurrent (EUC), flanked by the westward flowing south and north counter currents
312 are present in all models. This upper current structure is well reproduced (i.e the spatial structure
313 and intensity are consistent with observations) across the different models (see 2.1 “Model
314 analyzed”) compared to observations. Previous studies already discussed –the upper thermocline
315 current structure in the GFDL models suite (Busecke et al., 2019), NEMO2 and NEMO5 (e.g
316 Izumo, 2005, Lübecke et al., 2008), UVIC (Loeptien and Dietze, 2013); the upper thermocline will
317 not be further discussed in this study.

318

319 At intermediate depth, in the observations, a relatively strong (about 0.1 ms^{-1}) westward flowing
320 Equatorial Intermediate Current (EIC) is present below the EUC at about 400-600 m depth (Marin
321 et al., 2010). A complex structure of narrow and vertically alternating jets every 200 m, so-called
322 Equatorial Deep Jets (EDJ), extends below the EIC till 2000 m (Firing, 1987; Cravatte et al., 2012).
323 Laterally to the EIC, in the upper thermocline, the Low Latitude Subsurface Countercurrents
324 (LLSC) are observed. They include the North and South Subsurface Counter Currents (NSCC and
325 SSCC), located around $5^\circ\text{N}/5^\circ\text{S}$, and a series of jets between $5^\circ\text{N}/\text{S}$ and $15^\circ\text{N}/\text{S}$ (in particular the
326 Tsushima jets in the southern hemisphere, described by Rowe et al., 2000). Below the LLSCs, the
327 Low Latitude Intermediate Currents (LLICs) include the a series of westward and eastward zonal
328 jets (500–1500-m depth range) alternating meridionally from 3°S to 3°N ; the North and South
329 Intermediate Countercurrents (NICC and SICC) flow eastward at $1.5^\circ\text{--}2^\circ$ on both flanks of the
330 lower EIC. The North and South Equatorial Intermediate Currents (NEIC and SEIC) flow westward
331 at about 3° (Firing, 1987). A detailed schematic view of the tropical intermediate circulation is
332 shown in a recent review by Menesguen et al. (2019) and in Fig 1.

333

334 In coarse resolution models, the intermediate current system is not developed and sluggish (even
335 missing in UVIC and GFDL1). NEMO2 and NEMO05 display a “primitive” EICS as the LLSCs
336 are not represented. High resolution models (GFDL025, GFDL01, NEMO01) display a more
337 realistic picture, even if the mean velocity is still weaker than in observations (smaller than 5 cm.s⁻¹),
338 where it reaches more than 10 cm⁻¹ at 1000 m (Ascani et al., 2010; Cravatte et al., 2017). An
339 interesting feature is that the jets are broader and faster in NEMO01 than in GFDL01. Possible
340 causes include ~~a~~ different wind forcing, mixing strength or topographic features as all these
341 processes play a role in forcing the intermediate jets (see the review by Menesguen et al., 2019).
342 The intermediate currents are less consistent vertically in NEMO01 than in GFDL01, due to their
343 large temporal variability in NEMO01. A strong seasonal and interannual variability of the EICS
344 has been observed that displays varying amplitudes and somewhat positions of the main
345 currents/jets (Firing, 1998; Gouriou et al., 2006; Cravatte et al., 2017). A clear observational picture
346 of the EICS variability is however not yet available. Outside the tropics (in particular south of
347 15°S), the interior velocity pattern is similar in coarse and high resolution models, suggesting a
348 similar equatorward current transport at intermediate depth in the subtropics, in for instance
349 NEMO05 and NEMO01.

350

351 4.2 Transport by the EICS

352 4.2.1 Tracer spreading towards the eastern tropical Pacific

353 We released a conservative tracer in the subtropical domain in well oxygenated waters (see 2.2.2) in
354 a coarse (NEMO05) and a high resolution configuration (NEMO01). The tracer does not have
355 sources or sinks and is advected and mixed as any other model tracer and allows to assess the
356 spreading of tracer (such as oxygen) from oxygenated waters into the oxygen deficient eastern
357 tropical Pacific.

358

359 The ventilation by the oxygen rich waters, and in particular the IWM, is illustrated by the tropical
360 tracer concentration after 50 years (Fig 6a-e) of integration (mean 2002-2007). Concentrations
361 decrease from the release location to the northern part of the basin, where the lowest values (below
362 0.1) are located in NEMO05 and NEMO01. The 0.1 isoline is however located close to the equator
363 in NEMO05 while it is found around 7°N in NEMO01. This feature is associated with a pronounced
364 tongue of high tracer concentration (> 0.2) between 5°N and 5°S in NEMO01. Such a tongue is
365 absent in NEMO05. The enhanced tracer concentration in the equatorial region suggests a stronger
366 equatorial ventilation in NEMO01.

367

368 The preferential pathways of transport are highlighted by the determination of the transit time it
369 takes for the tracer to spread from the oxygen rich regions to the tropical regions. We define a
370 threshold called t10% when the tracer reaches a concentration of 0.1 (Fig 6**bd-f**) (similar to the
371 approach of SenGupta and England, 2007). t10% highlights a faster ventilation of the equatorial
372 regions in NEMO01 compared to NEMO05, as t10% displays maximum value of 10 (western part)
373 to 30 years (eastern part) between 5°N/5°S in NEMO01 compared to 30 years to more than 50 years
374 in NEMO05. The southern “shadow zone” is well individualized in NEMO01 compared to
375 NEMO05 as the oxygen levels are high in the equator in NEMO01, suggesting a strong transport by
376 the EICS. While t10% increases linearly at intermediate depth at 100°W in NEMO05 from 20°S to
377 the equator, suggesting a slow isopycnal propagation (consistent with the experiments performed
378 using NEMO2 in part 3.2), the tracer accumulation is faster in the equatorial regions than in the
379 mid-latitudes in NEMO01, suggesting a large role of advective transport, faster than a transport by
380 diffusive processes.

381

382 4.2.2 Equatorial lower thermocline water mass origin

383 Lagrangian Particles (see 2.2.3) allow us to understand the origin of the waters in the lower
384 thermocline. They also allow to disentangle the transport of the resolved currents of the EICS
385 (advection) from subgrid scale mixing processes, i.e. to assess the processes responsible for the
386 equatorial ventilation. Two releases [R1](#) and [R2](#) have been performed in the eastern and western part
387 of the basin in order to assess the equatorial circulation in NEMO05 and NEMO01.

388

389 The ~~particles of the first release~~ [R1](#) ~~in the eastern tropical Pacific (100°W, 5°N-5°S, at 1000 m~~
390 ~~depth where the EICS are located)~~ ~~origin from is- included in the larger~~ intermediate eastern tropical
391 ~~pacific (IETP) ocean region (160°W – coast / 10°N-10°S / 200 – 2000 m).~~ [The particles originate](#)
392 ~~close to the region of release (IETP);~~ in 60 % of the cases in NEMO05 and 50 % of the cases in
393 NEMO01, at a time scale of 50 years (Fig 7a-[e](#) and 8**ba**). In NEMO05, after 50 years, the particles
394 originating outside the IETP come either from the upper (0 – 200 m) ocean (5 %), deep (> 2000 m)
395 ocean (1%), higher (> 10°) latitudes (23 %), western (west of 160°W) part of the basin (21 %) (Fig
396 8**de**). The largest difference between NEMO05 and NEMO01 is the much larger amount of particles
397 originating from the deep ocean in NEMO01 (8 % in NEMO01), suggesting the presence of vertical
398 recirculation cells at intermediate depths. The advection processes are also considerably faster in
399 NEMO01, in particular the zonal advective ones. The relative difference between NEMO05 and
400 NEMO1 is particularly strong 15 years after the release (approximately corresponding to the t10%
401 at 1000 m at the equator in NEMO01), as already 10 % of the particles originate outside the IETP,

402 in regions where the oxygen levels are high, in NEMO01 while this fraction is close to 0 in
403 NEMO05.

404

405 The particles location of the second release R2 (160°E, 5°N-5°S, 1000 m depth) are originally is
406 included located in the intermediate western tropical pacific Ocean (IWTP) ocean region (160°W –
407 coast / 10°N-10°S / 200 – 2000 m) (Fig 7be-f). After 50 years, all the particles originate outside of
408 the IWTP is box in NEMO01 (Fig 8cb) (50 % originate in the eastern basin, 23 % in the deep
409 ocean, 24 % outside the equatorial band, 3 % in the upper 200 m) (Fig 8ed) while only 70 % of the
410 particles originate outside the IWTP in NEMO05 (39 % in the eastern basin, 27 % outside the
411 equatorial band, 2 % in the deep ocean and 2 % in the upper ocean).-

412

413 The Lagrangian particle experiments results point to a generally stronger ventilation at intermediate
414 depth in NEMO01 due to the EICS, which reinforcess the connectionss between western / eastern part
415 of the basin and thermocline / deep ocean.

416

417 | 4.3 Equatorial oxygen levels in models:

418 Our analyses above permit to better understand the distribution of the oxygen levels at the equator
419 in a suite of models characterized by an increasing resolution, such as the GFDL model suite. The
420 striking difference between GFDL01 and GFDL025 / GFDL1 are the high oxygen levels in the
421 eastern part of the ocean below 1000 m in GFDL01 compared to GFDL025/GFDL1 (Fig 2). The
422 oxygen levels are also more homogeneous zonally in GFDL01, with a weaker east/west gradient,
423 consistent with the tracer experiment that we performed in 4.2. The oxygen distribution fits with the
424 mean kinetic energy of the intermediate currents below 1000 m (Fig 9a), especially in the eastern
425 part of the basin (Fig 9b). Resolving the EICS results in a similar distribution results as what
426 Getzlaff and Dietze (2013) achievedd with a simple parameterization of the EICS (Fig 9a). To
427 compensate for the “missing” EICS in coarse resolution models, they enhanced anisotropically the
428 lateral diffusivity in the equatorial region. Implementing this approach tends to homogeneize
429 oxygen levels zonally, with an increase of the mean levels by 30-50 mmol.m⁻³ in the eastern basin
430 and a decrease of oxygen concentrations in the western basin.

431

432 A possibly not intuitive feature is that the oxygen levels are relatively similar in GFDL025 and
433 GFDL1, while the current system is relatively similar in GFDL025 and GFDL01 (see Fig 5 and Fig
434 9). An explanation lies in the relatively small net balance between large fluxes of respiration and
435 oxygen supply (Duteil et al., 2014). If the supply is slightly higher compared to the consumption by

436 respiration, it will lead to an increase of oxygen concentration. If it is slightly lower, the oxygen
437 levels will decrease. A small difference in supply (e.g slightly weaker currents) may therefore lead
438 to a large difference in oxygen levels when integrated over decades. For this reason, the impact of
439 the EICS is more visible below 1000 m as the respiration decreases following a power-law with
440 depth (Martin et al., 1987) and is therefore easier to offset even by a moderate oxygen supply.

441

442 | **5. Summary and conclusions**

443 Intermediate water masses (IWM) are subducted in the Southern Ocean and transported
444 equatorward to the tropics by isopycnal processes (Sloyan and Kamenkovich, 2007; Sallee et al.,
445 2013; Meijers, 2014). At lower latitudes they recirculate into the lower thermocline of the tropical
446 regions at 500 - 1500 m and into the EICS (Zenk et al., 2005; Marin et al., 2010; Cravatte et al.,
447 2012; 2017; Ascani et al., 2015; Menesguen et al., 2019) (see schema Fig 1). We show here that the
448 representation of this ventilation pathway is important to take into account when assessing tropical
449 oxygen levels and the extent of the OMZ in coupled biogeochemical circulation or climate models.
450 Particularly, we highlight two critical, yet typical, biases that hamper the correct representation of
451 the tropical oxygen levels.

452

453 | 5.1 Subducted IWM properties and tropical oxygen

454 First, the current generation of climate models, such as the CMIP5 models, show large deficiencies
455 in simulating IWM. Along with an unrealistic representation of IWM volume and properties
456 when the waters enter the subtropics, the models also lack the observed prominent oxygen
457 maximum associated with IWM. Restoring oxygen levels to observed concentrations at
458 30°S/30°N and at 1500 m depth in a coarse resolution model, comparable to CMIP5 climate models
459 in terms of resolution and oxygen bias, shows a significant impact on the lower thermocline (500 –
460 1500 m) oxygen levels : a positive anomaly of 60 mmol.m⁻³ translates into an oxygen increase by 10
461 mmol.m⁻³ in tropical regions after 50 years of integration.

462

463 The equatorward transport of the anomaly in the subtropics is mostly due to isopycnal subgrid scale
464 mixing processes as shown by the NEMO2 budget analysis. While the models with differing ocean
465 resolutions may differ in their transport of IWM between the subtropical regions and the tropics, it
466 nevertheless suggests that mesoscale activity in higher resolution models is important to spread
467 IWM (e.g Xu et al., 2016). This possibly includes subsurface eddies that show a signature well into
468 the IWM depth range (Frenger et al., 2018, see their Fig 2).

469

470 5.2 IMW transport and Equatorial Intermediate Current System

471 Second, the Equatorial Intermediate Current System (EICS) is not represented in coarse resolution
472 models and only poorly represented in high resolution ocean circulation models (0.25° and 0.1°), as
473 its strength remains too weak by a factor of two (consistent with previous studies, e.g Ascani et al.,
474 2015). The EICS transports the IWM that occupies the lower thermocline (500 – 1500 m depth) and
475 the recirculation of the IWM in the tropical ocean, as suggested by the observational study of Zenk
476 et al. (2005), and shown in our study.

477

478 We investigated the impact of the EICS on the oxygen supply with tracer release experiments: the
479 concentration of a conservative tracer that originates from the subtropical ocean, is, after 50 years,
480 30 % higher in the eastern equatorial (5°N - 5°S) Pacific in an ocean model with 0.1° resolution,
481 compared to an ocean model with 0.5° resolution. As the oxygen gradient along the equator is
482 similar to the gradient of the conservative tracer, we assume a similar enhancement of oxygen
483 supply by 30 % in the eastern equatorial Pacific at the same time scale. This means, if we account
484 for oxygen consumption due to respiration (about $1 \text{ mmol.m}^{-3}.\text{yr}^{-1}$ between 5°N - 5°S , see section
485 3.2), that the better resolved EICS in the higher resolution ocean leads roughly to higher
486 intermediate oxygen levels of $15 - 30 \text{ mmol.m}^{-3}$ compared to the lower resolution ocean experiment
487 in a timescale of 50 years. Consistently, 0.1° -ocean GFDL01 model displays oxygen concentrations
488 larger by about 30 mmol.m^{-3} in the eastern equatorial lower thermocline (500-1500 m) compared to
489 the 1° -ocean GFDL1 configuration (with higher subtropical oxygen concentrations of IWM of 15
490 mmol.m^{-3} in GFDL01 at 30°S)

491

492 We would like to highlight two potential implications of our finding of the important role of the
493 EICS for the Pacific eastern tropical oxygen supply: i) First, we have shown that the intermediate
494 current system EICS is important for the connection between the western and eastern Pacific Ocean
495 at a decadal / multidecadal time scale. This suggests that the EICS modulates the mean state and the
496 variability of the tropical oxygen in the lower thermocline, and subsequently the whole water
497 column by upwelling of deep waters. ii) Second, we have found an enhancement of the connections
498 between equatorial deep ocean ($> 2000 \text{ m}$) and lower thermocline in the high resolution model
499 compared to the lower resolution model. This result is consistent with the studies of Brandt et al.
500 (2011, 2012), who suggested, based on observational data and on an idealized model, that
501 Equatorial Deep Jets, part of the EICS (see Fig 1b), propagate their energy upward and impact the
502 upper ocean properties of the ocean, including their oxygen content. Taken this into account, we

503 hypothesize that the Pacific Deep Water has a larger role than previously thought in modulating the
504 intermediate and upper ocean properties.

505
506 A pragmatic approach to account for the missing EICS is to increase diffusion anisotropically, with
507 increased zonal mixing in the tropics (Getzlaff and Dietze, 2013). This parameterization mimics a
508 more vigorous EICS and improves the simulated shape of the OMZ in climate models. However,
509 the prominent bias of I_{MWM} in climate models, and therefore of the water masses entering the
510 EICS is not accounted for with this parameterization. Furthermore such a parameterization
511 improves the mean state but does not reproduce the variability of the EICS.-

512
513 5.3 Implication for biogeochemical cycles

514 The IWM are important supplier of oxygen to the tropical oceans, but also of nutrients (Palter et al.,
515 2010) as well as anthropogenic carbon (e.g Kathiwala et al., 2012), which accumulates in mode and
516 intermediate waters of the Southern Ocean (Sabine et al., 2004; Resplandy et al., 2013). The
517 mechanisms that we discussed here may therefore play a role in ocean carbon climate feedbacks on
518 time scales of decades to a century.

519
520 Finally, this study suggests that changes of the properties of the IWM may contribute to the still
521 partly unexplained deoxygenation of 5 mmol.m⁻³ / decade occurring in the lower thermocline of the
522 equatorial eastern Pacific Ocean (Schmidtko et al., 2017; Oschlies et al., 2018). In addition to an
523 oxygen decrease in tropical regions, Schmidtko et al. (2017) showed a decrease of oxygen levels by
524 2-5 mmol.m⁻³ in the regions of formations of AAIW. Based on repeated cruise observations,
525 Panassa et al. (2018) highlighted an increase of the apparent oxygen utilization in the core of the
526 AAIW, related to a 5 % increase in nutrient concentrations from 1990 to 2014. The transport of this
527 modified AAIW, poorer in oxygen and richer in nutrients, toward the low latitudes both by small
528 scale processes (section 3) and at the equator by the EICS (section 4), may explain a significant part
529 of the occurring deoxygenation in the equatorial ocean. In complement to changes in the AAIW
530 properties, little is known about the variability and long term trend of the strength of the EICS, an
531 oceanic “bridge” between the western and the eastern part of the basin. A possible way forward
532 could be to perform idealized model experiments in high resolution configurations, aiming to assess
533 both the effect of the observed change in the AAIW properties and of a potential change of EICS
534 strength on oxygen levels.

537 **Data and code availability**

538 The code for the Nucleus for European Modeling of the Ocean (NEMO) is available at:
539 <https://www.nemo-ocean.eu/>. The code for the University of Victoria (UVIC) model is available
540 at <http://terra.seos.uvic.ca/model/>. The Lagrangian particles ARIANE code is available at
541 <http://stockage.univ-brest.fr/~grima/Ariane/>. The Coordinated Ocean-ice Reference Experiments
542 (COREv2) dataset is available at: <https://data1.gfdl.noaa.gov/nomads/forms/core/COREv2.html>.
543 The experiments data is available on request.

544

545 **Authors contributions**

546 OD conceived the study, performed the NEMO model and ARIANE experiments and analyzed the
547 data. IF preprocessed and helped to analyze the GFDL data. JG preprocessed and helped to analyze
548 the UVIC data. All authors discussed the results and wrote the manuscript.

549

550 **Competing interest**

551 The authors declare that they have no conflict of interest.

552

553 **Acknowledgments**

554 This work is a contribution of the SFB754 “Climate-Biogeochemistry Interactions in the Tropical
555 Ocean”, supported by the Deutsche Forschungsgemeinschaft (DFG). The NEMO simulations were
556 performed at the North German Supercomputing Alliance (HLRN). We would like to thank Markus
557 Scheinert (research unit “Ocean Dynamics”, GEOMAR) for his technical support in compiling the
558 NEMO code and for providing the high resolution NEMO input files. We would like to thank
559 GFDL for producing the CM2-0 suite that involved a substantial commitment of computational
560 resources and data storage. [J. Getzlaff acknowledge support by the project "Reduced Complexity](#)
561 [Models" \(supported by the Helmholtz Association of German Research Centres \(HGF\) – grant no.](#)
562 [ZT-I-0010](#)

563

564

565

566

567

568

569

570

571 |

572 | **References**

573 Ascani, F., Firing, E., Dutrieux, P., McCreary, J. P., & Ishida, A. (2010). Deep Equatorial Ocean
574 Circulation Induced by a Forced–Dissipated Yanai Beam. *Journal of Physical Oceanography*, 40(5),
575 1118–1142. doi:10.1175/2010jpo4356.1

576 Ascani, F., Firing, E., McCreary, J. P., Brandt, P., & Greatbatch, R. J. (2015). The Deep Equatorial
577 Ocean Circulation in Wind-Forced Numerical Solutions. *Journal of Physical Oceanography*, 45(6),
578 1709–1734. doi:10.1175/jpo-d-14-0171.1

579 Bahl, A., Gnanadesikan, A., & Pradal, M. A. (2019). Variations in Ocean Deoxygenation Across
580 Earth System Models: Isolating the Role of Parameterized Lateral Mixing. *Global Biogeochemical
581 Cycles*, 33(6), 703–724. doi:10.1029/2018gb006121

582 Blanke, B., & Raynaud, S. (1997). Kinematics of the Pacific Equatorial Undercurrent: An Eulerian
583 and Lagrangian Approach from GCM Results. *Journal of Physical Oceanography*, 27(6), 1038–
584 1053. doi:10.1175/1520-0485(1997)027<1038:kotpeu>2.0.co;2

585 Brandt, P., Funk, A., Hormann, V., Dengler, M., Greatbatch, R. J., & Toole, J. M. (2011).
586 Interannual atmospheric variability forced by the deep equatorial Atlantic Ocean. *Nature*,
587 473(7348), 497–500. doi:10.1038/nature10013

588 Brandt, P., Greatbatch, R. J., Claus, M., Didwischus, S.-H., Hormann, V., Funk, A., ... Körtzinger,
589 A. (2012). Ventilation of the equatorial Atlantic by the equatorial deep jets. *Journal of Geophysical
590 Research: Oceans*, 117(C12), n/a–n/a. doi:10.1029/2012jc008118

591 Breitburg, D., Levin, L. A., Oschlies, A., Grégoire, M., Chavez, F. P., Conley, D. J., ... Zhang, J.
592 (2018). Declining oxygen in the global ocean and coastal waters. *Science*, 359(6371), eaam7240.
593 doi:10.1126/science.aam7240

594 Busecke, J. J. M., Resplandy, L., & Dunne, J. P. (2019). The Equatorial Undercurrent and the
595 Oxygen Minimum Zone in the Pacific. *Geophysical Research Letters*, 46(12), 6716–6725.
596 doi:10.1029/2019gl082692

597 Cabré, A., Marinov, I., Bernardello, R., & Bianchi, D. (2015). Oxygen minimum zones in the
598 tropical Pacific across CMIP5 models: mean state differences and climate change trends.
599 *Biogeosciences*, 12(18), 5429–5454. doi:10.5194/bg-12-5429-2015

600 Carrasco, C., Karstensen, J., & Farias, L. (2017). On the Nitrous Oxide Accumulation in
601 Intermediate Waters of the Eastern South Pacific Ocean. *Frontiers in Marine Science*, 4.
602 doi:10.3389/fmars.2017.00024

603 Cravatte, S., Kessler, W. S., & Marin, F. (2012). Intermediate Zonal Jets in the Tropical Pacific
604 Ocean Observed by Argo Floats. *Journal of Physical Oceanography*, 42(9), 1475–1485.
605 doi:10.1175/jpo-d-11-0206.1

606 Cravatte, S., Kestenare, E., Marin, F., Dutrieux, P., & Firing, E. (2017). Subthermocline and
607 Intermediate Zonal Currents in the Tropical Pacific Ocean: Paths and Vertical Structure. *Journal of*
608 *Physical Oceanography*, 47(9), 2305–2324. doi:10.1175/jpo-d-17-0043.1

609 Czeschel, R., Stramma, L., Schwarzkopf, F. U., Giese, B. S., Funk, A., and Karstensen, J. (2011),
610 Middepth circulation of the eastern tropical South Pacific and its link to the oxygen minimum zone,
611 *J. Geophys. Res.*, 116, C01015, doi:10.1029/2010JC006565

612 Delworth, T. L., Rosati, A., Anderson, W., Adcroft, A. J., Balaji, V., Benson, R., ... Zhang, R.
613 (2012). Simulated Climate and Climate Change in the GFDL CM2.5 High-Resolution Coupled
614 Climate Model. *Journal of Climate*, 25(8), 2755–2781. doi:10.1175/jcli-d-11-00316.1

615 Dietze, H., & Loeptien, U. (2013). Revisiting “nutrient trapping” in global coupled biogeochemical
616 ocean circulation models. *Global Biogeochemical Cycles*, 27(2), 265–284. doi:10.1002/gbc.20029

617 Dufour, C. O., Griffies, S. M., de Souza, G. F., Frenger, I., Morrison, A. K., Palter, J. B., ... Slater,
618 R. D. (2015). Role of Mesoscale Eddies in Cross-Frontal Transport of Heat and Biogeochemical
619 Tracers in the Southern Ocean. *Journal of Physical Oceanography*, 45(12), 3057–3081. doi:10.1175/
620 jpo-d-14-0240.1

621 Duteil, O., & Oschlies, A. (2011). Sensitivity of simulated extent and future evolution of marine
622 suboxia to mixing intensity. *Geophysical Research Letters*, 38(6), n/a–n/a.
623 doi:10.1029/2011gl046877

624 Duteil, O., Koeve, W., Oschlies, A., Aumont, O., Bianchi, D., Bopp, L., ... Segschneider, J. (2012).
625 Preformed and regenerated phosphate in ocean general circulation models: can right total
626 concentrations be wrong? *Biogeosciences*, 9(5), 1797–1807. doi:10.5194/bg-9-1797-2012

627 Duteil, O., Böning, C. W., & Oschlies, A. (2014). Variability in subtropical-tropical cells drives
628 oxygen levels in the tropical Pacific Ocean. *Geophysical Research Letters*, 41(24), 8926–8934.
629 doi:10.1002/2014gl061774

630 Duteil, O., Oschlies, A., & Böning, C. W. (2018). Pacific Decadal Oscillation and recent oxygen
631 decline in the eastern tropical Pacific Ocean. *Biogeosciences*, 15(23), 7111–7126. doi:10.5194/bg-
632 15-7111-2018

633 Duteil, O. (2019). Wind Synoptic Activity Increases Oxygen Levels in the Tropical Pacific Ocean.
634 *Geophysical Research Letters*, 46(5), 2715–2725. doi:10.1029/2018gl081041

635 Eden, C., & Dengler, M. (2008). Stacked jets in the deep equatorial Atlantic Ocean. *Journal of*
636 *Geophysical Research*, 113(C4). doi:10.1029/2007jc004298

637 Firing, E., Wijffels, S. E., & Hacker, P. (1998). Equatorial subthermocline currents across the
638 Pacific. *Journal of Geophysical Research: Oceans*, 103(C10), 21413–21423. doi:10.1029/98jc01944

639 Firing, E. (1987). Deep zonal currents in the central equatorial Pacific. *Journal of Marine Research*,
640 45(4), 791–812. doi:10.1357/002224087788327163

641 Frenger, I., Bianchi, D., Stührenberg, C., Oschlies, A., Dunne, J., Deutsch, C., ... Schütte, F.
642 (2018). Biogeochemical Role of Subsurface Coherent Eddies in the Ocean: Tracer Cannonballs,
643 Hypoxic Storms, and Microbial Stewpots? *Global Biogeochemical Cycles*, 32(2), 226–249.
644 doi:10.1002/2017gb005743

645 Galbraith, E. D., Dunne, J. P., Gnanadesikan, A., Slater, R. D., Sarmiento, J. L., Dufour, C. O., ...
646 Marvasti, S. S. (2015). Complex functionality with minimal computation: Promise and pitfalls of
647 reduced-tracer ocean biogeochemistry models. *Journal of Advances in Modeling Earth Systems*,
648 7(4), 2012–2028. doi:10.1002/2015ms000463

649 Getzlaff, J., & Dietze, H. (2013). Effects of increased isopycnal diffusivity mimicking the
650 unresolved equatorial intermediate current system in an earth system climate model. *Geophysical
651 Research Letters*, 40(10), 2166–2170. doi:10.1002/grl.50419

652 Gnanadesikan, A., Bianchi, D., & Pradal, M. (2013). Critical role for mesoscale eddy diffusion in
653 supplying oxygen to hypoxic ocean waters. *Geophysical Research Letters*, 40(19), 5194–5198.
654 doi:10.1002/grl.50998

655 Gouriou, Y., Delcroix, T., & Eldin, G. (2006). Upper and intermediate circulation in the western
656 equatorial Pacific Ocean in October 1999 and April 2000. *Geophysical Research Letters*, 33(10), n/
657 a–n/a. doi:10.1029/2006gl025941

658 Griffies, S. M., Winton, M., Anderson, W. G., Benson, R., Delworth, T. L., Dufour, C. O., ...
659 Zhang, R. (2015). Impacts on Ocean Heat from Transient Mesoscale Eddies in a Hierarchy of
660 Climate Models. *Journal of Climate*, 28(3), 952–977. doi:10.1175/jcli-d-14-00353.1

661 Iudicone, D., Rodgers, K. B., Schopp, R., & Madec, G. (2007). An Exchange Window for the
662 Injection of Antarctic Intermediate Water into the South Pacific. *Journal of Physical Oceanography*,
663 37(1), 31–49. doi:10.1175/jpo2985.1

664 Izumo, T. (2005). The equatorial undercurrent, meridional overturning circulation, and their roles in
665 mass and heat exchanges during El Niño events in the tropical Pacific ocean. *Ocean Dynamics*,
666 55(2), 110–123. doi:10.1007/s10236-005-0115-1

667 Khatiwala, S., Tanhua, T., Mikaloff Fletcher, S., Gerber, M., Doney, S. C., Graven, H. D., ...
668 Sabine, C. L. (2013). Global ocean storage of anthropogenic carbon. *Biogeosciences*, 10(4), 2169–
669 2191. doi:10.5194/bg-10-2169-2013

670 Kawabe, M., & Fujio, S. (2010). Pacific ocean circulation based on observation. *Journal of*
671 *Oceanography*, 66(3), 389–403. doi:10.1007/s10872-010-0034-8

672 Keller, D. P., Oschlies, A., & Eby, M. (2012). A new marine ecosystem model for the University of
673 Victoria Earth System Climate Model. *Geoscientific Model Development*, 5(5), 1195–1220.
674 doi:10.5194/gmd-5-1195-2012

675 Koshlyakov, M.N. and Tarakanov, R.Y. (2003). Antarctic Bottom Water in the Pacific sector of the
676 Southern Ocean, *Oceanology* 43(1):1-15

677 Kriest, I., Khatiwala, S., & Oschlies, A. (2010). Towards an assessment of simple global marine
678 biogeochemical models of different complexity. *Progress in Oceanography*, 86(3-4), 337–360.
679 doi:10.1016/j.pocean.2010.05.002

680 Lachkar, Z., Orr, J. C., & Dutay, J.-C. (2009). Seasonal and mesoscale variability of oceanic
681 transport of anthropogenic CO₂. *Biogeosciences*, 6(11), 2509–2523. doi:10.5194/bg-6-2509-2009

682 Large, W. G., & Yeager, S. G. (2008). The global climatology of an interannually varying air-sea
683 flux data set. *Climate Dynamics*, 33(2-3), 341–364. doi:10.1007/s00382-008-0441-3

684 Lübbecke, J. F., Böning, C. W., & Biastoch, A. (2008). Variability in the subtropical-tropical cells
685 and its effect on near-surface temperature of the equatorial Pacific: a model study. *Ocean Science*,
686 4(1), 73–88. doi:10.5194/os-4-73-2008

687 | Madec, G. Gurvan, M., Bourdallé-Badie, R., Pierre-Antoine Bouettier, Bricaud, C., Bruciaferri, D.,
688 Calvert, D., Chanut, J., Clementi, E., Coward, A., Delrosso, D., Ethé, C., Flavoni, S., Graham, T.,
689 Harle, J., Iovino, D., Lea, D., Lévy, C., Lovato, T., Martin, N., ... Vancoppenolle, M. (2017).
690 | <i>NEMO</i> ocean engine<i></i>. <https://doi.org/10.5281/ZENODO.3248739> Marin, F., Kestenare, E.,
691 Delcroix, T., Durand, F., Cravatte, S., Eldin, G., & Bourdallé-Badie, R. (2010). Annual Reversal of
692 the Equatorial Intermediate Current in the Pacific: Observations and Model Diagnostics. *Journal of*
693 *Physical Oceanography*, 40(5), 915–933. doi:10.1175/2009jpo4318.1

694 Martin, J. H., Knauer, G. A., Karl, D. M., & Broenkow, W. W. (1987). VERTEX: carbon cycling in
695 the northeast Pacific. *Deep Sea Research Part A. Oceanographic Research Papers*, 34(2), 267–285.
696 doi:10.1016/0198-0149(87)90086-0

697 Meijers, A. J. S. (2014). The Southern Ocean in the Coupled Model Intercomparison Project phase
698 5. *Philosophical Transactions of the Royal Society A: Mathematical, Physical and Engineering*
699 *Sciences*, 372(2019), 20130296. doi:10.1098/rsta.2013.0296

700 Méneguen, C., Delpech, A., Marin, F., Cravatte, S., Schopp, R., & Morel, Y. (2019). Observations
701 and Mechanisms for the Formation of Deep Equatorial and Tropical Circulation. *Earth and Space*
702 *Science*, 6(3), 370–386. doi:10.1029/2018ea000438

703 Molinelli EJ (1981) The Antarctic influence on Antarctic Intermediate Water. *J Mar Res* 39:267–
704 293

705 Oschlies, A., Brandt, P., Stramma, L., & Schmidtko, S. (2018). Drivers and mechanisms of ocean
706 deoxygenation. *Nature Geoscience*, 11(7), 467–473. doi:10.1038/s41561-018-0152-2

707 Palter, J. B., Sarmiento, J. L., Gnanadesikan, A., Simeon, J., and Slater, R. D. (2010). Fueling
708 export production: nutrient return pathways from the deep ocean and their dependence on the
709 Meridional Overturning Circulation, *Biogeosciences*, 7, 3549–3568, doi:10.5194/bg-7-3549-2010

710 Panassa, E., Santana-Casiano, J. M., González-Dávila, M., Hoppema, M., van Heuven, S. M. A. .,
711 Völker, C., ... Hauck, J. (2018). Variability of nutrients and carbon dioxide in the Antarctic
712 Intermediate Water between 1990 and 2014. *Ocean Dynamics*, 68(3), 295–308.
713 doi:10.1007/s10236-018-1131-2

714 Pardo, P. C., Pérez, F. F., Velo, A., & Gilcoto, M. (2012). Water masses distribution in the Southern
715 Ocean: Improvement of an extended OMP (eOMP) analysis. *Progress in Oceanography*, 103, 92–
716 105. doi:10.1016/j.pocean.2012.06.002

717 Paulmier, A., Ruiz-Pino (2009), D. Oxygen minimum zones (OMZs) in the modern ocean, *Progress*
718 in *Oceanography*, 80(3), 113-128, doi:10.1016/j.pocean.2008.08.001.

719 Qu, T., & Lindstrom, E. J. (2004). Northward Intrusion of Antarctic Intermediate Water in the
720 Western Pacific*. *Journal of Physical Oceanography*, 34(9), 2104–2118. doi:10.1175/1520-
721 0485(2004)034<2104:nioaiw>2.0.co;2

722 Resplandy, L., Bopp, L., Orr, J. C., & Dunne, J. P. (2013). Role of mode and intermediate waters in
723 future ocean acidification: Analysis of CMIP5 models. *Geophysical Research Letters*, 40(12),
724 3091–3095. doi:10.1002/grl.50414

725 Rowe, G. D., Firing, E., & Johnson, G. C. (2000). Pacific Equatorial Subsurface Countercurrent
726 Velocity, Transport, and Potential Vorticity*. *Journal of Physical Oceanography*, 30(6), 1172–1187.
727 doi:10.1175/1520-0485(2000)030<1172:pescvt>2.0.co;2

728 Russell, J. L., & Dickson, A. G. (2003). Variability in oxygen and nutrients in South Pacific
729 Antarctic Intermediate Water. *Global Biogeochemical Cycles*, 17(2), n/a–n/a.
730 doi:10.1029/2000gb001317

731 Sabine, C. L. (2004). The Oceanic Sink for Anthropogenic CO₂. *Science*, 305(5682), 367–371.
732 doi:10.1126/science.1097403

733 Sallée, J.-B., Shuckburgh, E., Bruneau, N., Meijers, A. J. S., Bracegirdle, T. J., Wang, Z., & Roy, T.
734 (2013). Assessment of Southern Ocean water mass circulation and characteristics in CMIP5
735 models: Historical bias and forcing response. *Journal of Geophysical Research: Oceans*, 118(4),
736 1830–1844. doi:10.1002/jgrc.20135

737 Schmidtko, S., Stramma, L., & Visbeck, M. (2017). Decline in global oceanic oxygen content
738 during the past five decades. *Nature*, 542(7641), 335–339. doi:10.1038/nature21399

739 Sen Gupta, A., & England, M. H. (2007). Evaluation of Interior Circulation in a High-Resolution
740 Global Ocean Model. Part II: Southern Hemisphere Intermediate, Mode, and Thermocline Waters.
741 *Journal of Physical Oceanography*, 37(11), 2612–2636. doi:10.1175/2007jpo3644.1

742 Shigemitsu, M., Yamamoto, A., Oka, A., & Yamanaka, Y. (2017). One possible uncertainty in
743 CMIP5 projections of low-oxygen water volume in the Eastern Tropical Pacific. *Global*
744 *Biogeochemical Cycles*, 31(5), 804–820. doi:10.1002/2016gb005447

745 Sloyan, B. M., & Kamenkovich, I. V. (2007). Simulation of Subantarctic Mode and Antarctic
746 Intermediate Waters in Climate Models. *Journal of Climate*, 20(20), 5061–5080.
747 doi:10.1175/jcli4295.1

748 Sloyan, B. M., & Rintoul, S. R. (2001). Circulation, Renewal, and Modification of Antarctic Mode
749 and Intermediate Water*. *Journal of Physical Oceanography*, 31(4), 1005–1030. doi:10.1175/1520-
750 0485(2001)031<1005:cramoa>2.0.co;2

751 Takano, Y., Ito, T., & Deutsch, C. (2018). Projected Centennial Oxygen Trends and Their
752 Attribution to Distinct Ocean Climate Forcings. *Global Biogeochemical Cycles*, 32(9), 1329–1349.
753 doi:10.1029/2018gb005939

754 Talley, L. D. (1993). Distribution and Formation of North Pacific Intermediate Water. *Journal of*
755 *Physical Oceanography*, 23(3), 517–537. doi:10.1175/1520-0485(1993)023<0517:dafonp>2.0.co;2

756 Weaver, A. J., Eby, M., Wiebe, E. C., Bitz, C. M., Duffy, P. B., Ewen, T. L., ... Yoshimori, M.
757 (2001). The UVic earth system climate model: Model description, climatology, and applications to
758 past, present and future climates. *Atmosphere-Ocean*, 39(4), 361–428.
759 doi:10.1080/07055900.2001.9649686

760 Xu, L., Li, P., Xie, S. et al. (2016). Observing mesoscale eddy effects on mode-water subduction
761 and transport in the North Pacific. *Nature Communications*, 10505 (2016),
762 doi.org/10.1038/ncomms10505

763 Zenk, W., Siedler, G., Ishida, A., Holfort, J., Kashino, Y., Kuroda, Y., ... Müller, T. J. (2005).
764 Pathways and variability of the Antarctic Intermediate Water in the western equatorial Pacific
765 Ocean. *Progress in Oceanography*, 67(1-2), 245–281. doi:10.1016/j.pocean.2005.05.003

766 Zhu, C., Liu, Z., & Gu, S. (2017). Model bias for South Atlantic Antarctic intermediate water in
767 CMIP5. *Climate Dynamics*, 50(9-10), 3613–3624. doi:10.1007/s00382-017-3828-1

768

769

770

771

772

773

774

775

776 **Table and Figures**

777

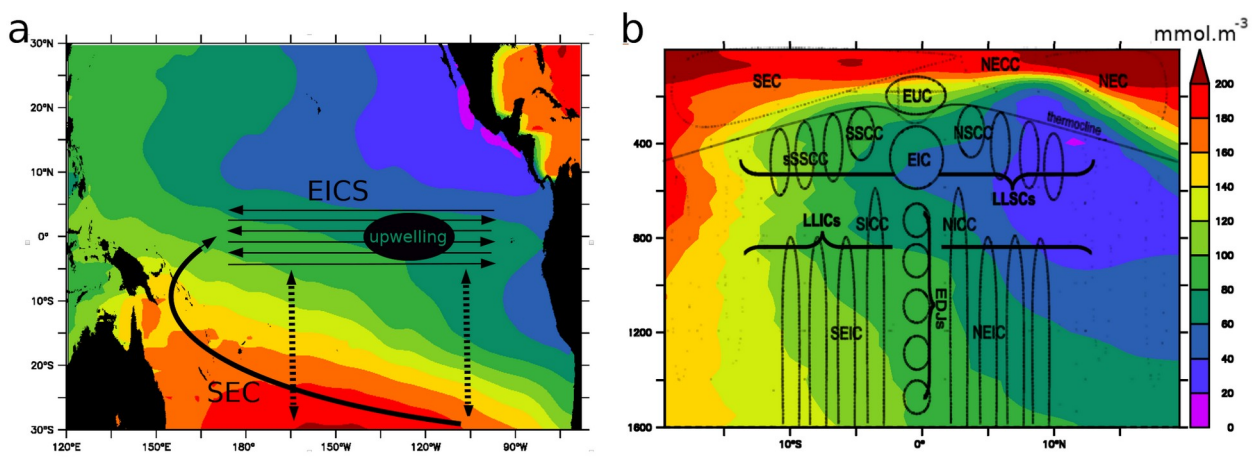
778 **Table 1:**

Model	Resolution	Atmosphere	BGC	Model Reference (circulation)	Model Reference (BGC)	
Mean state comparison						
UVIC	2.8°	Coupled (temperature, humidity) Forced (NCEP/NCA R-wind stress)	UVIC-BGC	Weaver et al., 2001	Keller et al., 2012	
NEMO2	2° (0.5 eq)	Forced COREv2 “normal year”	NPZD-θ2	Madec et al., 2017	Kriest et al., 2010 Duteil et al., 2014	
GFDL1	1°	Coupled (~50 km)	miniBL ING	Delworth et al., 2012, Griffies et al., 2015	Galbraith et al., 2015, Dufour et al., 2015	
GFDL025	0.25°	Coupled (~50 km)	miniBL ING	Griffies et al., 2015	Galbraith et al., 2015, Dufour et al., 2015	
GFDL01	0.1°	Coupled (~50 km)	miniBL ING			
Sensitivity experiments						
Model	Resolution	Atmosphere	BGC	Experiments		
NEMO2 (section 2.2.1)	2° (0.5 eq)	Forced COREv2 1948–2007	NPZD-θ2	REF: control experiment 30N30S: O ₂ restoring to WOA at 30°N/30°S 30N30S1500M: O ₂ restoring to WOA at 30°N/30°S/1500m		
NEMO05 (section 2.2.2)	0.5°	Forced COREv2 1948–2007	Tracer release	Tracer initialized to 1 (O ₂ WOA > 150 mmol.m ⁻³) or 0 (O ₂ WOA < 150 mmol.m ⁻³)		
NEMO01 (section 2.2.2)	0.1°	Forced COREv2 1948–2007	Tracer release			

779

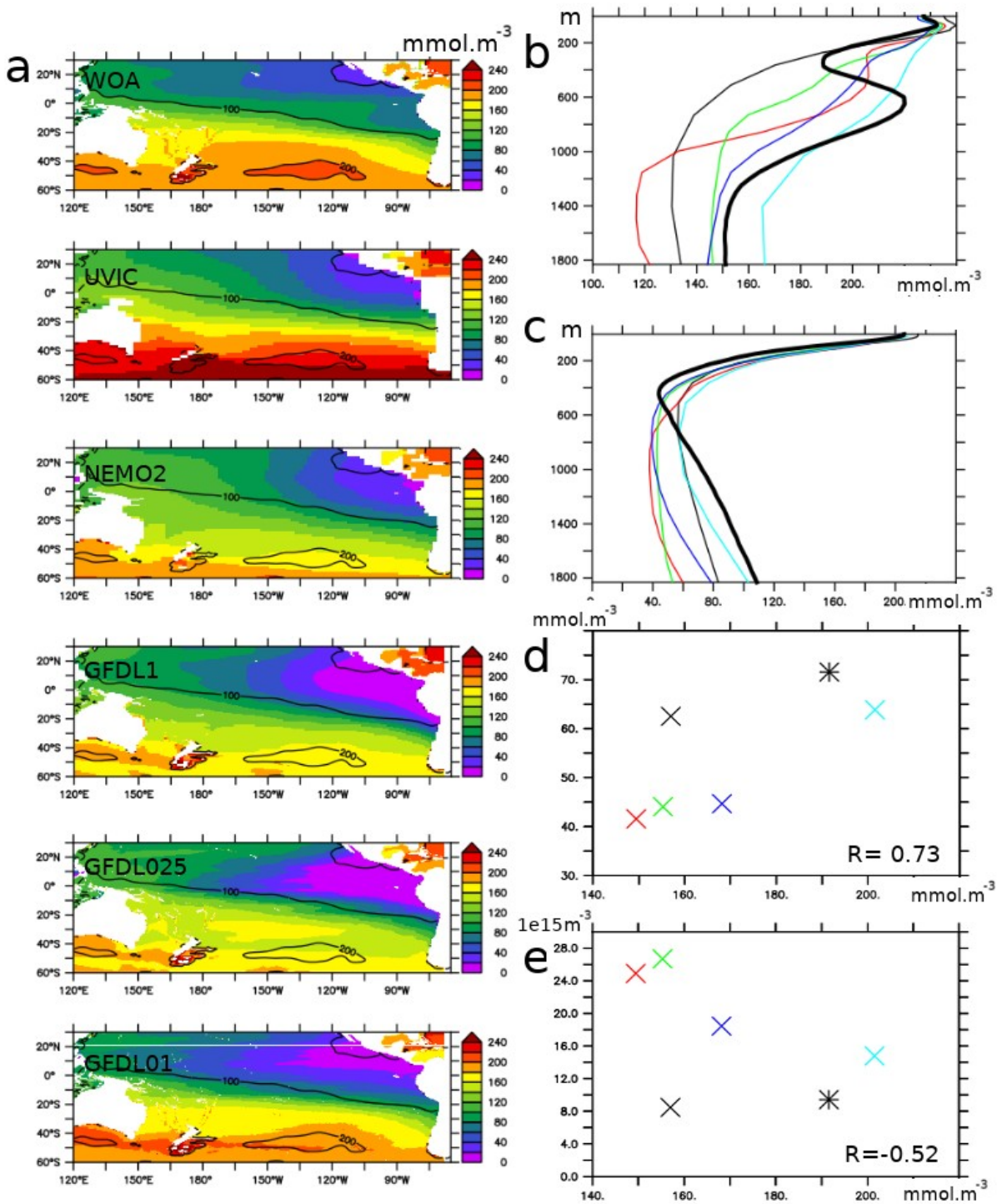
780

781
782
783
784
785
786



787
788
789

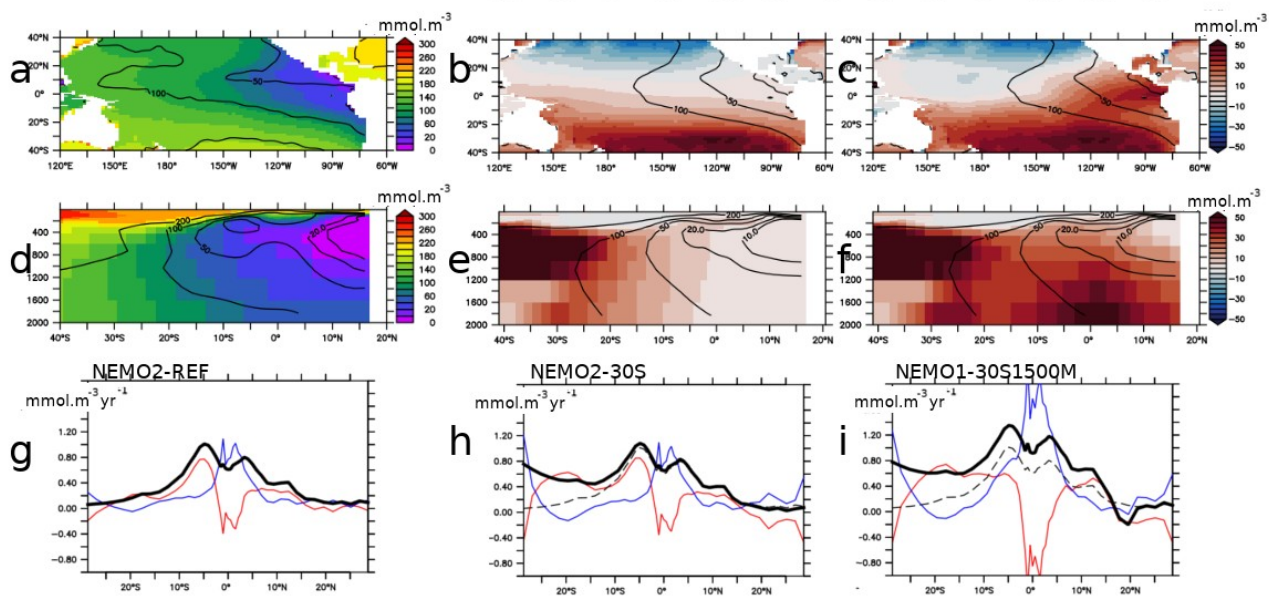
790 Figure 1 : a - schema summarizing the intermediate water masses (IWM) pathway from the
791 subtropics into the equatorial regions. EICS : Equatorial Intermediate Current System. SEC : South
792 Equatorial Current. Dashed line : isopycnal diffusive processes. Oxygen levels (mmol.m^{-3}) in the
793 lower thermocline (mean 500–1500m) are represented in color. b - schema (adapted from
794 Menesguen et al., 2019) illustrating the complexity of the EICS, extending below the thermocline
795 till more than 2000 m depth (see section 4.1 for a detailed description). Oxygen levels (mean 500–
796 1500m) at 160°W are represented in color (mmol.m^{-3}).



797

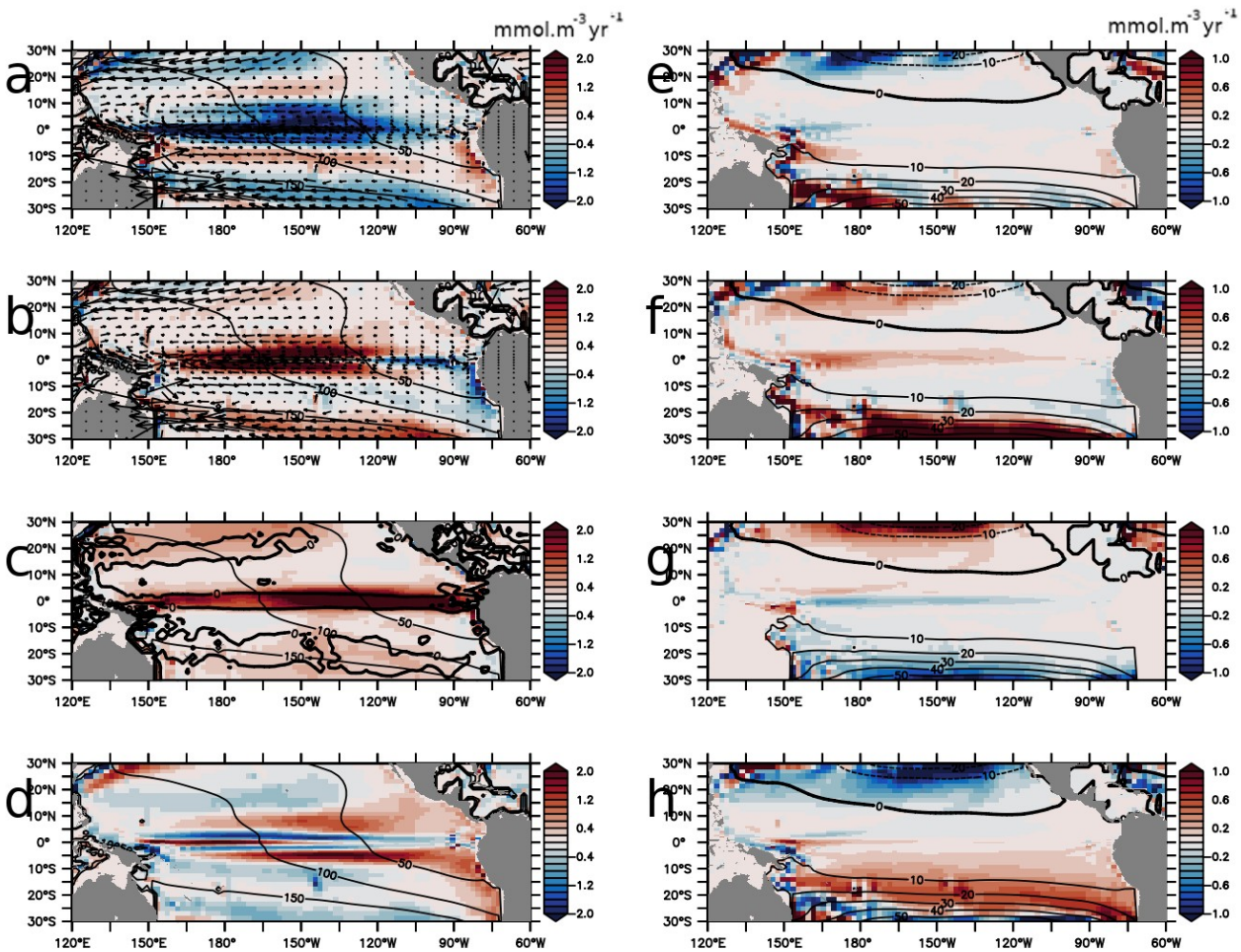
798 Figure 2 : a- oxygen levels (mmol.m⁻³) in observations (World Ocean Atlas - WOA) (mean 500-
 799 1500-m) and models (UVIC, NEMO2, GFDL1, GFDL025, GFDL01). Contours correspond to
 800 WOA values. b: average “30°S” (120°E-65°W, 30°S) c : average “tropics” (160°W-coast, 20°N-
 801 20°S). d: average “30°S” vs “tropics”. e: average “30°S” vs volume of tropical suboxic ocean
 802 (oxygen lower than 20 mmol.m⁻³) regions (10^{15} m^3). UVIC : black, NEMO2 : cyan, GFDL1 : red,
 803 GFDL025, green; GFDL01 : blue, WOA: star.

804
805
806



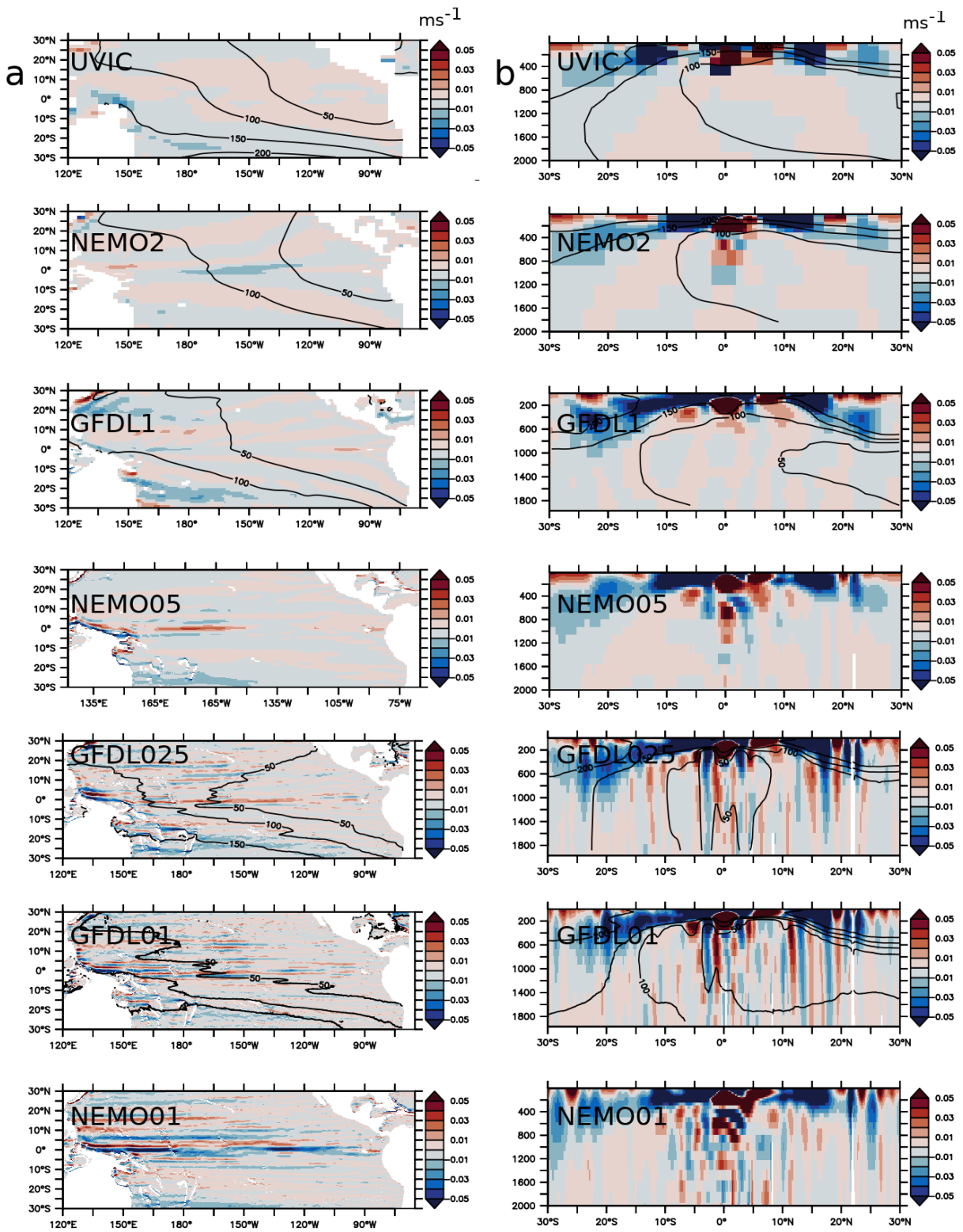
807

808 **Figure 3 :** a- Oxygen (mmol.m^{-3}) in the experiments NEMO2-REF (color) and World Ocean Atlas
809 (contour) (average 500–1500 m). b- Oxygen (mmol.m^{-3}) difference (average 500–1500 m) between
810 the experiments NEMO2-30S minus NEMO2-REF and c- NEMO2-30S1500M minus NEMO2-
811 REF (contour NEMO2-REF). d- Oxygen (mmol.m^{-3}) in the experiments NEMO2-REF (color) and
812 World Ocean Atlas (contour) (100°W). e- Oxygen (mmol.m^{-3}) difference (100°W) between the
813 experiments NEMO2-30S minus NEMO2-REF and f- NEMO2-30S1500M minus NEMO2-REF
814 (contour NEMO2-REF). g-i : basin zonal average (average 500 – 1500 m) of the oxygen total
815 supply (bold) ($\text{mmol.m}^{-3}.\text{year}^{-1}$), advective processes (blue) and isopycnal diffusion (red) in g-
816 NEMO2-REF, h- NEMO2-30DEG, i- NEMO2-30DEG1500M. The dashed line in is the oxygen
817 total supply in NEMO2-REF.



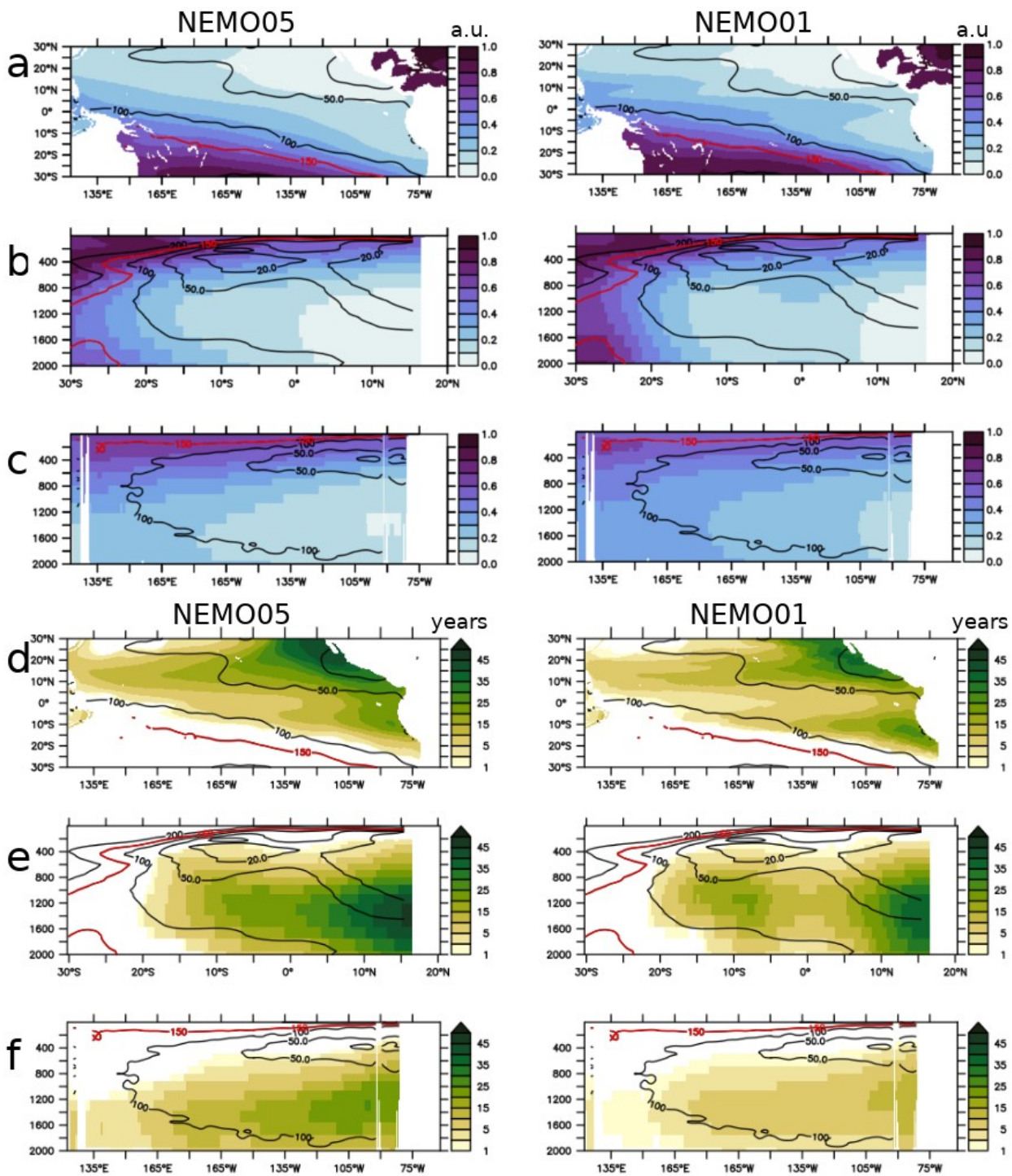
819

820 **Figure 4** : Oxygen supply processes ($\text{mmol.m}^{-3}.\text{year}^{-1}$ —average 500–1500m) in NEMO2-REF : a-
 821 zonal advection, b—meridional advection, c—vertical advection, d—isopycnal diffusion. The
 822 meridional and zonal currents are displayed as vectors in a,b and the vertical current as contour in c.
 823 Oxygen levels (mmol.m^{-3}) are displayed in contour. Difference in oxygen supply processes
 824 ($\text{mmol.m}^{-3}.\text{year}^{-1}$ —average 500–1500m) between NEMO2-30DEG and NEMO2-REF : e—zonal
 825 advection, f—meridional advection, g—vertical advection, h—isopycnal diffusion. The NEMO2-
 826 30DEG—NEMO2-REF oxygen anomaly (mmol.m^{-3}) is displayed in contour.



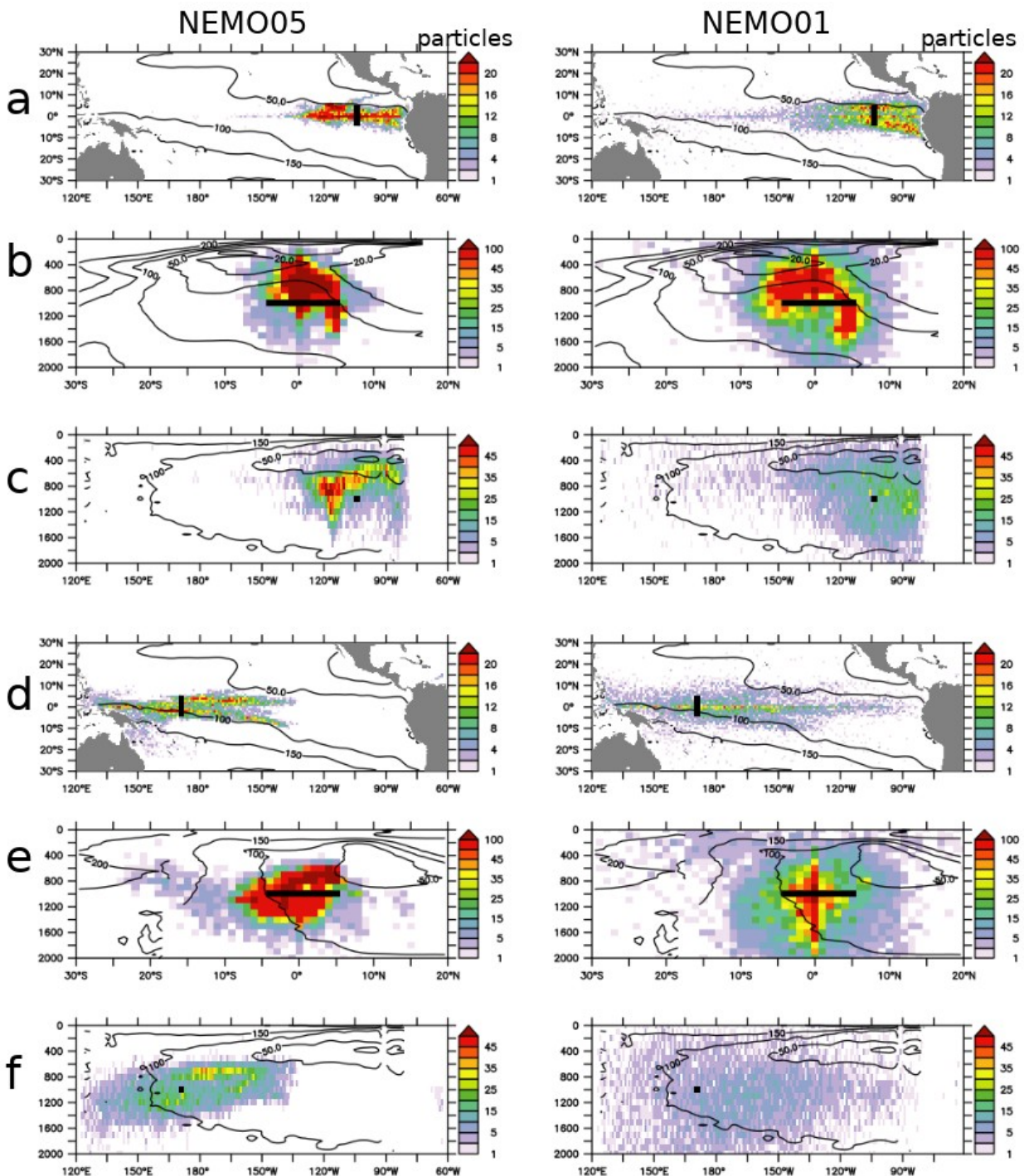
827

828 **Figure 5 : mean currents velocity (ms⁻¹) at a - 1000 m depth b - 100°W in UVIC, NEMO2,
 829 NEMO05, GFDL025, GFDL01, NEMO01. The mean oxygen levels (mmol.m⁻³) (when coupled
 830 circulation-biogeochemical experiments have been performed — see Table 1) are displayed in
 831 contour**



832

833 Figure 6: a-c : tracer concentration (arbitrary unit) after 60 years integration in NEMO05 (left) and
 834 NEMO01 (right). a-average 500-1500m, b-section 100°W, c-equatorial section. d-f: Time (years)
 835 at which the released tracer reaches the concentration 0.1 (t10%) in NEMO05 and NEMO01. d-
 836 average 500-1500m, e-section 100°W, f-equatorial section. In all the subpanels, the WOA oxygen
 837 levels are displayed in contour. The red contour is the WOA 150 mmol.m⁻³ oxygen isoline, used to
 838 initialize the tracer level.



841 Figure 7 : Density (number of particles in a $1^\circ \times 1^\circ \times 100\text{m}$ depth box) distribution of the location of
 842 released Lagrangian particles (15 years backward integration starting from the final experiment
 843 state) in NEMO05 (left) and NEMO01 (right). The release location is identified in bold and is
 844 located at $100^\circ\text{W}/5^\circ\text{N}/5^\circ\text{S}/1000\text{ m}$ depth. a- vertical integrated density; b- zonal integrated density;
 845 c- meridional integrated density. d-f : Similar to a-c but with a release location located at
 846 $160^\circ\text{E}/5^\circ\text{N}/5^\circ\text{S}/1000\text{ m}$ depth. The mean oxygen levels are displayed in contour.

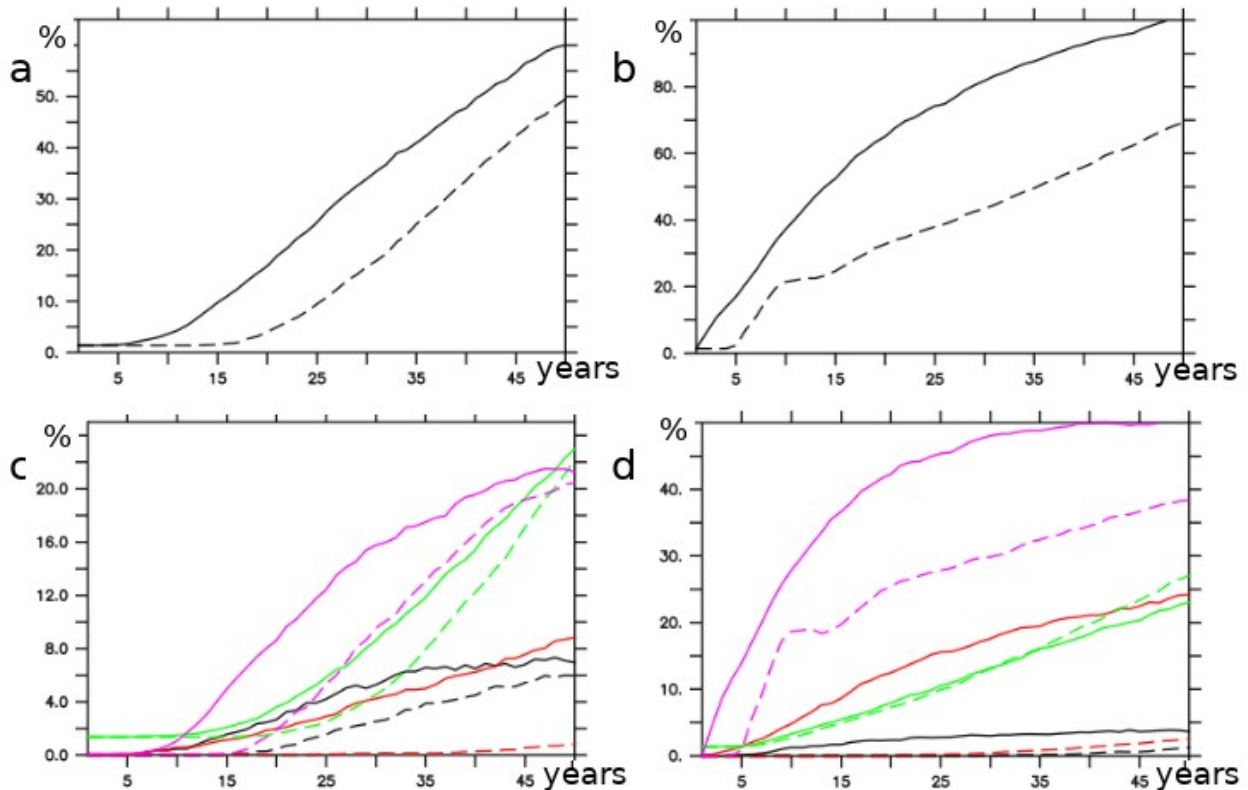
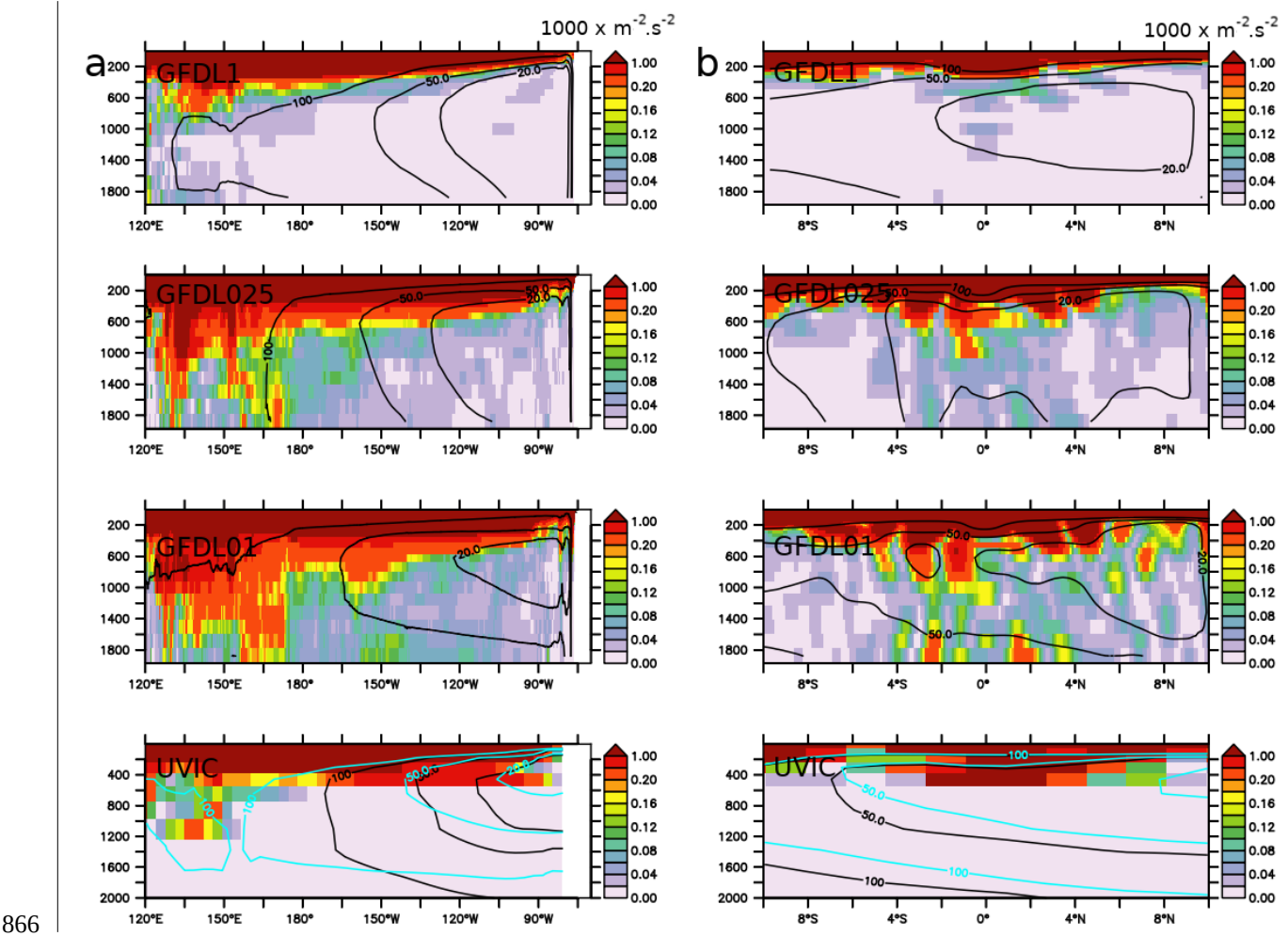


Figure 8 : a : percentage of particles originating from outside the Intermediate Eastern Tropical Pacific (IETP) ocean region (release $100^{\circ}\text{W} / 5^{\circ}\text{N}-5^{\circ}\text{S} / 1000 \text{ m}$) or b : originating from outside the Intermediate Western Tropical Pacific (IWTP) ocean region (release $160^{\circ}\text{E} / 5^{\circ}\text{N}-5^{\circ}\text{S} / 1000 \text{ m}$) in NEMO01 (black) and NEMO05 (dash). c,d ; percentage of particles originating from outside the IETP (c) and the IWTP (d): upper ocean ($< 200 \text{ m}$) (black), deep ocean ($> 2000 \text{ m}$) (red), subtropical region ($> 10^{\circ}\text{N/S}$) (green), panel c: western (west of 160°W) - or panel d: eastern (east of 160°W) part of the basin (magenta).



866

867

868

869

870 Figure 9 : a - Mean Kinetic Energy ($\text{m}^2\text{s}^{-2} \times 1000$) (average 10°N - 10°S) in GFDL01, GFDL025,
 871 GFDL01, UVIC, b - similar to a. but average 160°W coast. Oxygen levels (mmol.m^{-3}) are displayed
 872 in contour. The blue contour corresponds to UVIC GD13 (Getzlaff and Dietze, 2013, including an
 873 anisotropical increase of lateral diffusion at the equator)

874

875

876

877

878

879

880

881

882

883

884

885

886

887

888

889

890

891

892

893

894

895

896

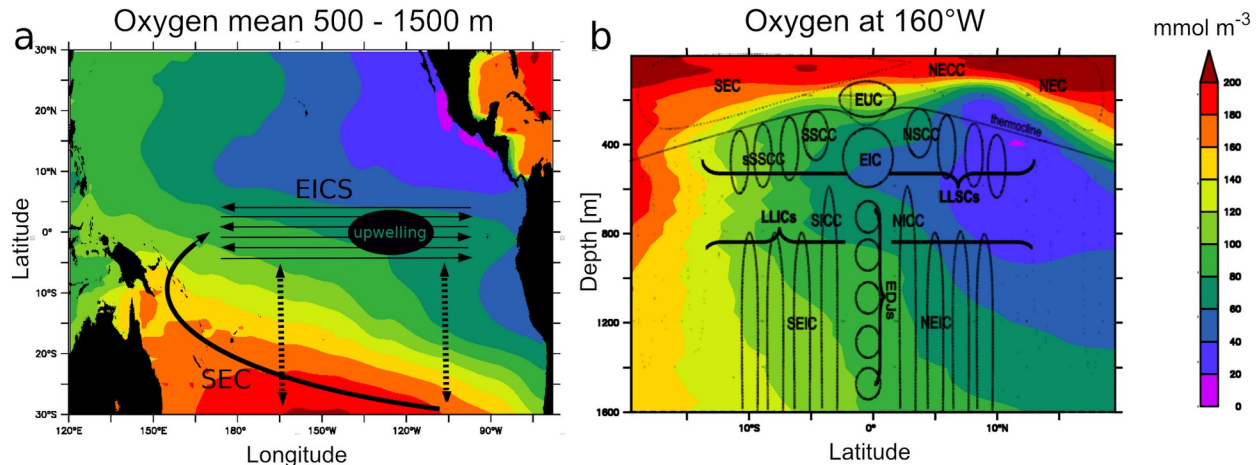
897

898

899

900

Figures and Table

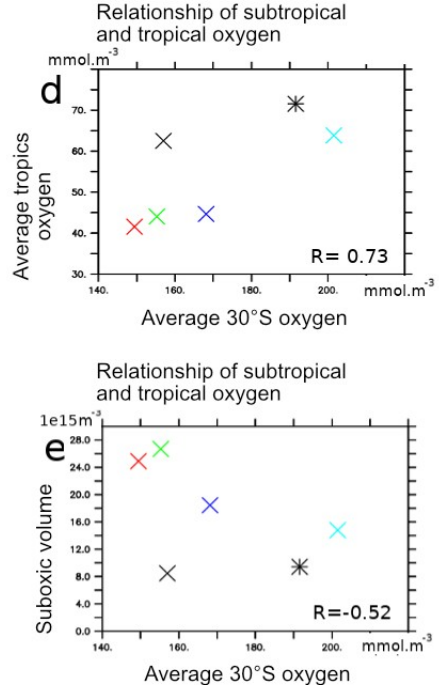
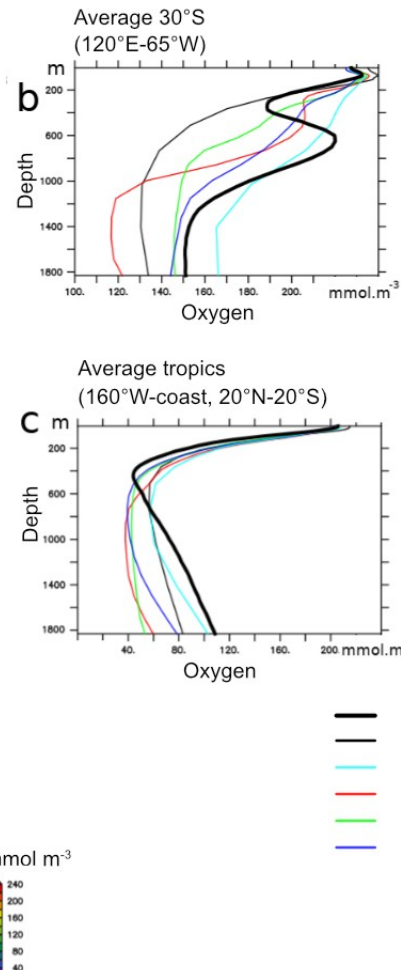
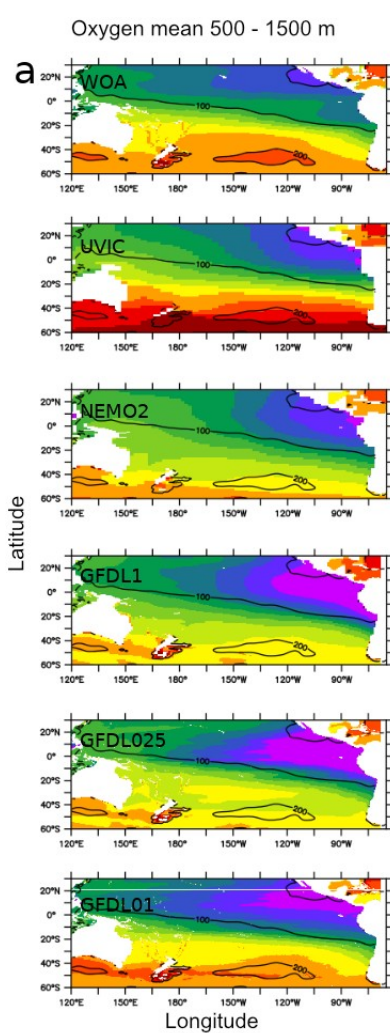


901

902

903 Figure 1 : a- schema summarizing the intermediate water masses (IWM) pathway from the
 904 subtropics into the equatorial regions. EICS : Equatorial Intermediate Current System. SEC : South
 905 Equatorial Current. Dashed line : isopycnal diffusive processes. Observed (World Ocean Atlas)
 906 oxygen levels (mmol.m⁻³) in the lower thermocline (mean 500-1500m) are represented in color. b -
 907 schema (adapted from Menesguen et al., 2019) illustrating the complexity of the EICS, extending

908 | below the thermocline till more than 2000 m depth (see section 4.1 for a detailed description).
909 | Observed (World Ocean Atlas) oxygen levels at 160°W are represented in color.
910 |
911 |
912 |
913 |
914 |
915 |
916 |
917 |
918 |
919 |
920 |
921 |
922 |
923 |
924 |
925 |
926 |



— WOA
— UVIC
— NEMO2
— GFDL1
— GFDL025
— GFDL01

mmol m⁻³

927

928 Figure 2 : a- oxygen levels (mmol.m⁻³) in observations (World Ocean Atlas - WOA) (mean 500 -

929 1500 m) and models (UVIC, NEMO2, GFDL1, GFDL025, GFDL01). Contours correspond to WOA

930 values. b: average "30°S" (120°E-65°W, 30°S) c : average "tropics" (160°W-coast, 20°N-20°S). d:

931 average "30°S" vs "tropics". e: average "30°S" vs volume of tropical suboxic ocean (oxygen lower

932 than 20 mmol.m⁻³) regions (1e15m³). b-e : UVIC : black, NEMO2 : cyan, GFDL1 : red, GFDL025,

933 green; GFDL01 : blue, WOA: bold line (b,c) and star (d,e).

934

935

936

937

938

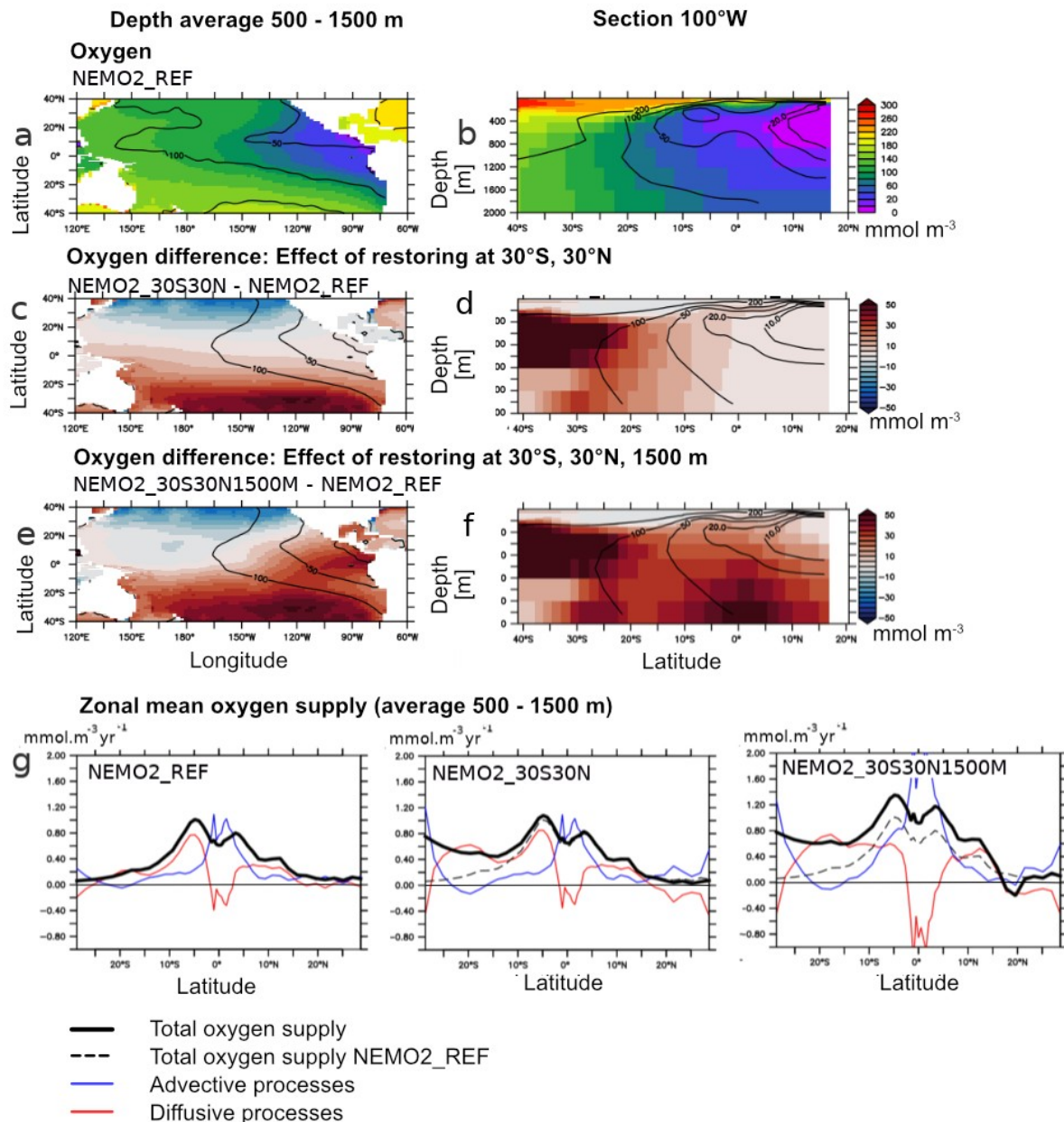
939

940

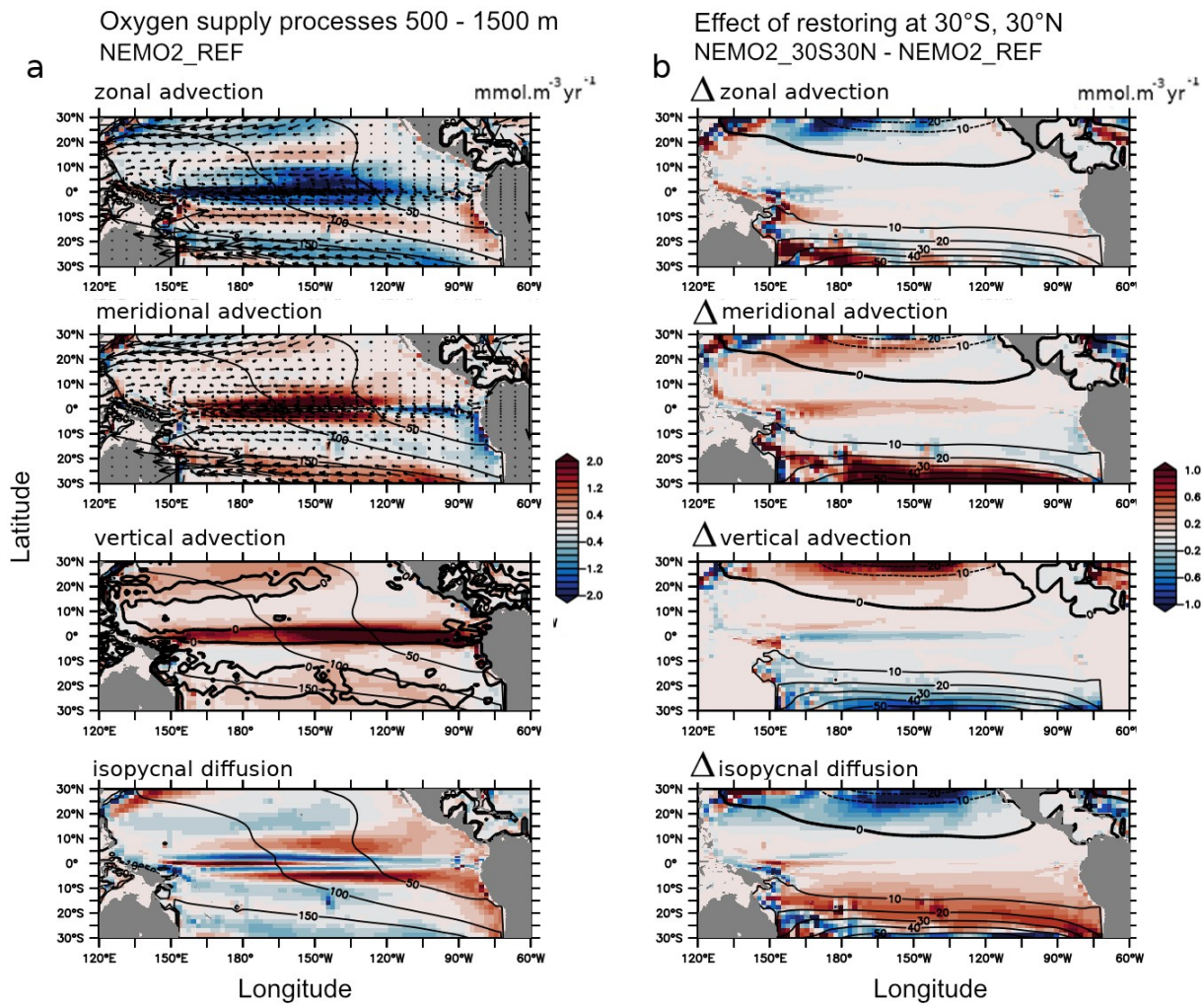
941

942

943



946 | Figure 3 : a,b: Oxygen (mmol.m⁻³) in the experiments NEMO2_REF (color) and World Ocean Atlas
947 | (contour) (a- average 500-1500 m, b- 100°W). c,d: Oxygen (mmol.m⁻³) difference (c- average 500 -
948 | 1500m, d- 100°W) between the experiments NEMO2_30S30N minus NEMO2_REF. e,f : Oxygen
949 | (mmol.m⁻³) difference (e- average 500-1500m, f- 100°W) between the experiments
950 | NEMO2_30S30N1500M minus NEMO2_REF. g- basin zonal average (average 500 - 1500 m) of
951 | the oxygen total supply (bold) (mmol.m⁻³.year⁻¹), advective processes (blue) and isopycnal diffusion
952 | (red) in NEMO2_REF, NEMO2_30S30N, NEMO2_30S30N1500M. The dashed line is the oxygen
953 | total supply in NEMO2_REF.



956 Figure 4 : a- Oxygen supply processes ($\text{mmol.m}^{-3} \text{year}^{-1}$ – average 500 - 1500m) in NEMO2_REF :
957 zonal advection, meridional advection, vertical advection, isopycnal diffusion. The mean meridional
958 and zonal currents are displayed as vectors (meridional, zonal advection). The mean vertical
959 current (0 isoline) is represented as bold contour (vertical advection). Oxygen levels (mmol.m^{-3})
960 are displayed in black contour. b- Difference in oxygen supply processes ($\text{mmol.m}^{-3} \text{year}^{-1}$ –
961 average 500-1500m) between NEMO2_30S30N and NEMO2_REF : zonal advection, meridional
962 advection, vertical advection, isopycnal diffusion. The NEMO2_30S30N – NEMO2_REF oxygen
963 anomaly (mmol.m^{-3}) is displayed in contour.

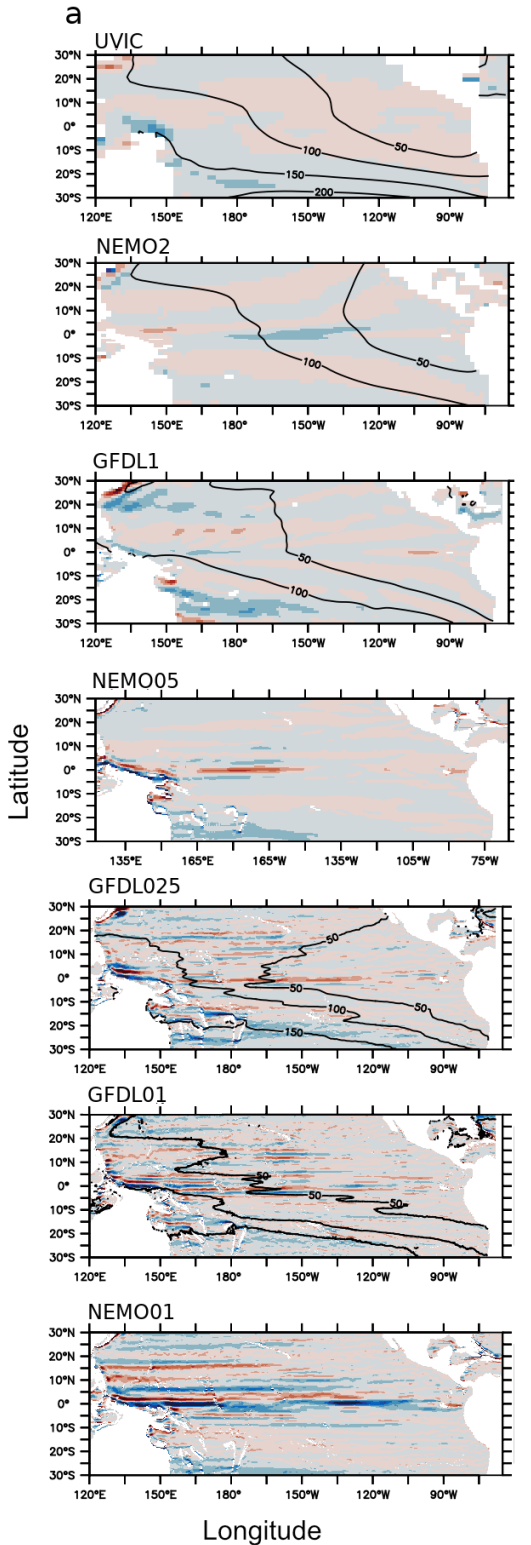
964

965

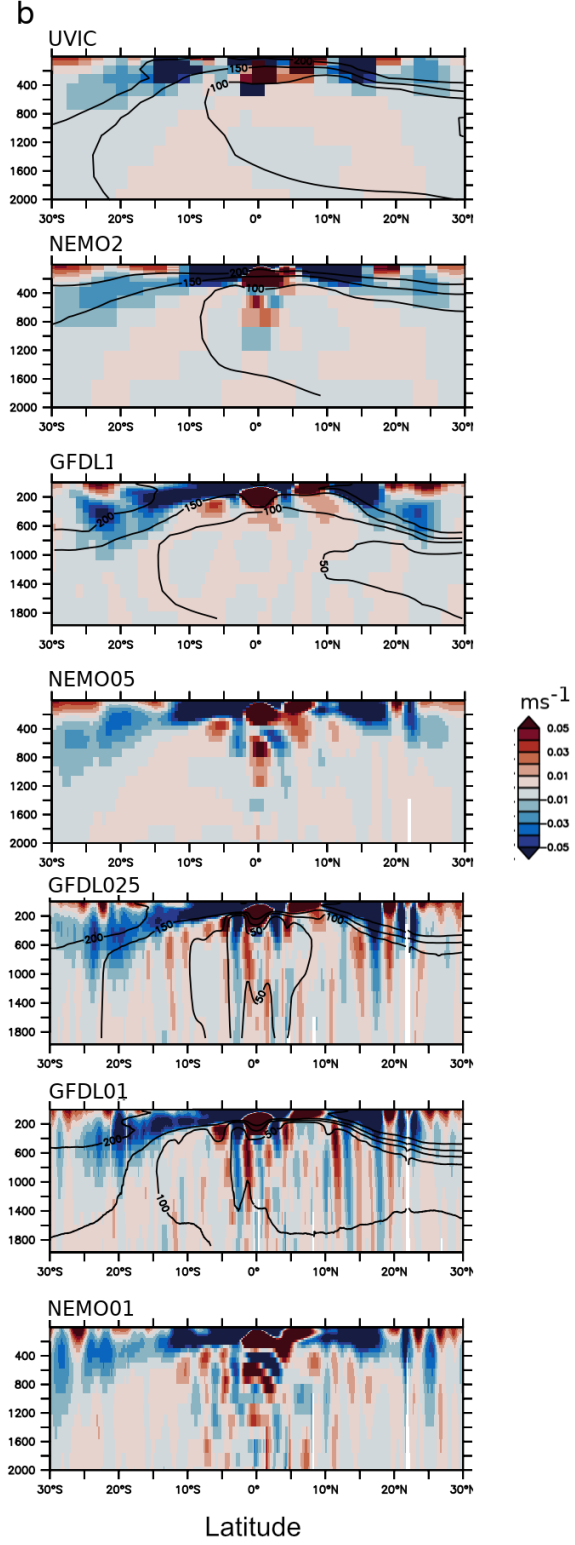
966

967

Zonal velocity component at 1000 m (colors) and oxygen (contours)



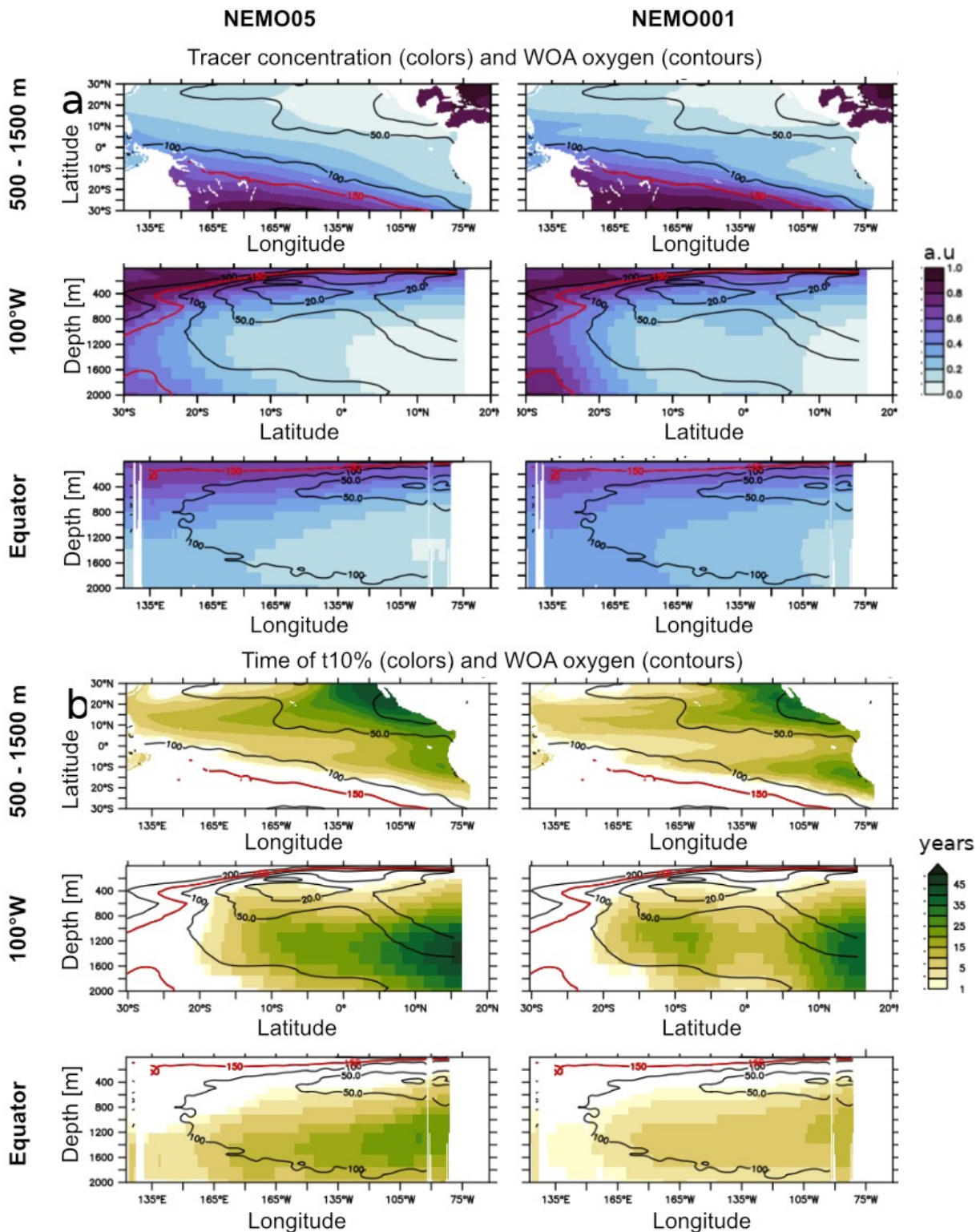
Zonal velocity component at 100°W (colors) and oxygen (contours)



968

969 | Figure 5 : mean currents velocity (ms⁻¹) at a- 1000 m depth b- 100°W in UVIC, NEMO2, NEMO05,
 970 | GFDL025, GFDL01, NEMO01. The mean oxygen levels (mmol.m⁻³) (when coupled circulation-
 971 | biogeochemical experiments have been performed – see Table 1) are displayed in contour

972 |

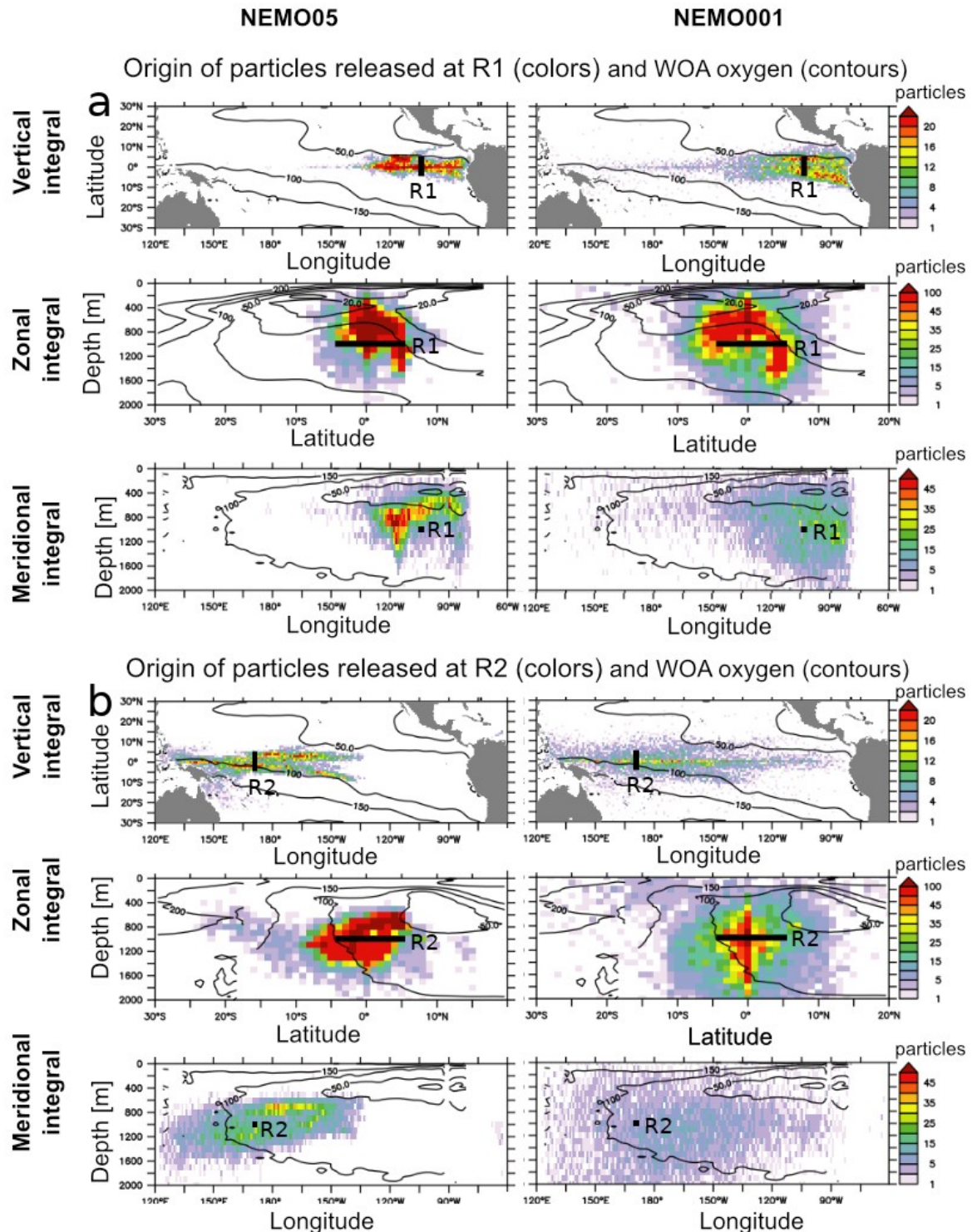


Fig

973
974
975
976
977

Figure 6: a : tracer concentration (arbitrary unit) after 60 years integration in NEMO05 and NEMO01: average 500-1500m, section 100°W, equatorial section. b: Time (years) at which the released tracer reaches the concentration 0.1 (t10%) in NEMO05 and NEMO01: average 500-1500m, section 100°W, equatorial section. In all the subpanels, the WOA oxygen levels are

978 | displayed in contour. The red contour is the WOA 150 mmol.m⁻³ oxygen isoline, used to initialize
 979 | the tracer level.



980 |
 981 | Figure 7 : Density (number of particles in a 1°x1°x100m depth box) distribution of the location of
 982 | released Lagrangian particles (15 years backward integration starting from the final experiment
 983 | state) in NEMO05 and NEMO01. The release location is identified in bold and is located a- at
 984 | [100°W/5°N-5S/1000 m depth \(R1\)](#). b- at [160°E/5°N-5°S/1000 m depth \(R2\)](#). The particles have

985 been integrated vertically, zonally and meridionally. The observed mean oxygen levels (WOA) are
986 displayed in contour.
987

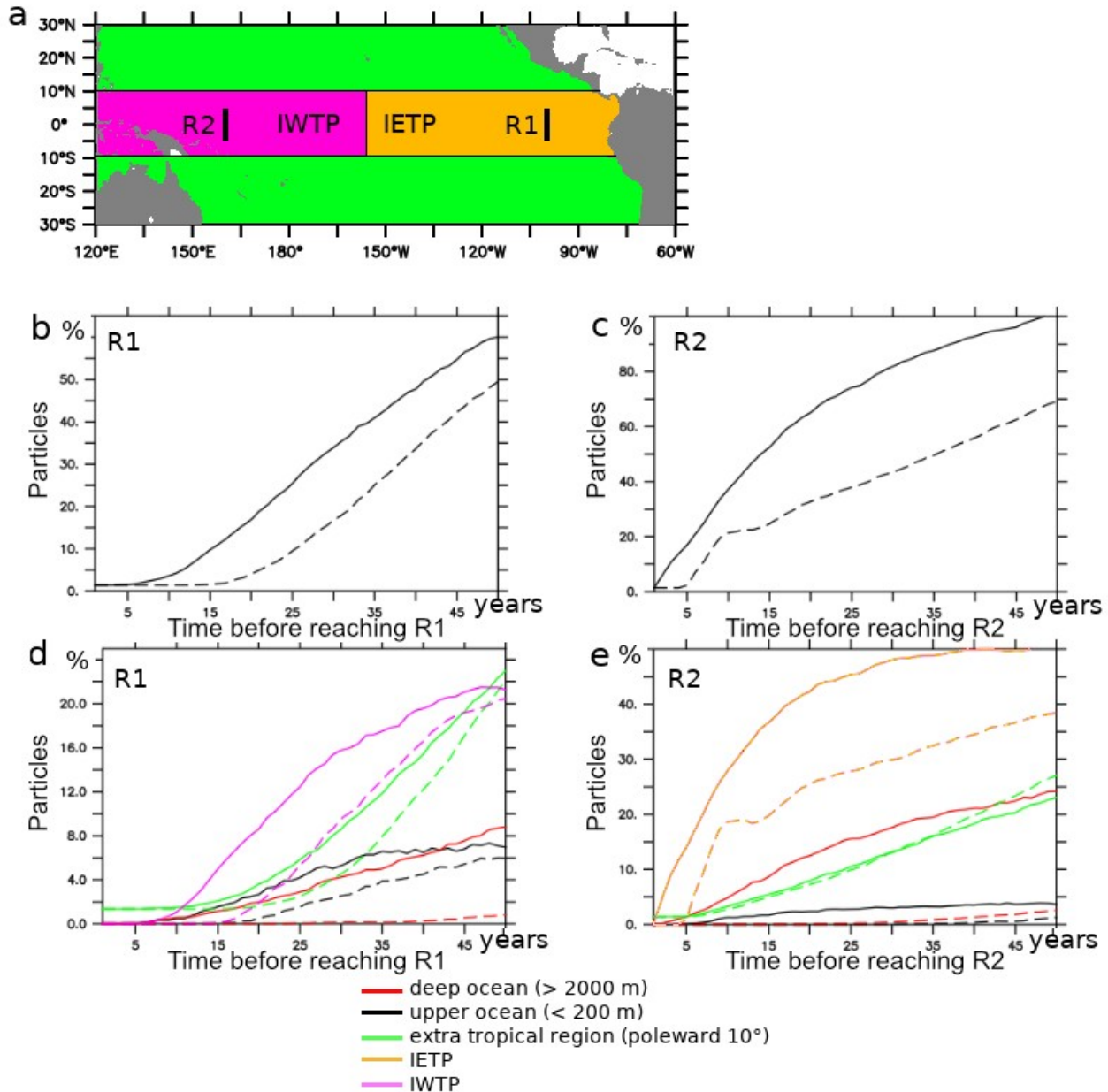
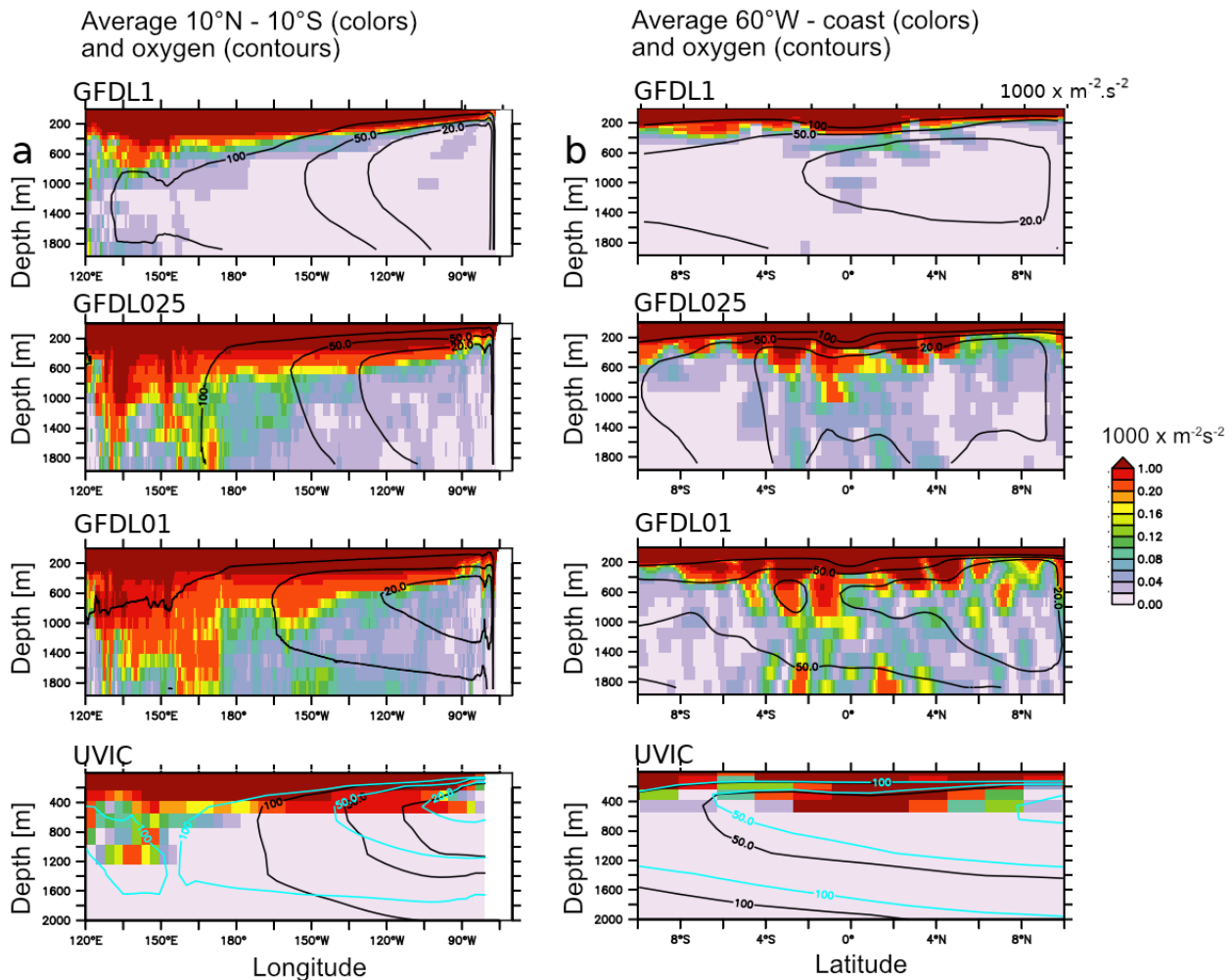


Figure 8 : a- schema summarizing the releases (R1: 100°W / 5°N-5°S / 1000 m , R2: 160°E / 5N°5S / 1000 m) location, the IETP (Intermediate Eastern Tropical Pacific), IWTP (Intermediate Western Tropical Pacific) regional extension. b. percentage of particles (release R1) originating from outside the IETP ocean region. b- percentage of particles (release R2) originating from outside the IWTP ocean region. d- percentage of particles (release R1) originating from the upper ocean (shallow than 200 m), the deeper ocean (deeper than 2000 m), subtropical regions (poleward 10°), the IWTP. e- percentage of particles (release R2) originating from the upper ocean

997 (shallower than 200 m), the deeper ocean (deeper than 2000 m), subtropical regions (poleward
998 10°), the IETP.

999
1000

Mean kinetic energy



1001
1002
1003 Figure 9 : a - Mean Kinetic Energy ($m^2.s^{-2} \times 1000$) (average 10°N-10°S) in GFDL01, GFDL025,
1004 GFDL1, UVIC, b - similar to a. but average 160°W- coast. Oxygen levels ($mmol.m^{-3}$) are displayed
1005 in black contour. The blue contour corresponds to UVIC GD13 (Getzlaff and Dietze, 2013,
1006 including an anisotropical increase of lateral diffusion at the equator)

1007
1008
1009
1010
1011

1012
1013
1014
1015

Table 1 :

Model	Resolution	Atmosphere	Integration (years)	BGC	Model Reference (circulation)	Model Reference (BGC)	
Mean state comparison							
UVIC	2.8°	Coupled (temperature, humidity) Forced (NCEP/NCAR wind stress)	10000	UVIC-BGC	Weaver et al., 2001	Keller et al., 2012	
NEMO2	2° (0.5 eq)	Forced COREv2 “normal year”	1000	NPZD-O2	Madec et al., 2015	Kriest et al., 2010 Duteil et al., 2014	
GFDL1	1°	Coupled	190	BLING	Delworth et al. 2012, Griffies et al., 2015	Galbraith et al., 2015	
GFDL025	0.25 °	Coupled	190	BLING			
GFDL01	0.1°	Coupled	190	BLING			
Process oriented experiments							
Model	Resolution	Atmosphere	Integration (years)	BGC	Characteristics		
NEMO2-REF-30N30S-30N30S1500M (section 2.2.1)	2° (0.5 eq)	Forced COREv2 1948-2007	60	NPZD-O2	<ul style="list-style-type: none"> - control experiment - O2 restoring to WOA at 30°N/30°S - O2 restoring to WOA at 30°N/30°S/1500m 		
NEMO05 (section 2.2.2)	0.5°	Forced COREv2 1948 - 2007	60	Tracer release	<ul style="list-style-type: none"> - Tracer initialized to 1 (O2 WOA > 150 mmol.m-3) or 0 (O2 WOA < 150 mmol.m-3) 		
NEMO01 (section 2.2.2)	0.1°	Forced COREv2 1948 – 2007	60	Tracer release			

1016
1017
1018
1019
1020
1021

1022 | [Annex A](#)

1023 |

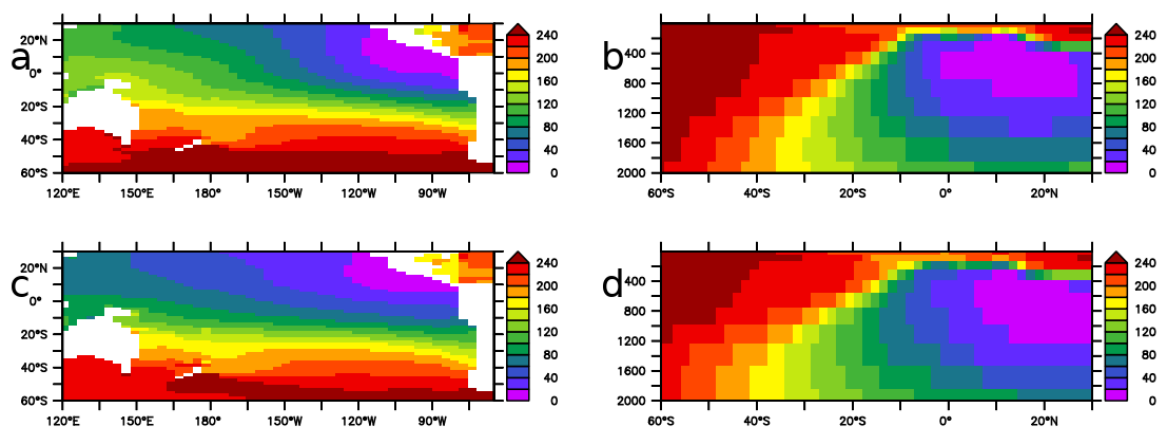
1024 | [The differences in oxygen levels between the “models groups” \(GFDL suite, UVIC, NEMO2\) are](#)
1025 | [partly related to differences in the atmospheric fields employed and the integration time \(see 2\).](#)

1026 |

1027 | [1. Wind forcing](#)

1028 | [Zonal wind mean stress typically vary by 5 to 20 % between the different wind products \(Chauduri](#)
1029 | [et al., 2013\). To test this impact, we performed an experiment using the UVIC model using 2](#)
1030 | [different wind products \(NCEP and COREv2 – Large and Yeager, 2009\) \(Figure A1\). While the](#)
1031 | [shape of the OMZ shows slight differences, the volume of the OMZ and the mean oxygen levels in](#)
1032 | [the tropical regions and in the mid latitudes are similar. Consistent with the Figure 2, higher oxygen](#)
1033 | [levels at 30°S lead to higher oxygen levels in the tropical ocean and to a smaller OMZ volume](#)
1034 | [\(Figure A2\)](#)

1035 |



1045 | [Figure A1 : Oxygen levels in UVIC \(10000 years integration\) a- mean 500-1500 m forcing NCEP.](#)
1046 | [b- section 120°W forcing NCEP. c- mean 500-1500 m forcing COREv2, d- section 120°W forcing](#)
1047 | [COREv2.](#)

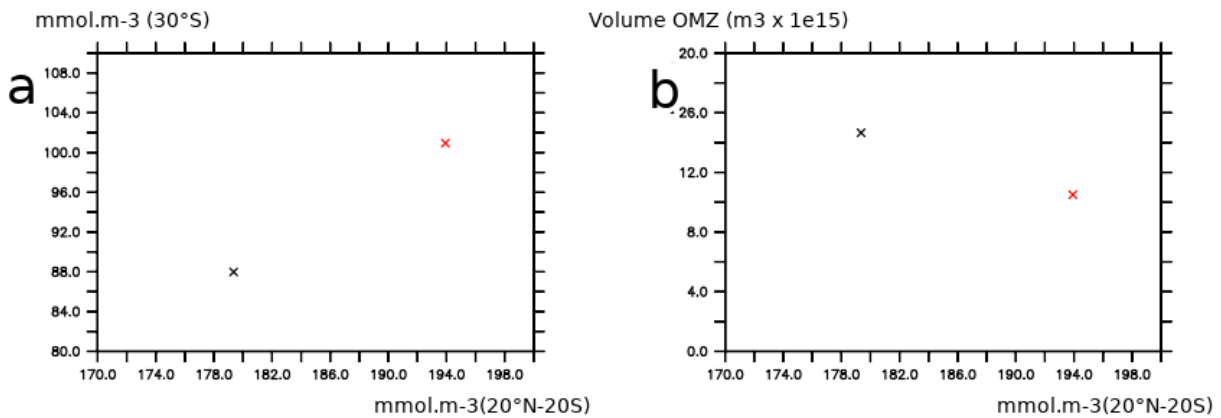
1048 |

1049 |

1050 |

1051 |

1052 |



1053 Figure A2 : a - Oxygen levels in UVIC (10000 years integration) at 30°S (zonal mean in the Pacific
1054 Ocean from surface to 2000 m depth) and in the tropical regions (20°S-20°N, averaged over the
1055 whole Pacific Ocean). b - Oxygen levels in UVIC (10000 years integration) at 30°S (zonal mean in
1056 the Pacific Ocean, from surface to 2000 m depth) and volume of the OMZ in the Pacific Ocean.
1057 The configuration forced by COREv2 is shown in black, the configuration forced by NCEP is shown
1058 in red.

1059

1060 2. Spinup state

1061 In complement, the spinup state of the model also impacts the oxygen levels as the deep ocean
1062 needs thousands of years to be in equilibrium. It may explain why UVIC (integrated for 10000
1063 years) is characterized by much larger oxygen levels than the GFDL model suite (integrated for
1064 190 years). As an example, the Figure A3 shows the evolution of oxygen levels during spinup in
1065 NEMO2. Larger oxygen levels at 30°S (e.g after 1000 years of integration) are characterized by a
1066 smaller OMZ volume (which is consistent with Fig 2) (Figure A4)

1067

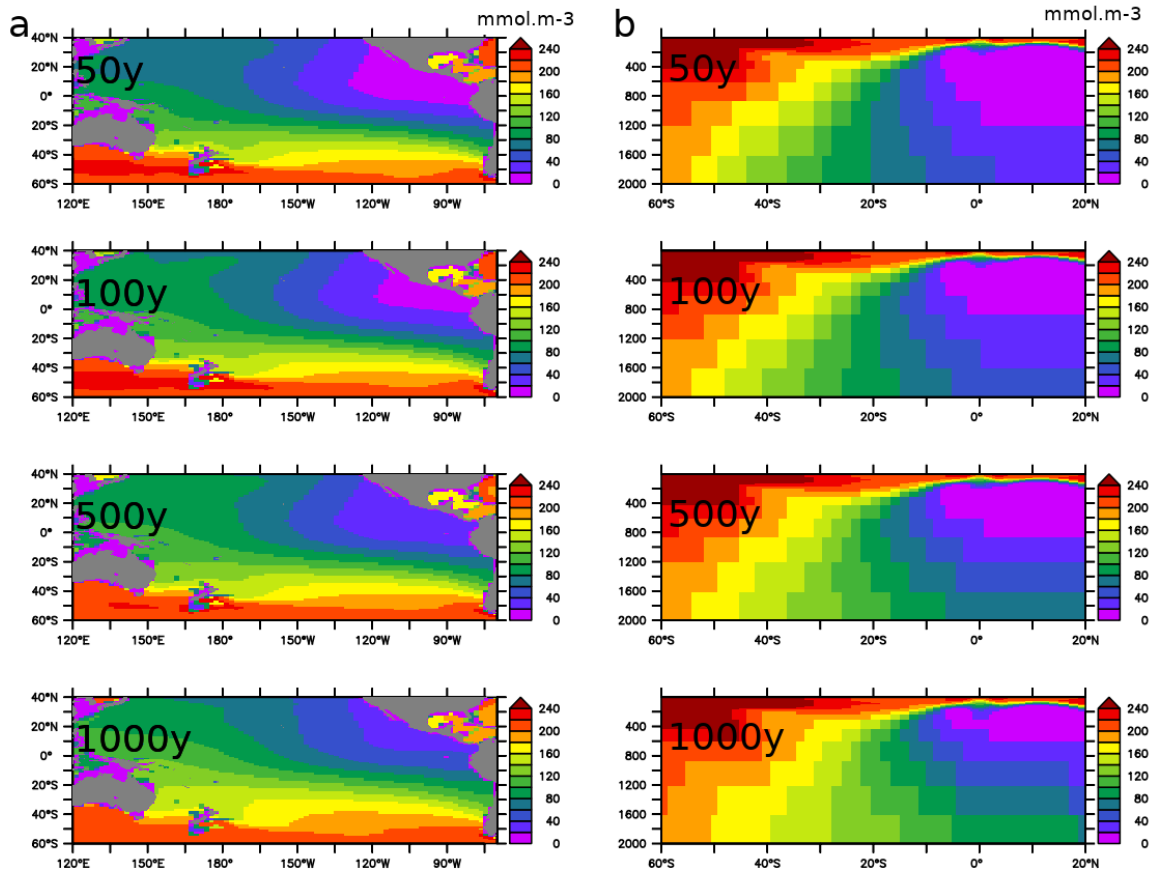


Figure A3 : oxygen levels at a - intermediate depth (average 500 – 2000 m) and b - 120°W in NEMO2 after 50, 100, 500 and 1000 years integration

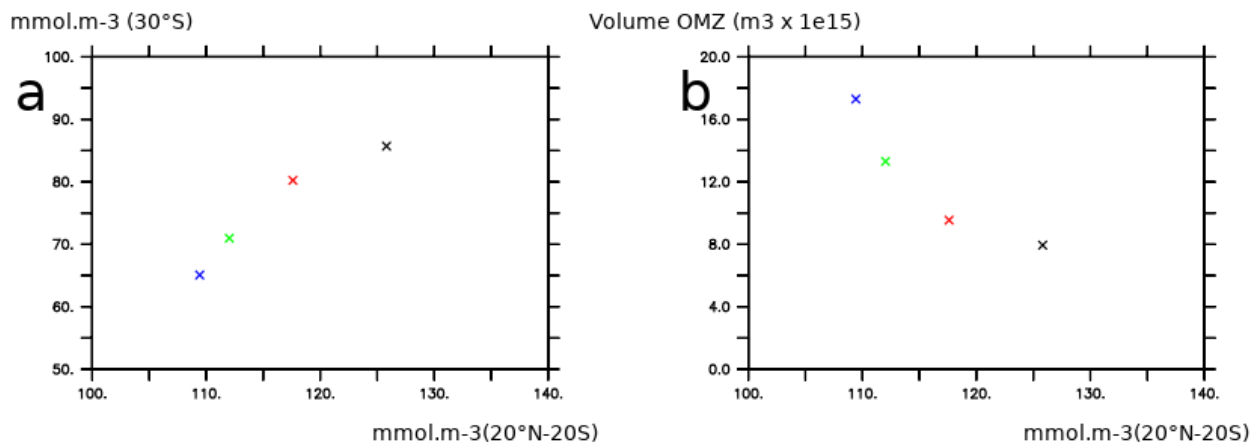


Figure A4 : a - Oxygen levels in NEMO2 at 30°S (zonal mean in the Pacific Ocean from surface to 2000 m depth) and in the tropical regions (20°S-20°N, averaged over the whole Pacific Ocean from surface to 2000 m depth). b - Oxygen levels in NEMO2 at 30°S (zonal mean in the Pacific Ocean from surface to 2000 m depth) and volume of the OMZ in the Pacific Ocean. The color of the cross

1076 | depends of the integration duration (black : 50 years, red : 100 years, green : 500 years, blue 1000
1077 | years).
1078 |
1079 |
1080 |
1081 | [References](#)
1082 | [Chaudhuri, Ayan & Ponte, Rui & Forget, Gael & Heimbach, Patrick. \(2013\). A Comparison of](#)
1083 | [Atmospheric Reanalysis Surface Products over the Ocean and Implications for Uncertainties in Air-](#)
1084 | [Sea Boundary Forcing. Journal of Climate. 26. 153-170. 10.1175/JCLI-D-12-00090.1.](#)
1085 | [Large, W.G., Yeager, S.G. \(2009\). The global climatology of an interannually varying air-sea flux](#)
1086 | [data set. Clim Dyn 33, 341–364. 10.1007/s00382-008-0441-3](#)